NUMERICAL SOLUTION OF ONE DIMENSIONAL DETONATION TUBE WITH
REACTIVE EULER EQUATIONS USING HIGH RESOLUTION METHOD

A THESIS SUBMITTED TO
THE GRADUATE SCHOOL OF MIDDLE EAST TECHINCAL UNIVERSITY
OF
MIDDLE EAST TECHNICAL UNIVERSITY

BY

YİĞİT UNGUN

IN PARTIAL FULFILLMENT OF THE REQUIREMENTS
FOR
THE DEGREE OF MASTER OF SCIENCE
IN
AEROSPACE ENGINEERING

FEBRUARY 2012

Approval of the thesis:

NUMERICAL SOLUTION OF ONE DIMENSIONAL DETONATION TUBE WITH REACTIVE EULER EQUATIONS USING HIGH RESOLUTION METHOD

submitted by **YİĞİT UNGUN** in partial fulfillment of the requirements for the degree of **Master of Science in Aerospace Engineering Department, Middle East Technical University** by,

Prof. Dr. Canan ÖZGEN
Dean, Graduate School of **Natural and Applied Sciences**   ———————

Prof. Dr. Ozan TEKİNALP
Head of Department, **Aerospace Engineering**   ———————

Prof. Dr. İ. Sinan AKMANDOR
Supervisor, **Aerospace Engineering Department, METU**   ———————

Examining Committee Members:

Prof. Dr. Cevdet ÇELENLİGİL
Aerospace Engineering, METU   ———————

Prof. Dr. İ. Sinan AKMANDOR
Aerospace Engineering, METU   ———————

Prof. Dr. İsmail H. TUNCER
Aerospace Engineering, METU   ———————

Prof. Dr. Yusuf ÖZYÖRÜK
Aerospace Engineering, METU   ———————

Prof. Dr. M. Haluk AKSEL
Mechanical Engineering, METU   ———————

Date: ———————

I hereby declare that all information in this document has been obtained and presented in accordance with academic rules and ethical conduct. I also declare that, as required by these rules and conduct, I have fully cited and referenced all material and results that are not original to this work.

Name, Last Name: YİĞİT UNGUN

Signature   :

ABSTRACT

NUMERICAL SOLUTION OF ONE DIMENSIONAL DETONATION TUBE WITH REACTIVE EULER EQUATIONS USING HIGH RESOLUTION METHOD

UNGUN, YİĞİT

M.S, Department of Aerospace Engineering

Supervisor   : Prof. Dr. İ. Sinan AKMANDOR

February 2012, 127 pages

In this thesis, numerical simulation of one dimensional detonation tube problem is solved with finite rate chemistry. For the numerical simulation, Euler equations have been used. Since detonation tube phenomena occurs in high speed flows, viscosity effects and gravity forces are negligible. In this thesis, Godunov type methods have been studied and afterwards high resolution method is used for the numerical solution of the detonation tube problem. To solve the chemistry aspect of the problem ZND theory have been used. For the numerical solution, a FORTRAN code is written and the numerical solution of the problems compared with the exact ZND solutions.

Keywords: detonation, high resolution, ZND theory, reactive Euler equations

ÖZ

REAKTİF EULER DENKLEMLERİNİ KULLANARAK YÜKSEK ÇÖZÜNÜRLÜK METODU İLE BİR BOYUTLU DETONASYON TÜPÜ SAYISAL ÇÖZÜMÜ

UNGUN, YİĞİT

Yüksek Lisans, Havacılık ve Uzay Mühendisliği Bölümü

Tez Yöneticisi   : Prof. Dr. İ. Sinan AKMANDOR

Şubat 2012, 127 sayfa

Bu tezde, tek boyutlu detonasyon tüp problemi sayısal olarak çözülmektedir. Sayısal simulasyon, Euler denklemleri ve sonlu hızla gerçekleşen kimyasal reaksiyonlar kullanarak gerçekleşmiştir. Detonasyon, yüksek hızlarda gerçekleşdiğinden viskozite etkiler ve yer çekimi kuvveti göz ardı edilmiştir. Bu tezde, Godunov tipi metodlar çalışılmıştır ve bu çalışma sonrasında sayısal çözüm için yüksek çözünürlük metodu kullanılmıştır. Problemin kimyasal kısmı için ZND teorisi kullanılmıştır. Sayısal Çözüm için FORTRAN kodu yazılmıştır. Sayısal sonuçlar doğru sonuçlar ile karşılaştırılmıştır.

Anahtar Kelimeler: detonasyon, yüksek çözünürlük metodu, ZND teorisi, reaktif Euler denklemleri

To my mom

ACKNOWLEDGMENTS

I would like to thank my advisor, Professor Dr. İ. SİNAN AKMANDOR for his guidance and support that helped me to complete this thesis. His ideas and comments were very helpful for me to overcome the problems that I encountered during my research.

I also would like to show my appreciation to my beloved mother for the support she has given me throughout my studies.

TABLE OF CONTENTS

LIST OF TABLES

LIST OF FIGURES

FIGURES

CHAPTER 1

INTRODUCTION

Detonation, which is a supersonic wave sustained by chemical reaction[1], is a process of combustion. Detonation waves are high speed combustion waves. In detonation, chemical reactions takes place very fast and time scale of the chemical reaction is very small compared to the time scale of the flow. This thesis concentrate on solving the detonation waves assuming a simple chemistry. In this chapter, first information on detonation waves will be given, then the Euler equations are examined and finally scope of this thesis will be stated.

1.1 DETONATION WAVES

Detonation waves are the combustion waves, which travel in supersonic speeds and led by a shock wave which heats the material and triggers a chemical reaction. Since this process happens rapidly, the energy is converted very fast[2].

Using the theory of the detonation, new types of engines are developing in order to use detonation waves in combustion. Pulse detonation engine is one of the propulsion systems that uses combustion waves[3]. In this thesis combustion waves are examined in one dimensional model.

The one dimensional model consists of a shock wave at the front and a reaction zone. The original model is developed by Chapman and Jouget, which uses the Rankine Hugoniot relations[4]. At the table 1.1, comparison of the wave speed of mixtures with the CJ model and experimental results are given. Differences between the experimental results and theoretical results which obtained from the CJ model are small enough to neglect, therefore CJ model can be used for calculating the wave speed.

Table 1.1: Comparison of the CJ model's wave speed with experimental results[5]

Mixture	Experimental wave speed (m/s)	Theoretical wave speed (m/s)
$4H_2 + O_2$	3344	3425
$3H_2 + O_2$	3156	3197
$2H_2 + O_2$	2825	2853
$H_2 + O_2$	2320	2333
$H_2 + 2O_2$	1909	1941
$H_2 + 3O_2$	1691	1759

Three simplifications have been made in this thesis, when solving for detonation waves. These are;

- Molecular diffusion, thermal conduction and viscous effects are negligible.

- Only one chemical reaction takes place.

- The detonation wave is one dimensional.

To visualize the one dimensional model, figure below can give an idea. As mentioned before, detonation wave is led by the shock wave which triggers the chemical reaction and the reaction zone is created behind the shock wave.
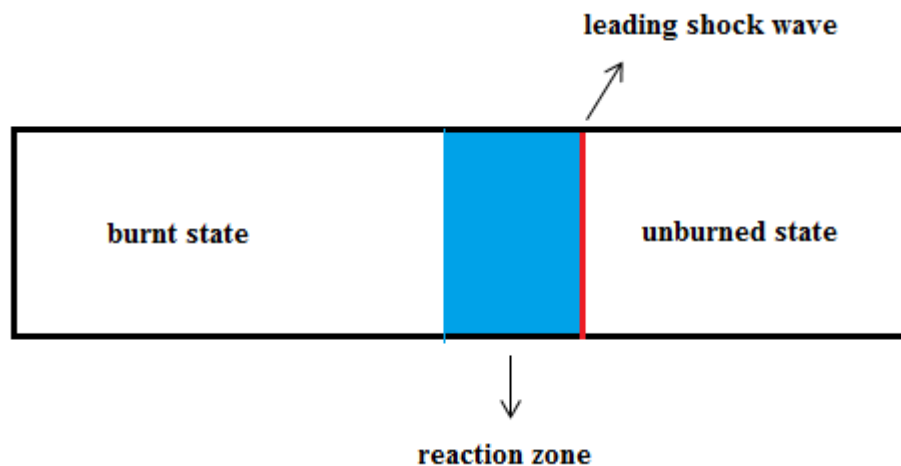
Figure 1.1: One dimensional model of the detonation wave.

This one dimensional model is solved numerically by using reactive Euler equations. The Chapman Jouget model gives the main idea on propagation of the wave speeds but does not

explain internal structure of the detonation wave[5]. The internal structure of the detonation waves are explained by the ZND model which is developed by Zel'dovich, von Neumann and Döring[1][2]. The ZND model is based on the shock wave that triggers an exothermic reaction behind the shock.

1.2 ONE DIMENSIONAL EULER EQUATIONS

The Euler equations derivation is based on the integral relations on control volume[6].

1.2.1 Conservation of Mass

The integral form of the conservation of mass is written as;

$$\int \int \int_V \frac{\partial \rho}{\partial t} dV + \int \int_A \vec{n} \cdot (\rho \vec{V}) dA = 0 \tag{1.1}$$

where ρ is the density, $\vec{V}$ is the velocity vector, V is the closed volume, A is the surface area, $\vec{n}$ is the normal direction vector. First term is written independent of time because of the fixed volume in space.

$$\int \int \int_V \frac{\partial \rho}{\partial t} dV = \frac{d}{dt} \int \int \int_V \rho dV \tag{1.2}$$

Applying the Gauss theorem on the second term.

$$\int \int_A \vec{n} \cdot (\rho \vec{V}) dA = \int \int \int_V div(\rho \vec{V}) dV \tag{1.3}$$

Then equation 1.1 is written as;

$$\int \int \int_V \left[\frac{\partial \rho}{\partial t} + div(\rho \vec{V}) \right] dV = 0 \tag{1.4}$$

Then the conservation of mass can be written in differential form as;

$$\rho_t + (\rho u)_x + (\rho v)_y + (\rho w)_z = 0 \tag{1.5}$$

where u, v, w is the velocity for the x,y and z directions. For the one dimensional form, y and z components are not used, thus;

$$\rho_t + (\rho u)_x = 0 \tag{1.6}$$

3

1.2.2 Conservation of Momentum

The integral form of the conservation of momentum is written as;

$$\int\int\int_V \frac{\partial \rho \vec{V}}{\partial t} dV + \int\int_A \vec{V}(\vec{n} \cdot \rho\vec{V})dA + \vec{f_S} + \vec{f_V} = 0 \qquad (1.7)$$

$\vec{f_S}$ is the surface forces, which is $\vec{f_S} = -\int\int_A \vec{S} dA$ and f_V is the volume forces; which is $f_V = -\int\int\int_V \rho\vec{g}dV$. First term is written independent of time because of the fixed volume in space.

$$\int\int\int_V \frac{\partial \rho \vec{V}}{\partial t} dV = \frac{d}{dt}\int\int\int_V \rho\vec{V}dV \qquad (1.8)$$

All the surface terms are written in a single integral; then the integral form becomes;

$$\int\int\int_V \frac{\partial \rho \vec{V}}{\partial t} dV + \int\int_A [\vec{V}(\vec{n} \cdot \rho\vec{V}) + p\vec{n} - \vec{n} \cdot \Pi]dA - \int\int\int_V \rho\vec{g}dV = 0 \qquad (1.9)$$

where Π is the viscous term. Applying the Gauss theorem on the second term. Second term becomes;

$$\int\int_A \vec{V}(\vec{n} \cdot \rho\vec{V}) + p\vec{n} - \vec{ni} \cdot \Pi dA = \int\int\int_V \left[div(\rho\vec{V} \times \vec{V} + grad(p) - div(\Pi)\right]dV \qquad (1.10)$$

For the Euler equations, viscous term and the gravity forces are negligible, then the equation 1.9 becomes;

$$\int\int\int_V \left[\frac{\partial \rho \vec{V}}{\partial t} + div(\rho\vec{V} \times \vec{V} + grad(p)\right]dV = 0 \qquad (1.11)$$

Then the conservation of momentum can be written in differential form in the x direction as;

$$(\rho u)_t + (\rho u^2 + p)_x + (\rho uv)_y + (\rho uw)_z = 0 \qquad (1.12)$$

For one dimensional form, y and z components are not used thus;

$$(\rho u)_t + (\rho u^2 + p)_x = 0 \qquad (1.13)$$

1.2.3 Conservation of Energy

The integral form of the conservation of energy is written as;

$$\int\int\int_V \frac{\partial \rho E}{\partial t} dV + \int\int_A (\vec{n} \cdot \rho E)dA + E_S + E_V + E_{in} = 0 \qquad (1.14)$$

where E is the total energy, E_S is the surface forces, which is $E_S = \int\int p(\vec{V} \cdot \vec{n})dA - \int\int_A \vec{V} \cdot (n \cdot \Pi)dA$, E_V is the volume forces, which is $E_V = -\int\int\int_V \rho(V \cdot \vec{g})dV$ and E_{in} is the influx

4

of energy into the volume, which is $E_{in} = \int \int_A (\vec{n} \cdot Q) dA$. Q is the energy flow vector. All the surface terms are written in a single integral; then integral form becomes;

$$\int \int \int_V \frac{\partial \rho E}{\partial t} dV + \int \int_A [(\vec{n} \cdot \rho E + p(\vec{V} \cdot \vec{n}) - \int \int_A \vec{V} \cdot (n \cdot \Pi)] dA \qquad (1.15)$$

First term is written independent of time because of the fixed volume in space.

$$\int \int \int_V \frac{\partial \rho E}{\partial t} dV = \frac{d}{dt} \int \int \int_V \rho E dV \qquad (1.16)$$

Applying the Gauss theorem on the second term, the second term becomes;

$$\int \int_A [\vec{n} \cdot (\rho E + p\vec{V} + \vec{Q}) - \vec{V} \cdot (\vec{n} \cdot \Pi)] dA = \int \int \int_V \left[div(\rho E + p)\vec{V} - \vec{V} \cdot \Pi + \vec{Q} \right] dV \quad (1.17)$$

For the Euler equations; energy influx, viscous term and the gravity forces are negligible then the equation 1.15 becomes;

$$\frac{d}{dt} \int \int \int_V \left[\rho E + div(\rho E + p)\vec{V} \right] dV = 0 \qquad (1.18)$$

The conservation of energy can be written in differential form in the x direction as;

$$(\rho E)_t + ((\rho E + p)u)_x + ((\rho E + p)v)_y + ((\rho E + p)w)_z = 0 \qquad (1.19)$$

For the one dimensional form, y and z components are not used thus;

$$(\rho E)_t + ((\rho E + p)u)_x = 0 \qquad (1.20)$$

The equation set for the one dimensional Euler equation can be written as;

$$U_t + F(U)_x = 0$$

$$U = \begin{bmatrix} \rho \\ \rho u \\ \rho E \end{bmatrix} \qquad F = \begin{bmatrix} \rho u \\ \rho u^2 + p \\ u(\rho E + p) \end{bmatrix} \qquad (1.21)$$

To solve the reactive Euler equations, conservation of the species has to be written.

1.2.4 Conservation of Species

The integral form of the conservation of mass is written as;

$$\int \int \int_V \frac{\partial \rho Y}{\partial t} dV + \int \int_A \vec{n} \cdot (\rho Y \vec{V}) dA = \int \int \int_V w Y dV \qquad (1.22)$$

5

where Y is the mass fraction of species, w is the reaction rate. First term is written independent of time because of the fixed volume in space.

$$\int \int \int_V \frac{\partial \rho Y}{\partial t} dV = \frac{d}{dt} \int \int \int_V \rho Y dV \tag{1.23}$$

Applying the Gauss theorem on the second term.

$$\int \int_A \vec{n} \cdot (\rho Y \vec{V}) dA = \int \int \int_V div(\rho Y \vec{V}) dV \tag{1.24}$$

Then equation 1.26 can be written as;

$$\int \int \int_V \left[\frac{\partial \rho Y}{\partial t} + div(\rho Y \vec{V}) \right] dV = \int \int \int_V wY dV \tag{1.25}$$

The conservation of species can be written in differential form as;

$$(\rho Y)_t + (\rho u Y)_x + (\rho v Y)_y + (\rho w Y)_z = w \tag{1.26}$$

For the one dimensional form, y and z components are not used thus;

$$(\rho Y)_t + (\rho u Y)_x = w \tag{1.27}$$

After the conservation of species is written in the differential form, it can be added to the equation set for one dimensional Euler equations. Then the equation set becomes;

$$U_t + F(U)_x = S(U)$$

$$U = \begin{bmatrix} \rho \\ \rho u \\ \rho E \\ \rho Y \end{bmatrix} \qquad F = \begin{bmatrix} \rho u \\ \rho u^2 + p \\ u(\rho E + p) \\ \rho u Y \end{bmatrix} \qquad S = \begin{bmatrix} 0 \\ 0 \\ 0 \\ w \end{bmatrix} \tag{1.28}$$

The detailed information of the derivation of the reactive equations is explained in the chapter 4.

6

1.3 PROPERTIES OF THE EULER EQUATIONS

The conservative formulation of one dimensional Euler equations are given in the equation 1.21. The equation set is written in conservative form, in order to solve the Euler equations numerically without violating the entropy condition[6].

The conservation laws can also written in quasi-linear form.

$$U_t + A(U)U_x = 0 \tag{1.29}$$

where $A(U)$ is the Jacobian matrix. The Jacobian matrix is a coefficient matrix and it is calculated from;

$$A(U) = \frac{\partial F}{\partial U} = \begin{bmatrix} \frac{\partial f_1}{\partial u_1} & \frac{\partial f_1}{\partial u_2} & \frac{\partial f_1}{\partial u_3} \\ \frac{\partial f_2}{\partial u_1} & \frac{\partial f_2}{\partial u_2} & \frac{\partial f_2}{\partial u_3} \\ \frac{\partial f_3}{\partial u_1} & \frac{\partial f_3}{\partial u_2} & \frac{\partial f_3}{\partial u_3} \end{bmatrix} \tag{1.30}$$

The Jacobian matrix is calculated for the Euler equations as;

$$A(U) = \begin{bmatrix} 0 & 1 & 0 \\ \frac{1}{2}(\gamma - 3)u^2 & (3 - \gamma)u & \gamma - 1 \\ (\gamma - 1)u^3 - \gamma uE & \gamma E - \frac{3}{2}(\gamma - 1)u^2 & \gamma u \end{bmatrix} \tag{1.31}$$

where γ is the ratio of the specific heats.

The Euler equations satisfy the homogeneity property. This property can be shown by multiplying the Jacobian matrix with the vector U. Result of this calculation is equal to $F(U)$. With that result the homogeneity property is satisfied.

Eigenvalues of the system show the characteristics of the problem. Eigenvalues of a system are calculated as;

$$|A - \lambda I| = 0 \tag{1.32}$$

λ is the eigenvalue of the system and I is the identity matrix.

For the one dimensional Euler equations, eigenvalues of the system are calculated as;

$$\lambda_1 = u - a, \qquad \lambda_2 = u, \qquad \lambda_3 = u + a \tag{1.33}$$

where a is the speed of sound. Eigenvectors are calculated from;

$$AK = \lambda K \tag{1.34}$$

7

where $K^{(i)}$ is right eigenvector. Right eigenvectors of the one dimensional Euler equations are calculated as;

$$K^{(1)} = [1, u - a, H - ua]^T, \quad K^{(2)} = [1, u, 0.5u^2]^T, \quad K^{(3)} = [1, u + a, H + ua]^T \quad (1.35)$$

where H is the total enthalpy.

All eigenvalues of the one dimensional Euler equations are real and distinct, therefore the Euler equations are hyperbolic equations.

1.4   SCOPE OF THESIS

The scope of this thesis is to solve the detonation tube problem numerically in one dimensional domain with the reactive Euler equations. Numerical solutions will be compared with exact solutions in order to check robustness and accuracy of the numerical method. The detonation process happens very fast, therefore to capture the detonation process with a numerical scheme is not an easy task, therefore more than one case has been studied with changing the input parameters of the detonation tube problem. Physical behavior of the waves and discontinuities have been discussed and accuracy of the numerical solutions has been examined.

The content of this thesis has the discussion on the numerical methods, introducing the detonation theory, that will be used for the solution of the reactive part, numerical tests with inviscid Burgers' equation and numerical simulations of the detonation tube.

First, Riemann problem have been studied in order to solve discontinuities and an exact Riemann solver is used for understanding the behavior of the waves. Then finite difference methods for the conservation laws have been introduced. Comparison of the solution of the exact Riemann solver with numerical methods is used to compare accuracy of the numerical methods. Afterwards high resolution methods have been studied, in order to solve the solution with better accuracy. Numerical solution with high resolution methods again compared with the exact solutions. The chemical part of the problem studied after the study of the high resolution method. The detonation theory, that will be used to solve reactive Euler equations have been introduced and the reactive Euler equations have been given. Finally numerical solutions are obtained for inviscid Burgers' equations and Euler equations with a second order method and solutions are sampled for different cases and input values.

CHAPTER 2

FINITE DIFFERENCE METHODS FOR CONSERVATION LAWS

First, in this chapter Riemann problem will be studied. The exact solution of Riemann problem will be introduced. The exact solutions are used to understand the accuracy and robustness of the numerical methods at the discontinuities for hyperbolic systems. In order to solve shock waves and rarefaction waves Riemann problem must be understood clearly. Riemann problem uses the characteristic lines, defines the discontinuities, whether it is a contact, rarefaction or a shock and it gives information about the unknown states.

Afterwards, the finite difference methods for solving non-reactive Euler equations have been studied. More than one numerical scheme has been tested. These numerical schemes are Godunov methods, Lax-Friedrichs scheme, Lax-Wendroff scheme and Roe's method. The solutions of the numerical schemes have been compared with the exact solution of the Riemann problem.

Inviscid Burgers' equation has solved with Godunov's method and Lax-Friedrichs scheme, then numerical schemes, Godunov's method, Lax-Friedrichs scheme, Richtmyer method, tested with 5 test cases.

After understanding the structure of the Riemann problem and numerical methods, that have been tested, Roe's method had been studied, which is an approximate Riemann solver. Roe's method tested with the same cases used in Godunov's method. Solutions have been compared with the previous tests[13, 14, 15, 16, 17, 18].

2.1 STRUCTURE OF THE RIEMANN PROBLEM

The Riemann Problem for the one dimensional time dependent Euler equations are given as[7];

$$U_t + F(U)_x = 0$$

$$U = \begin{bmatrix} \rho \\ \rho u \\ \rho E \end{bmatrix} \qquad F = \begin{bmatrix} \rho u \\ \rho u^2 + p \\ \rho u H \end{bmatrix} \tag{2.1}$$

where the initial values are,

$$U(x, 0) = \begin{cases} U_L & \text{if} \quad x < 0, \\ U_R & \text{if} \quad x > 0. \end{cases} \tag{2.2}$$

The primitive variable form will be used, when solving the Riemann problem. In the primitive variable form, understanding the behavior of shock waves and rarefaction waves and changes in the flow are easier are easier than the conservative form. Derivation of the primitive variables have been given in appendix B. $W = (\rho, u, p)^T$ is the primitive variable matrix for one dimensional Euler equations.
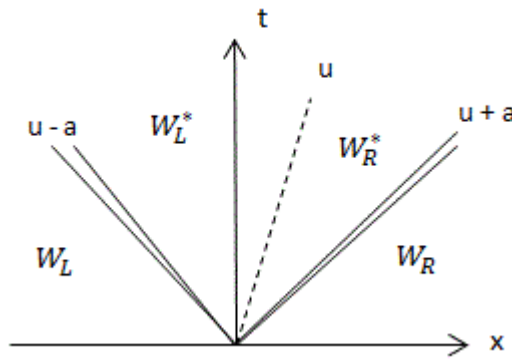
Figure 2.1: The general structure of the Riemann problem on x-t plane

The structure of the Riemann problem on x-t domain can be seen in figure 2.1. To fully characterize flow, Riemann problem flow structure need to be considered in four cases.
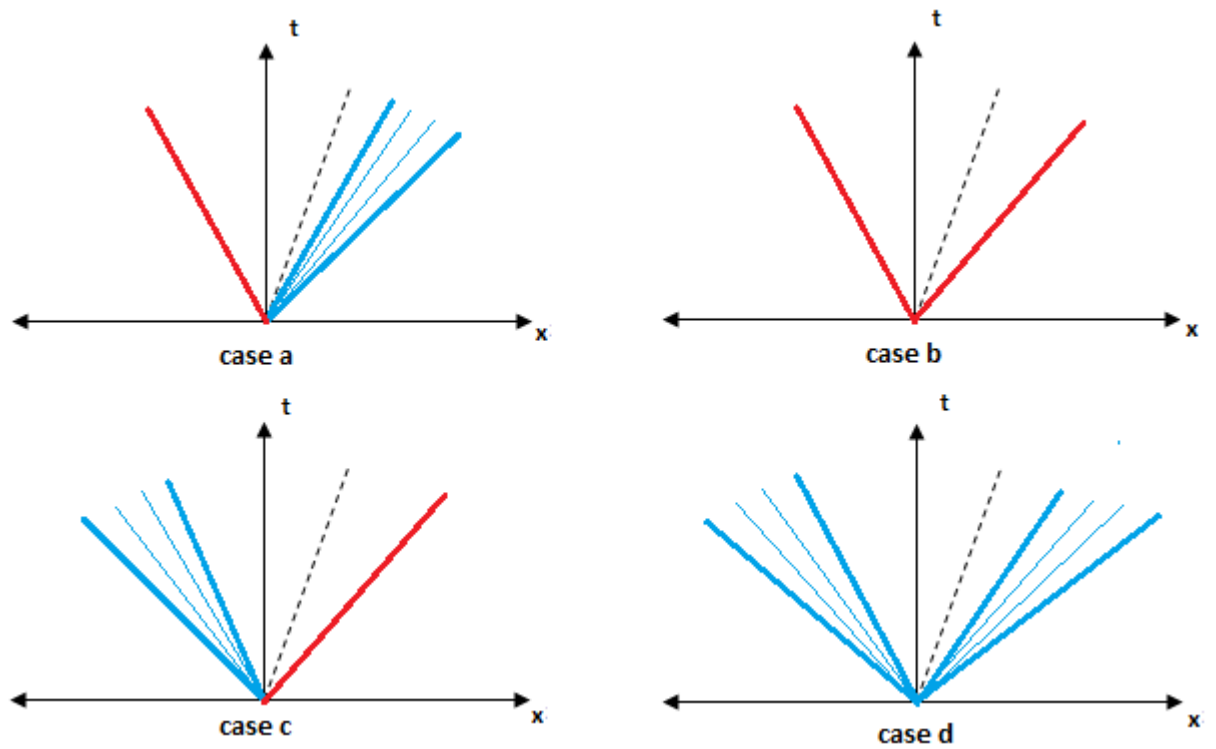
Figure 2.2: The four cases of the Riemann problem

In figure 2.2 all possible solution cases of the Riemann problem has been taken into account. Black dashed lines represent contact discontinuities, blue lines represent rarefaction waves and red lines represents shock waves. Case a consists of left shock wave, a contact discontinuity and right rarefaction wave. Case b consists of left shock wave, a contact discontinuity and right shock wave. Case c consists of left rarefaction wave, a contact discontinuity and right shock wave. Case d consists of left rarefaction wave, a contact discontinuity and right rarefaction wave. In all these cases, three waves separate the solution domain into four constant states.

2.2   THE EXACT SOLUTION PROCEDURE OF THE RIEMANN PROB-LEM

To solve the Riemann Problem exactly all four states has to be solved. States calculated from the relations across the waves.

2.2.1 ELEMENTARY WAVE SOLUTIONS

The solution of the Riemann problem consists of the elementary waves such as rarefaction waves, shock waves and contact discontinuities.
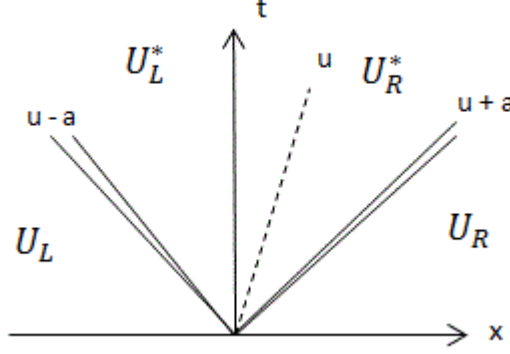
Figure 2.3: The general structure of the Riemann problem on x-t plane for one dimensional Euler equations with three wave families.

In figure 2.3 waves are associated with three characteristic fields corresponding to eigenvectors of $K^{(1)}, K^{(2)}, K^{(3)}$, where the corresponding eigenvalues are $\lambda_1 = u - a, \lambda_2 = u, \lambda_3 = u + a$.

Linearity of the characteristic fields are checked for understanding the relations across the waves.

$$\nabla\lambda_2(U) \cdot K^{(2)} = [-u/\rho, 1/\rho, 0] \cdot \left[1, u, \frac{1}{2}u^2\right]^T = -u/\rho + u/\rho = 0 \qquad (2.3)$$

$$\nabla\lambda_1(U) \cdot K^{(1)} = \left[-u/\rho + \frac{e}{\rho\sqrt{2e\gamma(\gamma-1)}}, 1/\rho, -\frac{1}{\rho\sqrt{e\gamma(\gamma-1)}}\right] \cdot [1, u-a, H-ua]^T \neq 0 \quad (2.4)$$

$$\nabla\lambda_3(U) \cdot K^{(3)} = \left[-u/\rho - \frac{e}{\rho\sqrt{2e\gamma(\gamma-1)}}, 1/\rho, \frac{1}{\rho\sqrt{e\gamma(\gamma-1)}}\right] \cdot [1, u+a, H+ua]^T \neq 0 \quad (2.5)$$

Above equations show that $K^{(1)}$ and $K^{(3)}$ characteristics fields are genuinely non linear but $K^{(2)}$ characteristic field is linearly degenerate.

$K^{(1)}$ and $K^{(3)}$ characteristics fields are rarefaction wave or shock wave, $K^{(2)}$ characteristic field is a contact discontinuity.

2.2.1.1 Contact Discontinuities

For contact discontinuity, $\lambda_2(U_{*L}) = \lambda_2(U_{*R}) = S$, where S is the speed of the contact wave. Using the Generalized Riemann Invariants, quantity change across the wave is calculated.

$$\frac{d\rho}{1} = \frac{d(\rho u)}{u} = \frac{d(\rho E)}{\frac{u^2}{2}} \tag{2.6}$$

From above relation, using the first and second variables, $ud(\rho) = ud(\rho) + \rho d(u)$, which shows that $d(u) = 0$; so across the contact discontinuity velocity is constant. Using second and third variables, $\frac{u^2}{2}d(\rho) = d(\frac{p}{\gamma-1} + \rho\frac{u^2}{2})$, opening up the derivatives should give;

$\frac{u^2}{2}d(\rho) - \frac{u^2}{2}d(\rho) - u\rho d(u) = \frac{d(p)}{\gamma-1}$. From the first relation u is constant so; $d(p) = 0$, which shows pressure is constant across the contact discontinuities.

2.2.1.2 Rarefaction Waves

Rarefaction waves are smooth transition, they consist a head and a tail wave and their structure is a fan shaped wave. In order to have a rarefaction wave, $\lambda_i(U_L) < \lambda_i(U_R)$. Rarefaction waves are associated with the genuinely non linear characteristic fields, which have the characteristic lines, λ_1 and λ_3. For better understanding wave structure, entropy formulation used as a primitive variable, then primitive variables, $W = [\rho, u, s]^T$, form is written as;

$$W_t + AW_x = 0 \tag{2.7}$$

$$A = \begin{bmatrix} u & \rho & 0 \\ a^2/\rho & u & \frac{1}{\rho}\frac{\partial p}{\partial s} \\ 0 & 0 & u \end{bmatrix} \tag{2.8}$$

where A is the Jacobian matrix.

Eigenvalues and eigenvectors are calculated for this system to build up a relationship in the characteristic field. Eigenvalues are calculated as; $\lambda_1 = u - a$, $\lambda_2 = u$ and $\lambda_3 = u + a$. Corresponding eigenvectors are $K^{(1)} = [1, -a/\rho, 0]^T$, $K^{(2)} = [-\frac{\partial p}{\partial s}, 0, a^2]^T$ and $K^{(3)} = [1, a/\rho, 0]^T$. As mentioned before, $K^{(1)}$ and $K^{(3)}$ characteristics fields will be used to obtain a relationship across the rarefaction waves because they are the genuinely non linear characteristic fields.

For λ_1, the Generalized Riemann Invariants is written and the relation becomes;

$$\frac{d\rho}{1} = \frac{du}{-a/\rho} = \frac{ds}{0} \tag{2.9}$$

13

From first and second variables, $u + \int \frac{a}{\rho} d\rho = constant$ relation is found. From third variable $ds = 0$ is found, this shows that s is constant, which means isentropic equations can be used. From isentropic relations, $\int \frac{a}{\rho} d\rho = \frac{2a}{\gamma-1}$ is founded and then putting it in to the first relation, the Riemann Invariants calculated for λ_1 and λ_3 as;

$$I_L(u, a) = u + \frac{2a}{\gamma - 1} = \text{constant} \tag{2.10}$$

$$I_R(u, a) = u - \frac{2a}{\gamma - 1} = \text{constant} \tag{2.11}$$

Using above relationships, primitive variables ρ, u, p is calculated across the rarefaction wave.

2.2.1.3 Shock Waves

Shock waves are discontinuous jumps. Shock waves are associated with the genuinely non linear characteristic fields, which have the characteristic lines, λ_1 and λ_3. In order to have a shock wave, $\lambda_i(U_R) > S_i > \lambda_i(U_R)$. Shock waves always occur from supersonic to subsonic states, otherwise it violates the entropy condition and gives unrealistic wave solutions[8].

The primitive variables, ρ, u, p change across the shock wave and they are found using of the Rankine-Hugoniot conditions with using a frame where shock speed is assumed to be zero[6]. Then velocities become for the new frame, $u_L - S = \bar{u}_L$ and $u_R - S = \bar{u}_R$. The Rankine-Hugoniot relations[30] written as;

$$\rho_L \bar{u}_L = \rho_R \bar{u}_R \tag{2.12}$$

$$\rho_L \bar{u}_L^2 + p_L = \rho_R \bar{u}_R^2 + p_R \tag{2.13}$$

$$\bar{u}_L(\rho_L \bar{E}_L + p_L) = \bar{u}_R(\rho_R \bar{E}_R + p_R) \tag{2.14}$$

Total energy is written in the form of the specific internal energy, e, then equation 2.14 becomes;

$$\bar{u}_L \rho_L(0.5\bar{u}_L^2 + e_L + p_L/\rho_L) = \bar{u}_R \rho_R(0.5\bar{u}_R^2 + e_R + p_R/\rho_R) \tag{2.15}$$

using specific enthalpy, h and using the relation at the equation 2.12, then the equation becomes;

$$\frac{1}{2}\bar{u}_L^2 + h_L = \frac{1}{2}\bar{u}_R^2 + h_R \tag{2.16}$$

To obtain a relation between velocities, density and pressure, equations 2.12 and 2.13 manipulated as;

$$\rho_L \bar{u}_L^2 = \rho_R \bar{u}_R^2 + p_R - p_L = \frac{(\rho_L \bar{u}_L)^2}{\rho_R} + p_R - p_L \tag{2.17}$$

Then $\bar{u}_L^2$ becomes;

$$\bar{u}_L^2 = \frac{\rho_L}{\rho_R} \frac{p_R - p_L}{p_R - p_L} \tag{2.18}$$

Using same methodology; $\bar{u}_R^2$ written as;

$$\bar{u}_R^2 = \frac{\rho_R}{\rho_L} \frac{p_L - p_R}{p_L - p_R} \tag{2.19}$$

Putting the above relations into the equation 2.16 gives;

$$h_L - h_R = \frac{1}{2}(p_L - p_R)\left(\frac{\rho_L + \rho_R}{\rho_L \rho_R}\right) \tag{2.20}$$

The equation 2.20 is written in the form of specific internal energy. Then the equation becomes;

$$e_L - e_R = \frac{1}{2}(p_L + p_R)\left(\frac{\rho_L - \rho_R}{\rho_L \rho_R}\right) \tag{2.21}$$

Assuming the gas is ideal caloric gas, internal energy is written in terms of density and pressure, so equation becomes;

$$\frac{p_L}{\rho_L(\gamma - 1)} - \frac{p_R}{\rho_R(\gamma - 1)} = \frac{1}{2}(p_L + p_R)\left(\frac{\rho_L - \rho_R}{\rho_L \rho_R}\right) \tag{2.22}$$

$$\frac{p_L \rho_R - p_R \rho_L}{\gamma - 1} = \frac{1}{2}(p_L + p_R)(\rho_L - \rho_R) \tag{2.23}$$

$$p_L \rho_R - p_R \rho_L = \frac{\gamma - 1}{2}(p_L \rho_L - p_L \rho_R + p_R \rho_L - p_R \rho_R) \tag{2.24}$$

$$p_L \rho_R + \frac{\gamma - 1}{2}p_L \rho_R + \frac{\gamma - 1}{2}p_R \rho_R = p_R \rho_L + \frac{\gamma - 1}{2}p_L \rho_L + \frac{\gamma - 1}{2}p_R \rho_L \tag{2.25}$$

$$\rho_R\left(\frac{\gamma + 1}{2}p_L + \frac{\gamma - 1}{2}p_R\right) = \rho_L\left(\frac{\gamma + 1}{2}p_R + \frac{\gamma - 1}{2}p_L\right) \tag{2.26}$$

$$\frac{\rho_L}{\rho_R} = \frac{\frac{p_L}{p_R} + \frac{\gamma - 1}{\gamma + 1}}{1 + \frac{p_L}{p_R}\frac{\gamma - 1}{\gamma + 1}} \tag{2.27}$$

From the above derivations, a relation between states are build.

2.2.2 Equations for Pressure and Velocity

In order to solve the Riemann problem exactly, functions $f_L(p_*, W_L)$ and $f_R(p_*, W_R)$ have been introduced. f_L and f_R build up a relation across the non linear waves and they able to calculate the star region in the Riemann problem.

2.2.2.1 Derivation of the function f_L

For shock wave;

Assuming shock is moving to the left direction with a speed of S_L. Then the Rankine-Hugoniot conditions that derived equations 2.12, 2.13 and 2.14 are adapted to the left state and star state. Then Rankine-Hugoniot becomes for this case given as;

$$\rho_L \bar{u}_L = \rho_{*L} \bar{u}_* \tag{2.28}$$

$$\rho_L \bar{u}_L^2 + p_L = \rho_{*L} \bar{u}_*^2 + p_* \tag{2.29}$$

$$\bar{u}_L(\rho_L \bar{E}_L + p_L) = \bar{u}_*(\rho_{*L} \bar{E}_{*L} + p_*) \tag{2.30}$$

Mass flux m_L have been introduced, 2.28 is written as;

$$m_L = \rho_L \bar{u}_L = \rho_{*L} \bar{u}_* \tag{2.31}$$

Then using equation 2.28, equation 2.29 is written as;

$$\rho_L \bar{u}_L(\bar{u}_* - \bar{u}_L) = p_* - p_L \tag{2.32}$$

$$m_L = -\frac{p_* - p_L}{\bar{u}_* - \bar{u}_L} = -\frac{p_* - p_L}{u_* - u_L} \tag{2.33}$$

$$u_* = u_L - \frac{p_* - p_L}{m_L} \tag{2.34}$$

Then assuming as;

$$u_* = u_L - f_L(p_*, W_L) \tag{2.35}$$

m_L has to be written in terms of p_* and data on the left side in order to represent $f_L(p_*, W_L)$ correctly. Manipulating the equation 2.29, m_L becomes;

$$\frac{m_L^2}{\rho_L} - \frac{m_L^2}{\rho_{*L}} = p_* - p_L \tag{2.36}$$

$$m_L^2 = -\frac{p_* - p_L}{\frac{1}{\rho_{*L}} - \frac{1}{\rho_L}} \tag{2.37}$$

At equation 2.27 the relation for the density across the shock has been derived. Then ρ_{*L} becomes in term of left state and p_*;

$$\rho_{*L} = \rho_L \left(\frac{\frac{\gamma-1}{\gamma+1} + \frac{p_*}{p_L}}{\frac{\gamma-1}{\gamma+1}\frac{p_*}{p_L} + 1} \right) \tag{2.38}$$

Using the above relation, equation 2.37 is written in a general form as;

$$m_L = \sqrt{\frac{p_* + B_L}{A_L}} \tag{2.39}$$

where $A_L = \frac{2}{(\gamma+1)\rho_L}$ and $B_L = \frac{(\gamma-1)}{(\gamma+1)}p_L$.

For left shock wave function $f_L(p_*, W_L)$ written in the form as;

$$u_* = u_L - f_L(p_*, W_L) \tag{2.40}$$

$$f_L(p_*, W_L) = (p_* - p_L)\sqrt{\left[\frac{A_L}{p_* + B_L}\right]} \tag{2.41}$$

For rarefaction wave;

Assuming the rarefaction wave is traveling to the left direction. From the properties of the rarefaction waves, isentropic relations and the Generalized Riemann Invariants are used to define star region. From isentropic relations;

$$\rho_{*L} = \rho_L \left(\frac{p_*}{p_L}\right)^{\frac{1}{\gamma}} \tag{2.42}$$

Using the Generalized Riemann Invariants at the equations 2.10 and 2.11;

$$u_L + \frac{2a_L}{\gamma - 1} = u_* + \frac{2a_{*L}}{\gamma - 1} \tag{2.43}$$

Using the density relation for the isentropic case, speed of sound for the star region is represented as;

$$a_{*L} = a_L \left(\frac{p_*}{p_L}\right)^{\frac{\gamma-1}{2\gamma}} \tag{2.44}$$

Then the equation 2.43 is written in a general form as;

$$u_* = u_L - f_L(p_*, W_L) \tag{2.45}$$

where function $f_L(p_*, W_L)$ is calculated in terms of p_* and left state data given as;

$$f_L(p_*, W_L) = \frac{2a_L}{\gamma - 1}\left[\left(\frac{p_*}{p_L}\right)^{\frac{\gamma-1}{2\gamma}} - 1\right] \tag{2.46}$$

2.2.2.2 Derivation of the function f_R

For shock wave;

The methodology is same with the left state but now shock wave is traveling to the right with

the speed of S_R. The Rankine-Hugoniot conditions are

$$\rho_{*R}\bar{u}_* = \rho_R\bar{u}_R \tag{2.47}$$

$$\rho_{*R}\bar{u}_*^2 + p_* = \rho_R\bar{u}_R^2 + p_R \tag{2.48}$$

$$\bar{u}_*(\rho_{*R}\bar{E}_{*R} + p_*) = \bar{u}_R(\rho_R\bar{E}_R + p_R) \tag{2.49}$$

Mass flux m_R have been introduced, 2.47 is written as;

$$-m_R = \rho_{*R}\bar{u}_* = \rho_R\bar{u}_R \tag{2.50}$$

For left shock wave function $f_R(p_*, W_R)$ written in the form as;

$$u_* = u_R + f_R(p_*, W_R) \tag{2.51}$$

$$f_R(p_*, W_R) = (p_* - p_R)\sqrt{\left[\frac{A_R}{p_* + B_R}\right]} \tag{2.52}$$

where $A_R = \frac{2}{(\gamma+1)\rho_R}$ and $B_R = \frac{(\gamma-1)}{(\gamma+1)}p_R$.

For rarefaction wave;

The methodology is same with the left state but now rarefaction wave is moving to the right. For this case isentropic relation is written as;

$$\rho_{*R} = \rho_R\left(\frac{p_*}{p_R}\right)^{\frac{1}{\gamma}} \tag{2.53}$$

The Generalized Riemann Invariants is written as;

$$u_* - \frac{2a_{*R}}{\gamma - 1} = u_R - \frac{2a_R}{\gamma - 1} \tag{2.54}$$

Using the density relation for the isentropic case, speed of sound for the star region is represented as;

$$a_{*R} = a_R\left(\frac{p_*}{p_R}\right)^{\frac{\gamma-1}{2\gamma}} \tag{2.55}$$

Then the equation 2.54 is written in a general form as;

$$u_* = u_R + f_R(p_*, W_R) \tag{2.56}$$

where function $f_R(p_*, W_R)$ calculated as in terms of p_* and right state data given as;

$$f_R(p_*, W_R) = \frac{2a_R}{\gamma - 1}\left[\left(\frac{p_*}{p_R}\right)^{\frac{\gamma-1}{2\gamma}} - 1\right] \tag{2.57}$$

18

2.2.2.3 Derivation of the function $f(p_*, W_L, W_R)$

The general form of the functions $f_L(p_*, W_L)$ and $f_R(p_*, W_R)$ written as;

$$u_* = u_L - f_L(p_*, W_L) \tag{2.58}$$

$$u_* = u_R + f_R(p_*, W_R) \tag{2.59}$$

The general function, $f(p_*, W_L, W_R)$, is written by canceling the u_*;

$$f(p_*, W_L, W_R) = f_L(p_*, W_L) - f_R(p_*, W_R) + \Delta u = 0 \tag{2.60}$$

If the equations are written in a more compact form ;

$$f(p, W_L, W_R) = f_L(p, W_L) + f_R(p, W_R) + \Delta u = 0 \tag{2.61}$$

$$f_L(p, W_L) = \begin{cases} (p - p_L)\left(\frac{A_L}{p + B_L}\right)^{\frac{1}{2}} & \text{if} \quad p > p_L, \\ \frac{2a_L}{(\gamma - 1)}\left[\left(\frac{p}{p_L}\right)^{\frac{\gamma - 1}{2\gamma}} - 1\right] & \text{if} \quad p \le p_L, \end{cases} \tag{2.62}$$

$$f_R(p, W_R) = \begin{cases} (p - p_R)\left(\frac{A_R}{p + B_R}\right)^{\frac{1}{2}} & \text{if} \quad p > p_R, \\ \frac{2a_R}{(\gamma - 1)}\left[\left(\frac{p}{p_R}\right)^{\frac{\gamma - 1}{2\gamma}} - 1\right] & \text{if} \quad p \le p_R, \end{cases} \tag{2.63}$$

and constants of the functions are

$$A_L = \frac{2}{(\gamma + 1)\rho_L} , \quad B_L = \frac{(\gamma - 1)}{(\gamma + 1)}p_L$$
$$A_R = \frac{2}{(\gamma + 1)\rho_R} , \quad B_R = \frac{(\gamma - 1)}{(\gamma + 1)}p_R \tag{2.64}$$

The star region velocity u_* is formulated as;

$$u_* = \frac{1}{2}(u_L + u_R) + \frac{1}{2}[f_R(p_*) - f_L(p_*)] \tag{2.65}$$

An iterative scheme is used to calculate p_* value at the equation 2.61. Newton-Raphson iterative scheme is used in this thesis and it is formulated as;

$$p_k = p_{k-1} - \frac{f(p_{k-1})}{f'(p_{k-1})} \tag{2.66}$$

After calculating the p_* value, u_* is calculated from the equation 2.65. The only unknown states are ρ_{*L} and ρ_{*R}. If there is a rarefaction wave, isentropic relation is used to calculate star region density. From equations 2.42 and 2.53, ρ_{*L} and/or ρ_{*R} are calculated for isentropic case.

If there is a shock wave, the equation 2.27 is used to calculate ρ_{*L} and/or ρ_{*R}.

19

2.3 CONSERVATIVE METHODS

2.3.1 BASIC DEFINITIONS

In this thesis, high speed one dimensional shocked flow solutions are obtained. Conservative formulation is used to obtain results. Formulation of the equations other than the conservative formulation gives incorrect shock solutions. Because of the increase in entropy dissipation, non conservative variables give incorrect solutions at the discontinuities. The amplitude of the discontinuous jumps affect the error done by the non conservative variables[19].

A conservative scheme in a numerical method can be written as;

$$u_i^{n+1} = u_i^n + \frac{\Delta t}{\Delta x}\left[f_{i-\frac{1}{2}} - f_{i+\frac{1}{2}}\right] \tag{2.67}$$

$f_{i+\frac{1}{2}}$ is the numerical flux, which is needed to be calculated by the numerical methods. Discretization of the domain is done by;

$$\Delta x = x_{i+\frac{1}{2}} - x_{i-\frac{1}{2}} = \frac{L}{M} \tag{2.68}$$

where L is the length of the domain and M is the number of cells.

2.3.2 GODUNOV'S FIRST-ORDER UPWIND METHOD

Godunov's method[7] is a conservative method in a form of equation 2.67. In Godunov's method numerical fluxes are computed with the solution of the local Riemann problem. Godunov's method is the first method that defines the Riemann problem and solve it without using an iterative scheme or non linear functions. Iterative schemes or non linear functions are expensive to solve, so Godunov constructs a method, which treats weak and strong shocks automatically and gives thin shock solutions. After Godunov introduced his method, Godunov-type methods have emerged. Godunov-type methods are great for their robustness and accuracy in very complicated shock structures. For the solution with Godunov's method, a piece-wise constant distribution in the cells is assumed as;

$$U_i^n = \frac{1}{\Delta x}\int_{x_{i-\frac{1}{2}}}^{x_{i+\frac{1}{2}}} U(x, t^n)dx \tag{2.69}$$

For the solution, Godunov suggest that, solve the two Riemann problems $RP(U_{i-1}^n, U_i^n)$ and $RP(U_i^n, U_{i+1}^n)$, which gives the solution for $U_{i-\frac{1}{2}}^n$ and $U_{i+\frac{1}{2}}^n$, locally. Then taking an inte-

gral average of the solutions, $U^n_{i-\frac{1}{2}}$ and $U^n_{i+\frac{1}{2}}$, will give the value of U^{n+1}_i. Since the piecewise constant distribution is used, information of the cell value is depending on the inter-cell boundaries. For cell i, inter-cell boundaries $i - \frac{1}{2}$ and $i + \frac{1}{2}$ are using to compute piece-wise constant distribution. This is the main idea behind to use the solutions of $RP(U^n_{i-1}, U^n_i)$ and $RP(U^n_i, U^n_{i+1})$. Δt has to be chosen carefully, otherwise the characteristic lines of the inter-cell boundaries can clash and wrong solutions will emerge. Figure 2.4 shows the importance of the Δt and the inter-cell boundaries of the cell i.
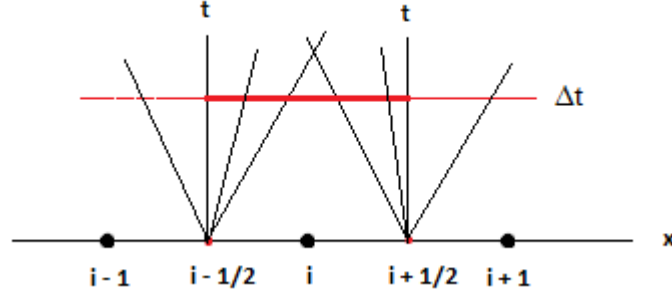
Figure 2.4: Averaging the inter-cell boundaries with the time step Δt

For the linear advection equations, where $f(u) = au, a > 0$, the exact solution of $RP(U^n_{i-1}, U^n_i)$ is;

$$U_{i-\frac{1}{2}}(x/t) = \begin{cases} U^n_{i-1} & \text{if} \quad x/t < a, \\ U^n_i & \text{if} \quad x/t > a, \end{cases} \tag{2.70}$$

The exact solution of $RP(U^n_i, U^n_{i+1})$ is;

$$U_{i+\frac{1}{2}}(x/t) = \begin{cases} U^n_i & \text{if} \quad x/t < a, \\ U^n_{i+1} & \text{if} \quad x/t > a, \end{cases} \tag{2.71}$$

So the general solution for first order Godunov's method for the U^{n+1}_i is;

$$U^{n+1}_i = \frac{1}{\Delta x} \left[\int_0^{\frac{1}{2}\Delta x} U_{i-\frac{1}{2}}(x/\Delta t)dx + \int_{-\frac{1}{2}\Delta x}^0 U_{i+\frac{1}{2}}(x/\Delta t)dx \right] \tag{2.72}$$

2.3.3 SECOND VERSION OF THE GODUNOV'S METHOD

Second version of the Godunov's method is easier to apply with conservative formula, equation 2.67. In the second version of the Godunov's method, the integral average of the solution

21

of the Riemann problems, $RP(U_{i-1}^n, U_i^n)$ and $RP(U_i^n, U_{i+1}^n)$ written in the form as;

$$U_i^{n+1} = \frac{1}{\Delta x} \int_{x_{i-\frac{1}{2}}}^{x_{i+\frac{1}{2}}} \tilde{U}(x, \Delta t) dx. \tag{2.73}$$

where $\tilde{U}(x, t)$ is the combined solution of the Riemann problem. Since $\tilde{U}(x, t)$ is an exact solution of conservation law, it is written in integral form as;

$$\int_{x_{i-\frac{1}{2}}}^{x_{i+\frac{1}{2}}} \tilde{U}(x, \Delta t) dx = \int_{x_{i-\frac{1}{2}}}^{x_{i+\frac{1}{2}}} \tilde{U}(x, 0) dx + \int_0^{\Delta t} F(\tilde{U}(x_{i-\frac{1}{2}}, t)) dt - \int_{\Delta t}^0 F(\tilde{U}(x_{i+\frac{1}{2}}, t)) dt \tag{2.74}$$

The inter-cell fluxes defines as;

$$F_{i-\frac{1}{2}} = \frac{1}{\Delta t} \int_0^{\Delta t} F(\tilde{U}_{i-\frac{1}{2}}, t) dt \tag{2.75}$$

$$F_{i+\frac{1}{2}} = \frac{1}{\Delta t} \int_0^{\Delta t} F(\tilde{U}_{i+\frac{1}{2}}, t) dt \tag{2.76}$$

Fluxes are depending on the solution of $\tilde{U}(x, t)$, the exact solution of the Riemann problem at the local coordinates.

$$(\tilde{U}_{i-\frac{1}{2}}, t) = U_{i-\frac{1}{2}}(0) \text{ and } (\tilde{U}_{i+\frac{1}{2}}, t) = U_{i+\frac{1}{2}}(0) \tag{2.77}$$

The inter-cell fluxes become;

$$F_{i-\frac{1}{2}} = F(U_{i-\frac{1}{2}}(0)) \tag{2.78}$$

$$F_{i+\frac{1}{2}} = F(U_{i+\frac{1}{2}}(0)) \tag{2.79}$$

From the above equations, Godunov's method inter-cell flux generalized as;

$$F_{i+\frac{1}{2}}^{god} = F(U_{i+\frac{1}{2}}(0)) \tag{2.80}$$

2.3.4   THE LAX-FRIEDRICHS SCHEME

The Lax-Friedrichs scheme is a finite difference method and it helps to solve partial differential equations[20]. It is a conservative method, so it is applicable to the hyperbolic system of equations. It is a monotone scheme. The Lax-Friedrichs scheme is space-centered explicit scheme with a first order accuracy. The Lax-Friedrichs scheme has been studied in this thesis, because it is one of the first schemes that solves Euler equations numerically and it helps to understand the finite difference methods. Although it is a successful numerical method, it has poor accuracy because of it's order and it gives oscillations at the discontinuities, which is a important subject for this thesis.

If the integral form of conservation law is written at time $1/2\Delta t$;

$$\int_{-\frac{1}{2}\Delta x}^{\frac{1}{2}\Delta x} \tilde{U}(x, \frac{1}{2}\Delta t)dx = \int_{-\frac{1}{2}\Delta x}^{\frac{1}{2}\Delta x} \tilde{U}(x, 0)dx + \int_0^{\frac{1}{2}\Delta t} F(\tilde{U}(-\frac{1}{2}\Delta x, t))dt - \int_{\frac{1}{2}\Delta t}^0 F(\tilde{U}(\frac{1}{2}\Delta x, t))dt \tag{2.81}$$

Replacing the U_i^n with $(U_{i-1}^n + U_{i+1}^n)/2$, direct evaluation form of integrals become;

$$U_i^{n+1} = \frac{1}{2}(U_{i-1}^n + U_{i+1}^n) + \frac{1}{2}\frac{\Delta t}{\Delta x}(F_{i-1}^n - F_{i+1}^n) \tag{2.82}$$

If the Lax-Friedrichs scheme is written in conservative form, above equation becomes;

$$U_i^{n+1} = U_i^n + \frac{\Delta t}{\Delta x}\left[F_{i-\frac{1}{2}} - F_{i+\frac{1}{2}}\right] \tag{2.83}$$

with the Lax-Friedrichs inter-cell flux is given as;

$$F_{i+\frac{1}{2}}^{LF} = \frac{1}{2}(F_i^n + F_{i+1}^n) + \frac{1}{2}\frac{\Delta x}{\Delta t}(U_i^n - U_{i+1}^n) \tag{2.84}$$

2.3.5   THE LAX-WENDROFF SCHEME

The Lax-Wendroff scheme is a finite difference method and it is a second order scheme[15, 21]. It has got a better accuracy than the Lax-Friedrichs scheme because it is a second order both in time and space but it is not a monotone scheme, therefore oscillations are increased in discontinuous regions, which isn't wanted, when solving the shock waves. The Lax-Wendroff inter-cell flux is given as;

$$F_{i+\frac{1}{2}}^{LW} = F(U_{i+\frac{1}{2}}^{n+\frac{1}{2}}); \qquad U_{i+\frac{1}{2}}^{n+\frac{1}{2}} = \frac{1}{\Delta x}\int_{-\frac{1}{2}\Delta x}^{\frac{1}{2}\Delta x} U_{i+\frac{1}{2}}(x, \frac{1}{2}\Delta t)dx \tag{2.85}$$

$U_{i+\frac{1}{2}}(x, t)$ is the solution of the $RP(U_i^n, U_{i+1}^n)$. Because it is using U_{i+1}^n and U_i^n for the solution, this scheme called Weighted Average Flux method. By using the calculated fluxes, equation 2.83 is solved for non-linear hyperbolic systems.

If the Lax-Wendroff scheme is written in the integral form of the conservation law;

$$\int_{-\frac{1}{2}\Delta x}^{\frac{1}{2}\Delta x} \tilde{U}(x, \frac{1}{2}\Delta t)dx = \int_{-\frac{1}{2}\Delta x}^{\frac{1}{2}\Delta x} \tilde{U}(x, 0)dx + \int_0^{\frac{1}{2}\Delta t} F(\tilde{U}(-\frac{1}{2}\Delta x, t))dt - \int_{\frac{1}{2}\Delta t}^0 F(\tilde{U}(\frac{1}{2}\Delta x, t))dt \tag{2.86}$$

Replacing the $U_{i+\frac{1}{2}}^{n+\frac{1}{2}}$ with $(U_i^n + U_{i+1}^n)/2$, direct evaluation form of integrals become;

$$U_{i+\frac{1}{2}}^{n+\frac{1}{2}} = \frac{1}{2}(U_i^n + U_{i+1}^n) + \frac{1}{2}\frac{\Delta t}{\Delta x}(F_i^n - F_{i+1}^n) \tag{2.87}$$

If the Lax-Wendroff scheme is written in conservative version, the inter-cell flux becomes;

$$F_{i+\frac{1}{2}}^{LW} = F(U_{i+\frac{1}{2}}^{n+\frac{1}{2}});$$

(2.88)

This scheme is called the two step Richtmyer version of the Lax-Wendroff method and it is used for comparison of numerical solutions in this thesis.

2.4   SOLUTION OF THE INVISCID BURGERS' EQUATION

For comparison of the numerical schemes inviscid Burgers' equation is used. Inviscid Burgers' equation can create shock waves and rarefactions. Using a basic equation such as inviscid Burgers' equation, will help to understand the behavior of numerical methods at the discontinuities. The inviscid Burgers' equation can be shown as;

$$u_t + f(u)_x = 0, \qquad f(u) = \frac{1}{2}u^2$$

(2.89)

For boundary conditions, transmissive boundary conditions applied. Ghost cells created at the start and at the end of the domain.

$$u_0^n = u_1^n, \qquad u_{M+1}^n = u_M^n$$

(2.90)

For choosing time step, the maximum Courant number C_{CFL} has been computed.

$$C_{cfl} = \Delta t S_{max}^n / \Delta x$$

(2.91)

S_{max}^n is the maximum wave speed in the domain for time level n. For the case of a shock, S_{max}^n is equal to the shock speed. For the case of the rarefaction wave S_{max}^n is equal to head or tail speeds of the expansion.

C_{cfl} is chosen between $0 < C_{cfl} \leq 1$ for stability reasons. For our problem $C_{cfl} = 0.8$.

After setting the C_{cfl}, Δt is calculated from equation 2.91.

Domain length of the problem is between $[0, \frac{3}{2}]$ and initial conditions are set as;

$$u(x,0) = \begin{cases} -\frac{1}{2} & \text{if} \quad x \leq \frac{1}{2}, \\ 1 & \text{if} \quad \frac{1}{2} \leq x \leq 1, \\ 0 & \text{if} \quad x \geq 1, \end{cases}$$

(2.92)

The problem consists of left rarefaction wave and a right shock wave. The domain is discretized by 75 cells so $\Delta x = 0.02$. Solutions are sampled at $t = 0.5$ units.
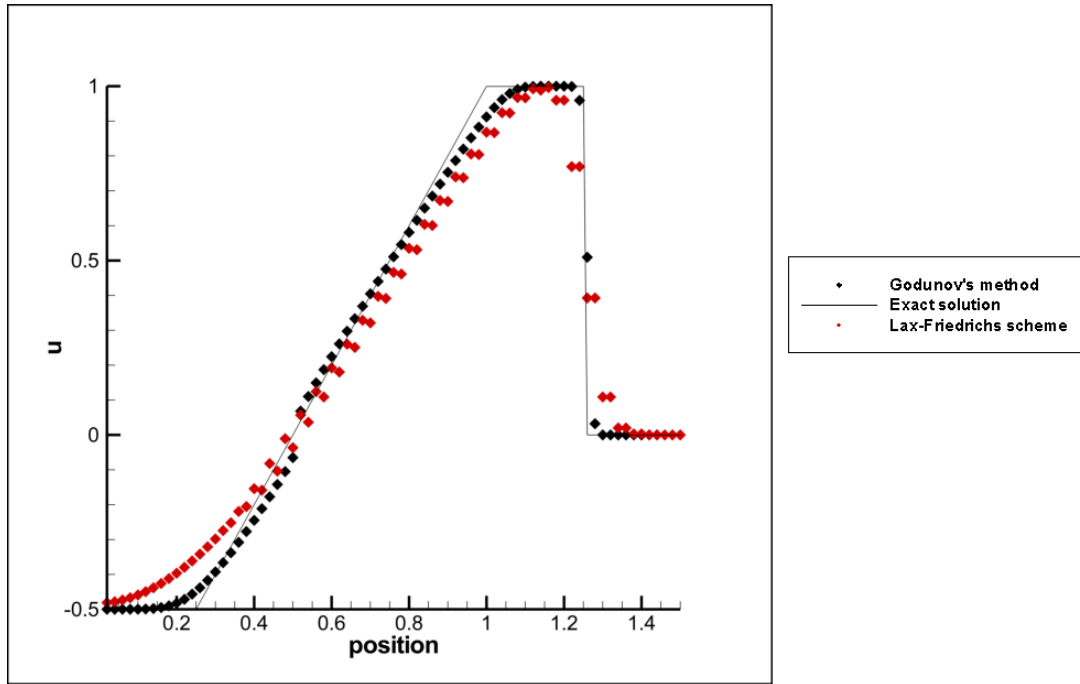
Figure 2.5: Comparison of the Godunov's method (black symbols) and Lax-Friedrichs scheme (red symbols) with exact solution (black line) for the inviscid Burgers' equation

At the first look at the figure 2.5, diffusivity of the Godunov's method is less than the Lax-Friedrichs scheme. When looked at the shock wave, Godunov's method solves the shock wave in 3 cells but Lax-Friedrichs scheme solves shock wave in10 cells. Because of solving the Riemann problem locally, Godunov-type methods are better at solving discontinuities and this example clearly shows that. But when looked at the sonic point, $x = 0.5$, a glitch is seen at the Godunov's method. This is an unrealistic result and it is called entropy glitch. More information is given on entropy glitch at section 2.7.2 and an entropy fix will be told. The initial data on the left boundary is calculated wrong with the Lax-Friedrichs scheme, because upwind term has a larger weight in the solution.

This problem is a good example for comparing Godunov-type methods and centered schemes. In this thesis, solutions at the discontinuities are important, so Godunov-type methods are more important.

2.5 THE GODUNOV'S METHOD FOR ONE DIMENSIONAL NON-REACTIVE EULER EQUATIONS

$$PDEs : U_t + F(U)_x = 0,$$

$$ICs : U(x, 0) = U^{(0)}(x),$$

$$BCs : U(0, t) = U_l(t), U(L, t) = U_r(t),$$

$$U = \begin{bmatrix} \rho \\ \rho u \\ \rho E \end{bmatrix} \qquad F = \begin{bmatrix} \rho u \\ \rho u^2 + p \\ \rho u H \end{bmatrix}$$

$$(2.93)$$

The Godunov's method is written in conservative form at the equation 2.83, where the intercell numerical flux computed from;

$$F_{i+\frac{1}{2}} = F(U_{i+\frac{1}{2}}(0)) \qquad (2.94)$$

There are 10 possible wave patterns for the solution of non-reactive Euler equations, shown at figure 2.6. For case 1, $0 \leq u_*$ and for case 2, $0 \geq u_*$. Each case has 5 possible wave patterns.
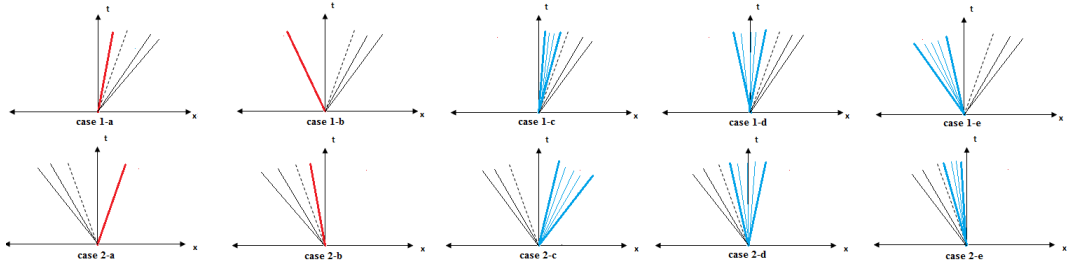
Figure 2.6: Possible wave pattern when solving the Riemann Problem for the Godunov's method

At the figure 2.6 red line represents shock wave, a blue fan represents a rarefaction wave, a dashed black line represents contact discontinuity and pair of thin black lines represents an unknown case.

For case 1, $(0 \leq u_*)$ of the figure 2.6, case 1-a is a right shock wave, case 1-b is a left shock wave, case 1-c is a right rarefaction wave, case 1-d is a sonic rarefaction wave and case 1-e is a left rarefaction wave.

For case 2, $(0 \leq u_*)$ of the figure 2.6, case 2-a is a right shock wave, case 2-b is a left shock wave, case 2-c is a right rarefaction wave, case 2-d is a sonic rarefaction wave and case 2-e is a left rarefaction wave.

2.5.1 TIME STEP

Time step is chosen according to the C_{cfl} condition.

$$\Delta t = \frac{C_{cfl}\Delta x}{S^n_{max}} \qquad (2.95)$$

Where $0 < C_{cfl} \leq 1$. S^n_{max} is chosen as;

$$S^n_{max} = max\{|u^n_i| + a^n_i\} \qquad (2.96)$$

S^n_{max} is taken as an underestimated value because when Δt is high, there can be instabilities.

2.5.2 BOUNDARY CONDITION

Transmissive boundary condition is used for our problem. Ghost cells created at the start and at the end of the domain.

$$
\begin{aligned}
\rho^n_0 &= \rho^n_1, & \rho^n_{M+1} &= \rho^n_M, \\
u^n_0 &= u^n_1, & u^n_{M+1} &= u^n_M, \\
p^n_0 &= p^n_1, & p^n_{M+1} &= p^n_M
\end{aligned}
\qquad (2.97)
$$

2.6 NUMERICAL RESULTS

2.6.1 NUMERICAL SOLUTIONS WITH EXACT RIEMANN SOLVER

Five Riemann case are used to test the exact Riemann solver. Test case 1 is modified version of Sod's test[9], its solution consist of a left rarefaction wave, a contact discontinuity and a right shock wave. Test case 2 is the 123 problem[10], its solution consist of two rarefaction waves and a contact discontinuity. Test case 3 is the left half of the blast wave problem[11], its solution consist of a left rarefaction wave, a contact discontinuity and a right shock wave. Test 4 consist of three strong discontinuities. Test 5 consists of a left rarefaction wave, a right shock wave and a stationary contact discontinuity.

Table 2.1: Data for the five test cases

Test	ρ_L	u_L	p_L	ρ_R	u_R	p_R
1	1.0	0.75	1.0	0.125	0.0	0.1
2	1.0	-2.0	0.4	1.0	2.0	0.4
3	1.0	0.0	1000.0	1.0	0.0	0.01
4	5.99924	19.5975	460.894	5.99242	-6.19633	46.0950
5	1.0	-19.597545	1000.0	1.0	-19.59745	0.01

Initial data for the five Riemann problem tests given at the table 2.1. For the solution of the problems, ratio of the specific heat is $\gamma = 1.4$, 100 cells have been use for each tests, domain length has taken as 1.

Solution for the star region is given at table 2.2.

Table 2.2: Exact solution for the Riemann problem tests

Test	p_*	u_*	ρ_{*L}	ρ_{*R}
1	0.466294	1.360906	0.579867	0.339700
2	0.001894	0.00000	0.021852	0.021852
3	460.893768	19.597450	0.575062	5.999241
4	1691.647217	8.689775	14.282351	31.042604
5	460.893768	-0.000095	0.575062	5.999241

For exact Riemann problem solver, Toro's HE-E1RPEXACT code[12] have been used. Plots of these test cases is given below. In this thesis, the exact Riemann solutions will used to compare the accuracy and the correctness of the numerical schemes and it will help to define the characteristics of the solutions.

2.6.1.1 Test Case 1

For this test output time is taken as 0.2 units and initial discontinuity position taken as $x_0 = 0.3$.
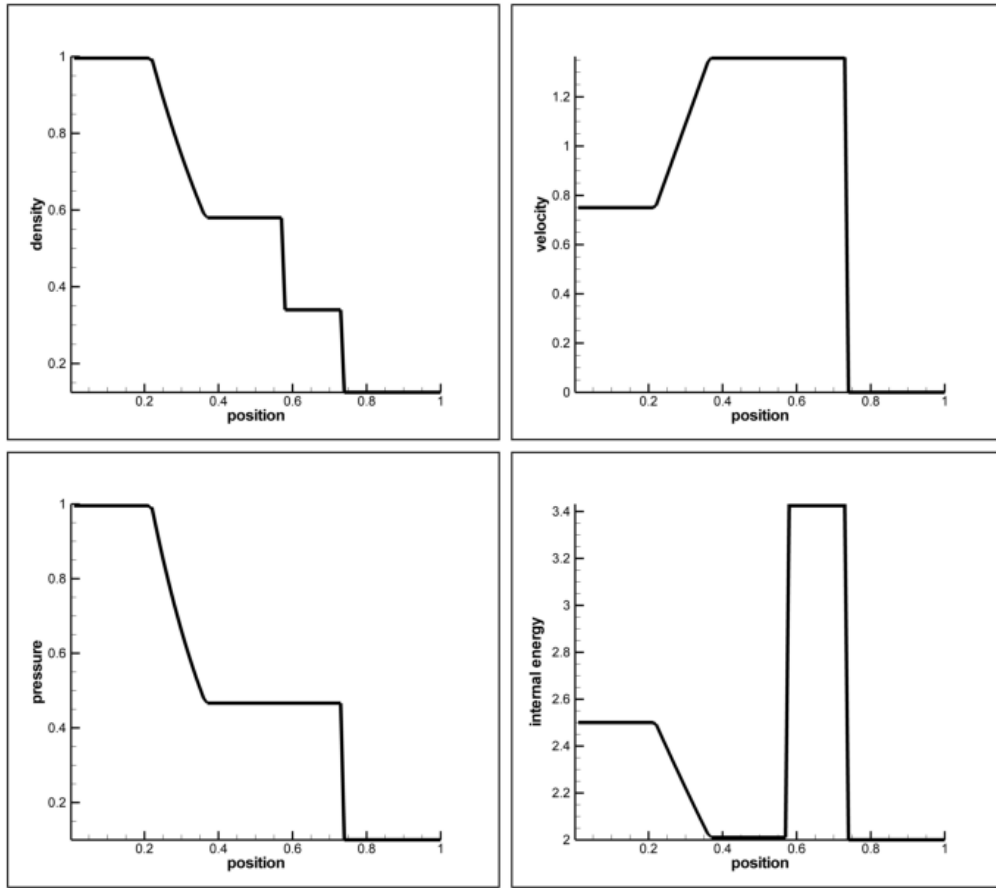
Figure 2.7: Exact solution of the Riemann problem for density, velocity, pressure and internal energy for test case 1

Characteristic of the problem is seen from the figure 2.7. The problem consists of a left rarefaction wave, a contact discontinuity and a right shock wave. Left rarefaction wave is seen at the position between $x = 0.2$ and $x = 0.4$. As rarefaction waves' characteristic property, velocity is increasing in that region. Position of contact discontinuity is at the first density jump location, where $x = 0.58$. Characteristic of the contact discontinuity is seen from the figure. u and p values constant across the contact discontinuity, meanwhile the density value is decreasing. Internal energy is also changing at the contact because the temperature changes as the density change. Because density is decreasing, temperature has to be increase, while pressure is constant. So change in the internal energy is expected. Shock wave is at the position, where all the variables show a jump. Shock wave is at position $x = 0.74$. As

a characteristic of the shock, velocity, pressure, density and the internal energy subjected to sudden decrease. The initial values of the left and the right states are seen at the end of the rarefaction and the shock wave, this is the reason that the velocities are zero in these regions.

2.6.1.2 Test Case 2

For this test output time is taken as 0.15 units and initial discontinuity position taken as $x_0 = 0.5$.
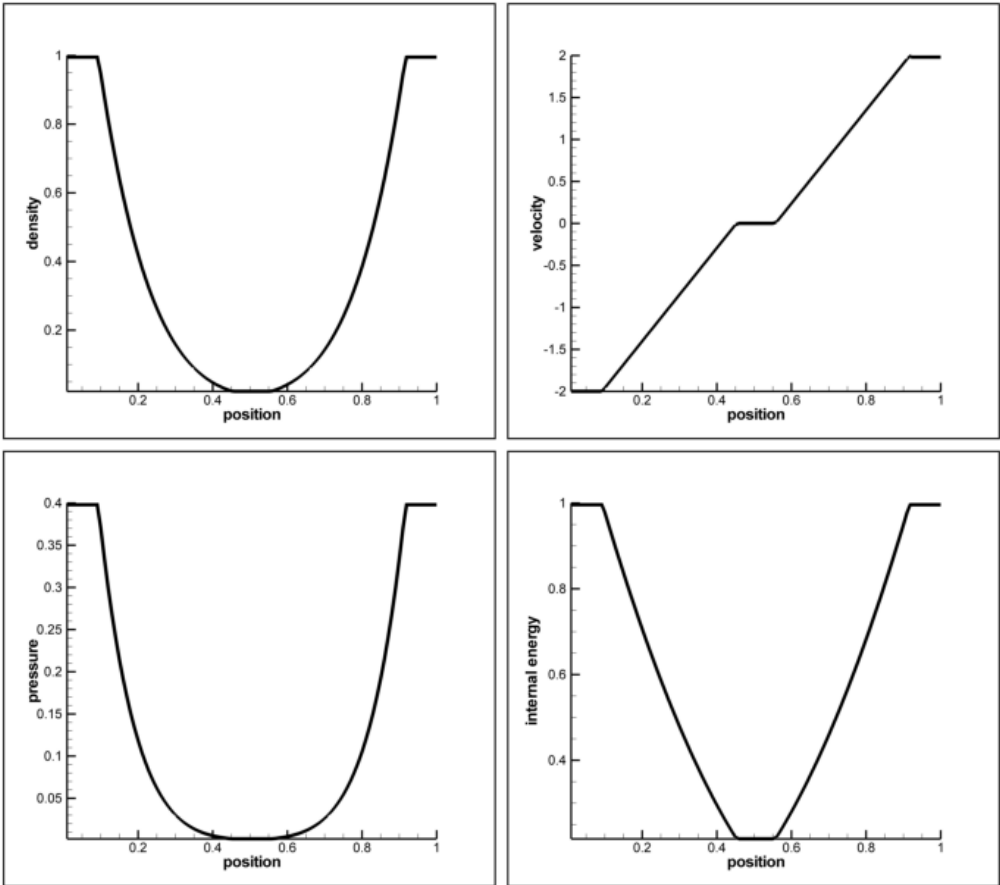
Figure 2.8: Exact solution of the Riemann problem for density, velocity, pressure and internal energy for test case 2

In this case, problem consists of two rarefaction waves and a contact discontinuity. Position of rarefaction waves are seen better in the velocity profile. Because of the amplitude of rarefaction waves are equal, contact discontinuity stayed at the $x = 0.5$, which is the same with the initial discontinuity position. This problem is important because problem has very small pressure value, $p_* = 0.00189$ at the $x = 0.5$. To solve numerically low pressure or low density is hard. Because some numerical schemes create oscillations, which give negative pressure or

density in low regions and that results give an error in the solution.

2.6.1.3 Test Case 3

For this test output time is taken as 0.012 units and initial discontinuity position taken as $x_0 = 0.5$.
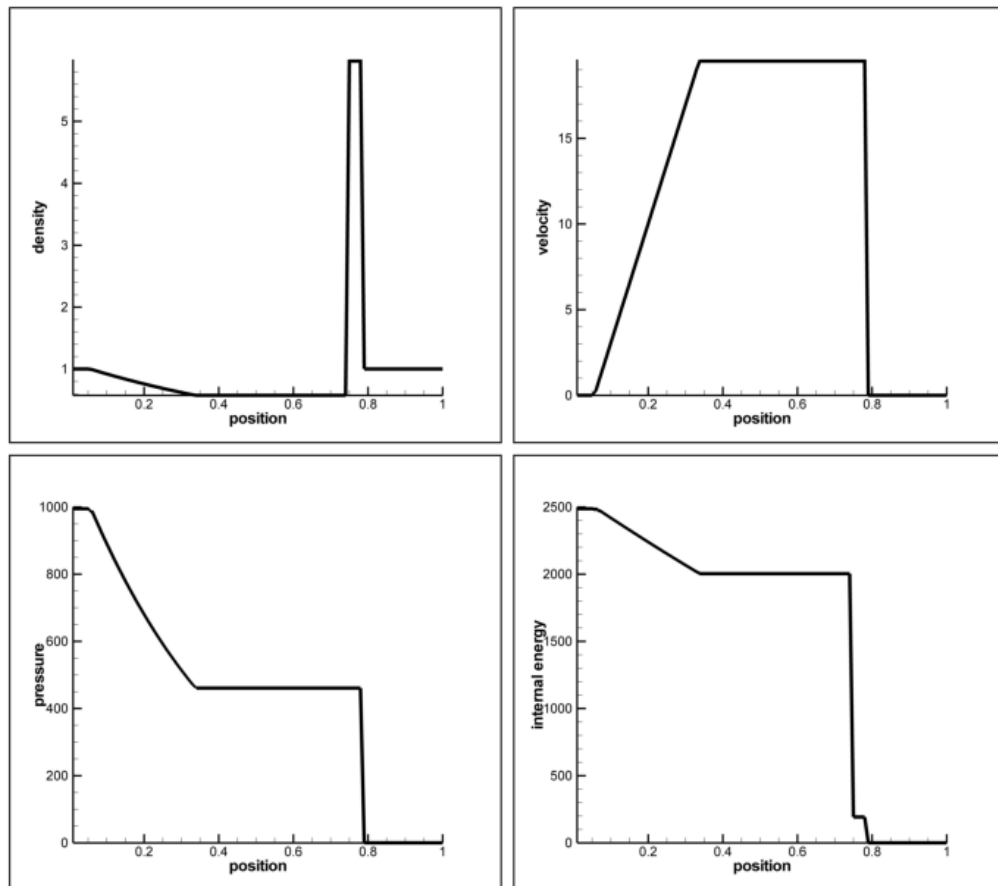
Figure 2.9: Exact solution of the Riemann problem for density, velocity, pressure and internal energy for test case 3

This case shows similarities with the first case but in this case effect of the pressure is seen. The characteristic of the problem is same with the first case, a left rarefaction, a contact discontinuity and a shock wave. But in this case the shock wave and the rarefaction wave are stronger than first case. When looked at initial data of the problem, ratio of p_L and p_R is 100000, which is a high ratio.

2.6.1.4 Test Case 4

For this test output time is taken as 0.035 units and initial discontinuity position taken as $x_0 = 0.4$.

Figure 2.10: Exact solution of the Riemann problem for density, velocity, pressure and internal energy for test case 4

In this case, two shocks and a contact discontinuity is seen. Again comparing the density profile with pressure profile reveals the contact and the shocks location. Looking at the initial data a right moving wave and a left moving wave is seen to be colliding, the collision creates a high change in the pressure. Because of sign of the velocities of the waves are different, negative velocity is seen after the right shock wave.

2.6.1.5 Test Case 5

For this test output time is taken as 0.012 units and initial discontinuity position taken as $x_0 = 0.8$.
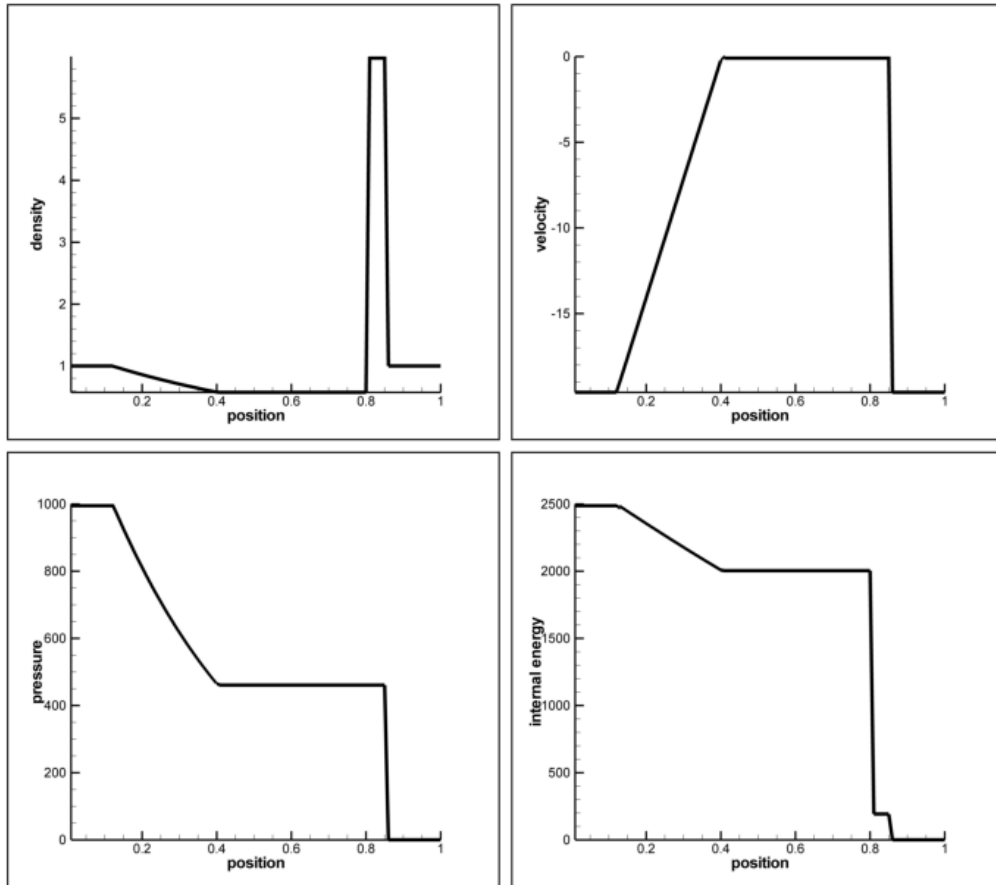
Figure 2.11: Exact solution of the Riemann problem for density, velocity, pressure and internal energy for test case 5

This case is the similar with the test case 3, only difference is the direction of the waves. When initial data examined, ratio of p_L and p_R is 100000. Because of the pressured state is at left state, fluid's velocity at the star region is near to the zero value. This means a stationary contact waves is created. Position of the discontinuities are found by looking at the density profile, first jump left to right corresponds to position of the contact wave because velocity and pressure are constant at that jump. The initial data of this problems show that waves are moving to the left direction because they have a negative velocity value.

2.6.2   NUMERICAL SOLUTIONS WITH NUMERICAL METHODS

Five cases have been solved with the Godunov's method. For comparison Lax-Friedrichs and two-step Lax-Wendroff (Richtmyer) methods have been used.

Test 1 is chosen because it shows the entropy satisfaction of a numerical method. Test 2 is chosen for the numerical methods performance at low density flows. Test 3, 4 and 5 chosen because they show accuracy of the numerical methods.

In each test case an appropriate initial discontinuity position and an output time is chosen to analyze the results.

The ratio of specific heats (γ) is = 1.4. Domain length is 1 and it is between [0,1]. Computing cells (M) are taken as 100. C_{cfl} is chosen as 0.9 but for the first 5 time steps C_{cfl} reduced by a factor of 0.2. Because at the first steps of the calculation, more reliable waves wanted to be formed.

2.6.2.1 Test Case 1

For this test output time is taken as 0.2 units and initial discontinuity position taken as $x_0 = 0.3$.

Figure 2.12: Comparison of the Godunov's method (black symbols), Lax-Friedrichs method (red symbols) and Richtmeyer method (blue symbols) with exact solution (line) for the test case 1.

At the figure 2.12, numerical solution of the test case 1 is seen. As expected a left rarefaction wave, a contact discontinuity then a right shock wave is seen at the solution. The Godunov's method solves the shock wave faster than Lax-Friedrichs method. The Godunov's method uses 3 cells but the Lax-Friedrichs method uses 8 cells. The Richtmyer method has a good accuracy in the overall but at the shock wave oscillations are increased as a characteristic of a second order accurate numerical method, so unexpected and unrealistic results occur. For this thesis solutions at the shock waves are important, therefore second order finite volume methods has no use for this thesis. The Godunov's method shows good accuracy and robustness for this test case and it brings the Godunov-type methods forward when solving discontinuities. The Godunov's method shows entropy glitch when solving rarefaction wave, an entropy fix required for more realistic results. Entropy fix and entropy glitch will be studied at section 2.7.2. There is also pairing in the neighbor cells when solving with Lax-Friedrichs method. It occurs because of the U_i^n replaces with $(U_{i-1}^n + U_{i+1}^n)/2$ when constructing the solution. In

summary, test case 1 show that, Godunov-type methods are more accurate than finite volume methods when solving shock waves.
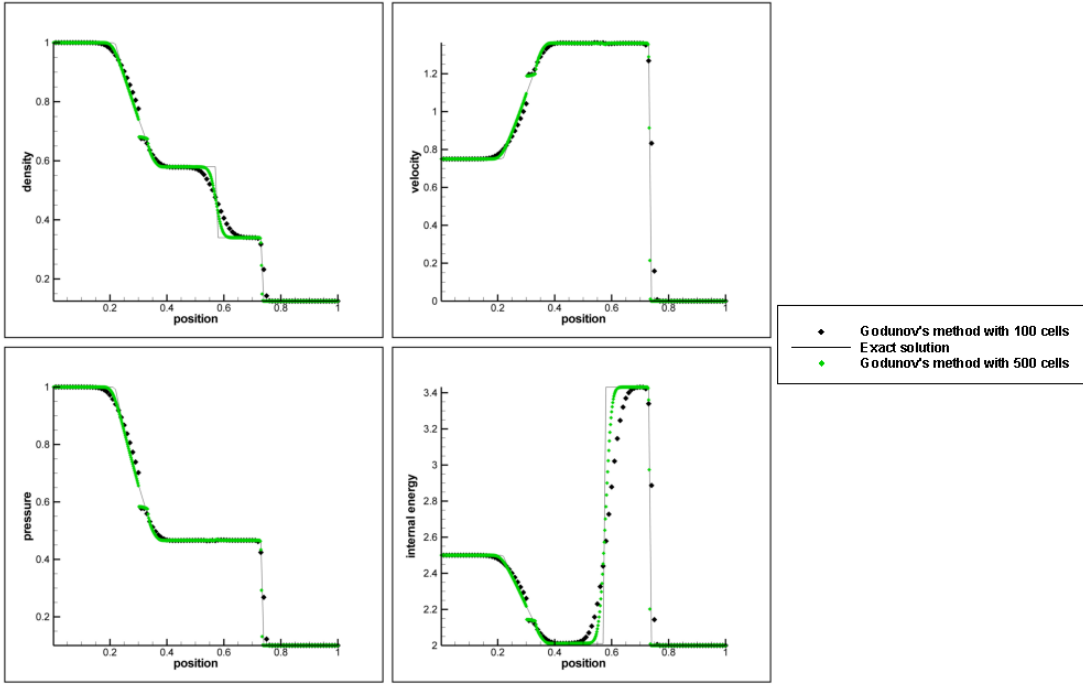
Figure 2.13: Effect of the computing cells for the Godunov's method M=100 cells (black symbols), M=500 cells (green symbols) with exact solution (line) for the test case 1.

The effect of the computing cells is seen at the figure 2.13. As expected increase in the cells increases the solution accuracy but it does not effect sharpness of the solution at the shock wave. The shock wave resolved in 3 cells in both methods. Accuracy increases in the contact discontinuity and this effect seen best in the internal energy. However, the entropy glitch has given a more unrealistic result at the increased cell case. Increasing the computing cells is increasing the computing time, so number of the computing cells has to be chosen according to needs. For this chapter 100 computing cells are enough to see the accuracy and robustness of the numerical methods.

2.6.2.2 Test Case 2

For this test output time is taken as 0.15 units and initial discontinuity position taken as $x_0 = 0.5$.
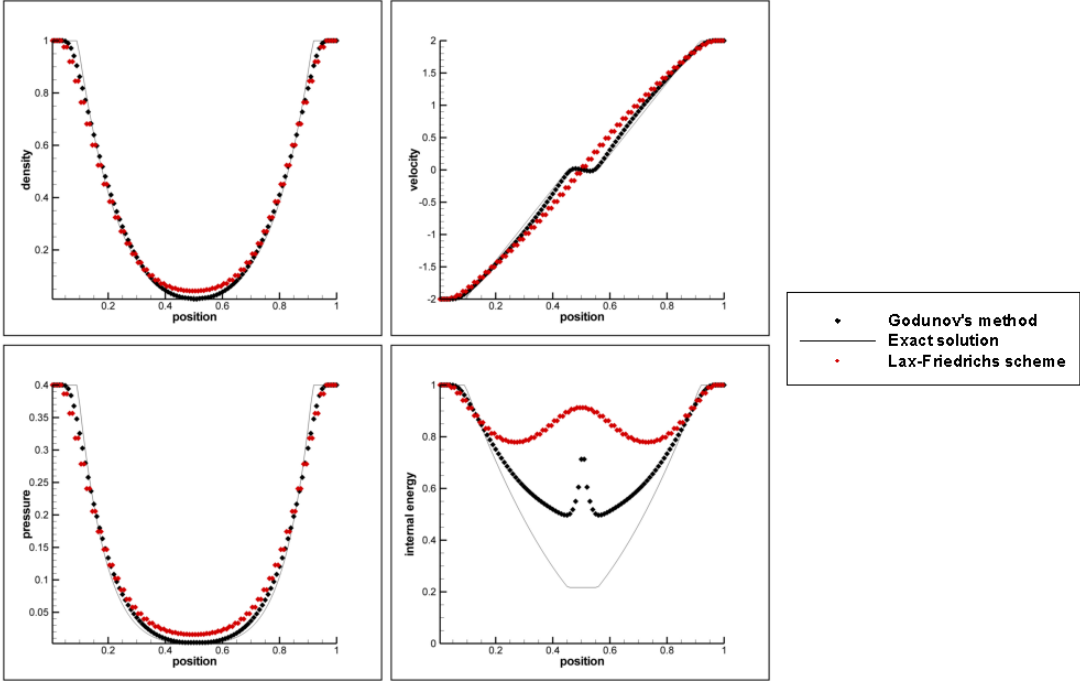
Figure 2.14: Comparison of the Godunov's method (black symbols), Lax-Friedrichs method (red symbols) with exact solution (line) for the test case 2.

This case is a low density problem, which isn't this thesis problem but in order to under-stand the numerical methods behavior, it has been studied. When looked at the figure 2.14 Godunov's method superiority over the Lax-Friedrichs method is seen. Godunov's method gives more accurate results at the two rarefactions and contact discontinuity. But Godunov's method is inaccurate at low density regions. When internal energy is analyzed, a sudden increase is seen at the $x = 0.5$ position. Density and pressure cannot be solved correctly, therefore internal energy calculated wrong. Godunov's method assumes piece-wise constant distribution at the cells, this is reason of the unrealistic results emerges, when calculating internal energy. Therefore at low regions Godunov's method calculates wrong pressure and density. Lax-Friedrichs method have pairing of the neighbor cells at this case too.

2.6.2.3 Test Case 3

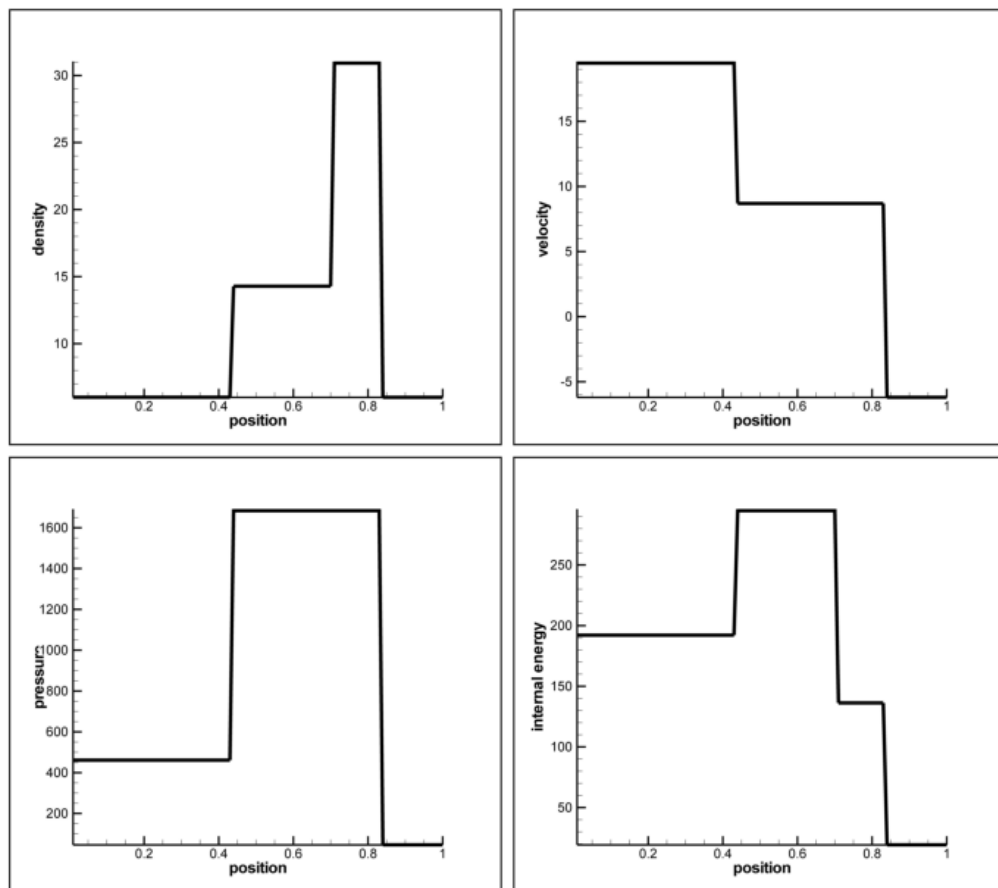For this test output time is taken as 0.012 units and initial discontinuity position taken as $x_0 = 0.5$.
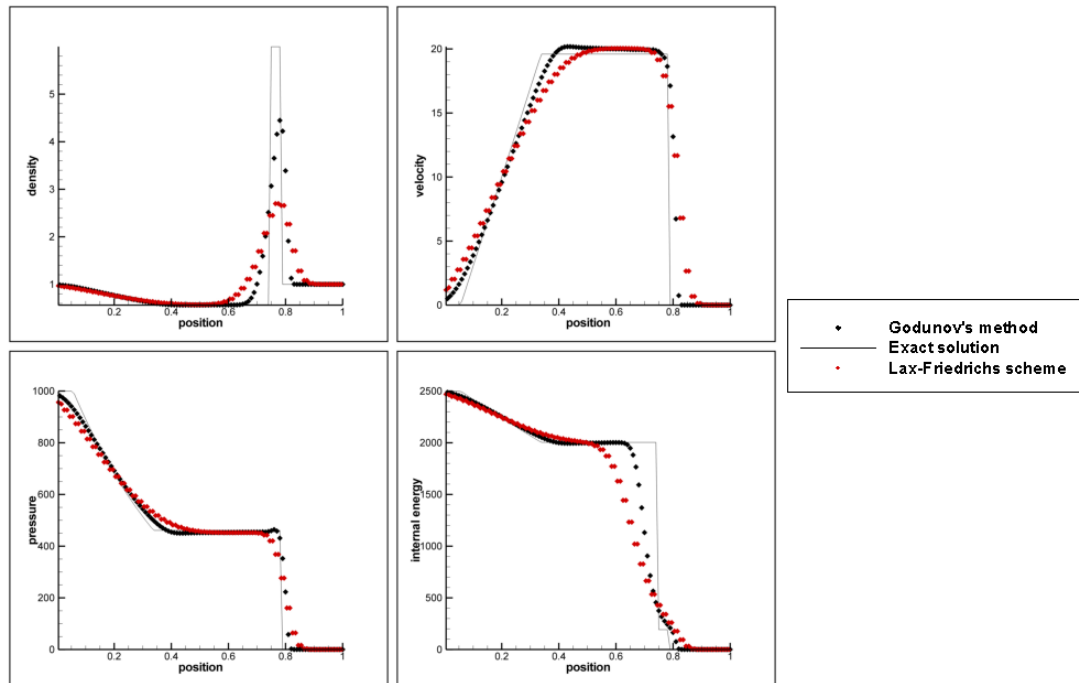
Figure 2.15: Comparison of the Godunov's method (black symbols), Lax-Friedrichs method (red symbols) with exact solution (line) for the test case 3.

As it can be seen from figure 2.15, test case consists of a strong shock. Due to the strong shock, two numerical methods cannot solve the strong shock region accurately. Again Godunov's method solves shock region faster than the Lax-Friedrichs method but that isn't accurate enough to have a good solution. When density variable inspected, Godunov's method gives better result than Lax-Friedrichs method but due to sudden increase and decrease in the density, Godunov's method is can not resolve this region correctly. Because of the inaccurate calculation at the density, internal energy is computed inaccurate. But still Godunov's method is giving more realistic results than the Lax-Friedrichs method. When looked at the left boundary values of the two numerical methods, numerical diffusion of the Lax-Friedrichs method is affecting the solution. The diffusivity of this method is more than diffusivity of the Godunov's method. If the solution output time have been increased, the Lax-Friedrichs methods left boundary values become unrealistic.

2.6.2.4 Test Case 4

For this test output time is taken as 0.035 units and initial discontinuity position taken as $x_0 = 0.4$.
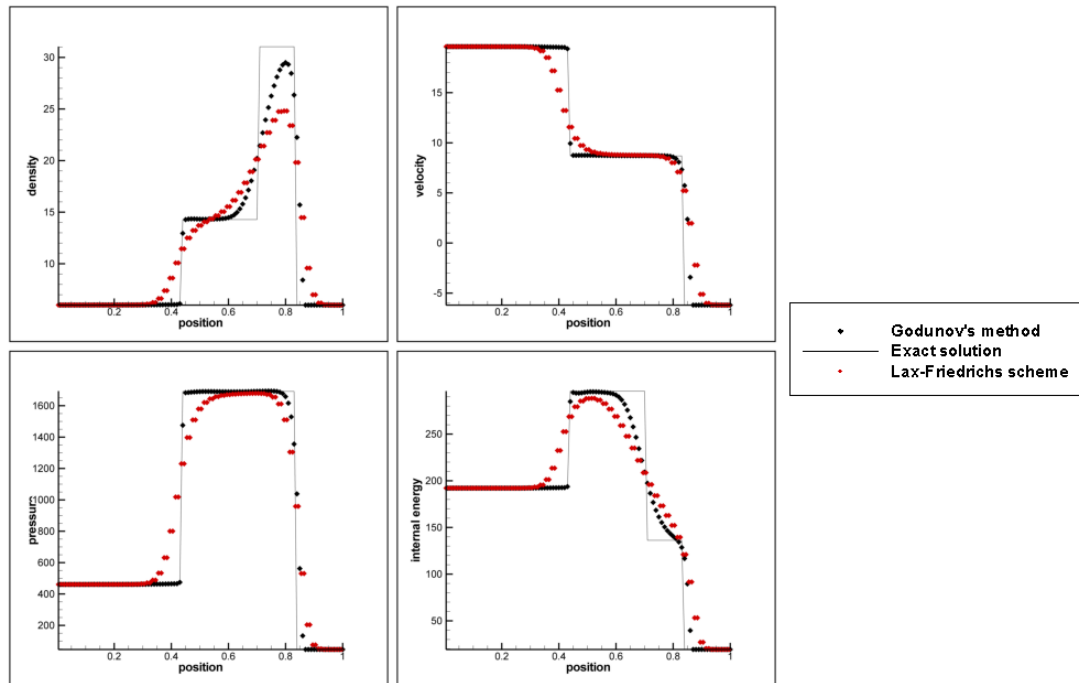
Figure 2.16: Comparison of the Godunov's method (black symbols), Lax-Friedrichs method (red symbols) with exact solution (line) for the test case 4.

For this test case, there are two shock waves and it can be seen from figure 2.16. Right shock wave is stronger than the left shock wave so, solving the left shock wave was easier. Godunov's method has solved it in 1 cell but faster shock wave is solved over 5 cells. Because of these reasons, contact discontinuity solution can not solved accurately, effect of the inaccurate solutions is seen from the internal energy profile.

2.6.2.5 Test Case 5

For this test output time is taken as 0.012 units and initial discontinuity position taken as $x_0 = 0.8$.

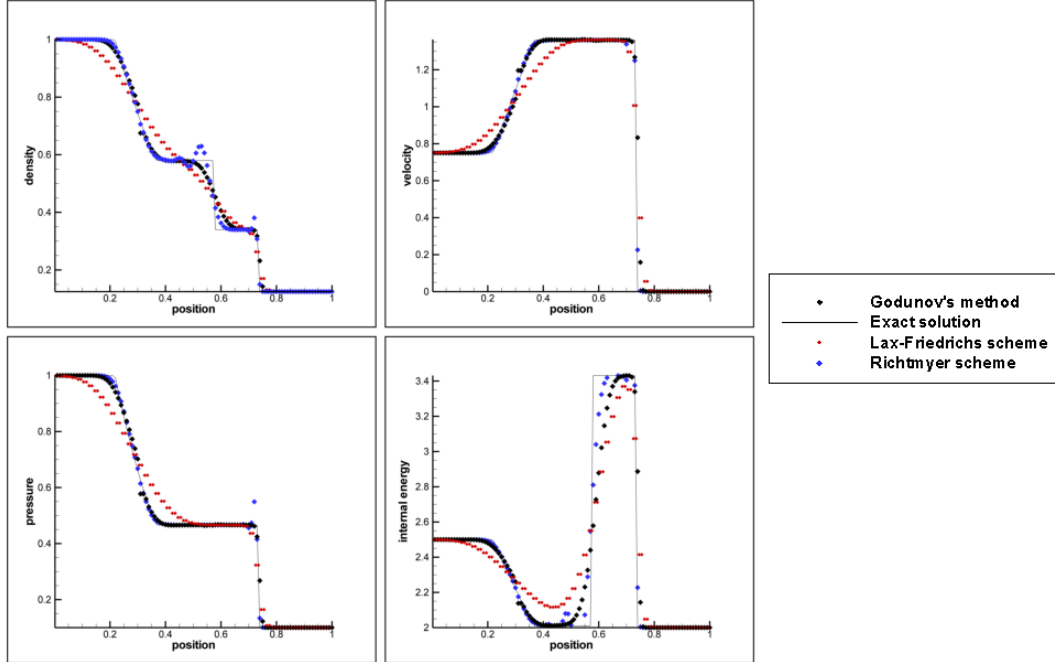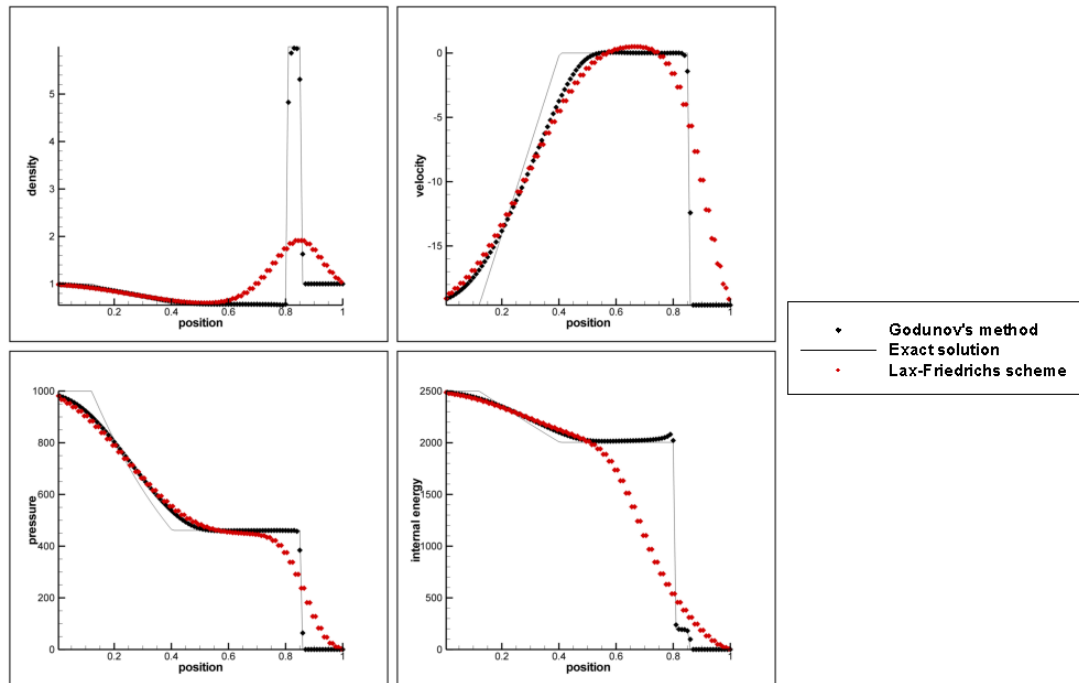Figure 2.17: Comparison of the Godunov's method (black symbols), Lax-Friedrichs method (red symbols) with exact solution (line) for the test case 5.

This case is a similar case with the test case 3. The differences between two cases are the initial velocities. In this case a stationary contact discontinuity is seen. Stationary contact discontinuity have been solved accurately with the Godunov method. In test case 3 moving contact discontinuity isn't solved sharp as the stationary one. Since the contact wave is solved accurately, shock wave after the contact discontinuity is solved accurately but in the test case 3, because of the inaccurate solution of the contact discontinuity shock wave isn't solved accurately.

2.7 ROE'S METHOD

From previous section, it is seen that Godunov's method have better numerical accuracy than finite volume methods. But Godunov's method solves Riemann problem locally in every step, which increases the solution time. However, the approximate Riemann solvers, solves the Riemann problem approximately, which decreases the solution time[22]. Roe's method is one of the approximate Riemann solvers that has been used nowadays[23].

Roe's method solves the Riemann problem approximately. Roe uses the averaged Jacobian matrix for solving Riemann Problem approximately. The Jacobian matrix is;

$$A(U) = \frac{\partial F}{\partial U} \tag{2.98}$$

Then the conservation laws are written as;

$$U_t + A(U)U_x = 0 \tag{2.99}$$

Roe replaces matrix $A(U)$ with a constant Jacobian matrix $\bar{A}(U_L, U_R)$. Now, conservation laws are written as;

$$U_t + \bar{A}U_x = 0 \tag{2.100}$$

For replacing the Jacobian matrix with the Roe Jacobian matrix, it has to satisfy these properties;

- $\bar{A}$ has to have real and distinct eigenvalues, which is the system has to be hyperbolic.

- It has to be consistent with the exact Jacobian matrix.

- It has to conserve across discontinuities.

$\bar{A}(U_L, U_R)$ has eigenvalues $\bar{\lambda}_i(U_L, U_R)$ and right eigenvectors $\bar{K}^{(i)}(U_L, U_R)$. Data difference can be written as;

$$\Delta U = U_R - U_L = \sum_{i=1}^{3} \bar{\alpha}_i \bar{K}^{(i)} \tag{2.101}$$

where $\bar{\alpha}_i$ is the wave strengths. The solution of $U_{i+\frac{1}{2}}(0)$ can be written as;

$$U_{i+\frac{1}{2}}(0) = U_L + \sum_{i=1}^{3} \bar{\alpha}_i \bar{K}^{(i)} \text{ for negative eigenvalues} \tag{2.102}$$

42

$$U_{i+\frac{1}{2}}(0) = U_R - \sum_{i=1}^{3} \bar{\alpha}_i \bar{K}^{(i)} \text{ for positive eigenvalues} \tag{2.103}$$

The numerical flux is obtained from integral relations.

$$F_{OL} = F_L - S_L U_L - \frac{1}{t} \int_{TS_L}^{0} U(x,t)dx \tag{2.104}$$

$$F_{OR} = F_R - S_R U_R + \frac{1}{t} \int_{0}^{TS_R} U(x,t)dx \tag{2.105}$$

where S_L and S_R are the smallest and largest signal speeds in the exact solution of the problem. F_{OL} and F_{OR} are the flux along the t-axis. From consistency condition $F_{OL} = F_{OR}$.

Integrals in the equations 2.104 and 2.105 for $\bar{U}_{i+\frac{1}{2}}(x,t)$ are;

$$\int_{TS_L}^{0} \bar{U}_{i+\frac{1}{2}}(x,t)dx = t\left[\bar{F}(U_L) - \bar{F}(U_{i+\frac{1}{2}}(0))\right] - tS_L U_L \tag{2.106}$$

$$\int_{0}^{TS_R} \bar{U}_{i+\frac{1}{2}}(x,t)dx = t\left[\bar{F}(U_{i+\frac{1}{2}}(0)) - \bar{F}(U_R)\right] + tS_R U_R \tag{2.107}$$

Substituting the integrals in to the equations 2.104 and 2.105, fluxes are obtained as;

$$F_{OL} = \bar{F}((\bar{U}_{i+\frac{1}{2}}(0)) + F_L - \bar{F}_L \tag{2.108}$$

$$F_{OR} = \bar{F}((\bar{U}_{i+\frac{1}{2}}(0)) + F_R - \bar{F}_R \tag{2.109}$$

The definition of the numerical flux is $\bar{F} = \bar{A}\bar{U}$ and using the equations 2.102 and 2.103 inter-cell flux is calculated as;

$$F_{i+\frac{1}{2}} = \frac{1}{2}(F_L + F_R) - \frac{1}{2}\sum_{i=1}^{3} \bar{\alpha}_i |\bar{\lambda}_i| \bar{K}^{(i)} \tag{2.110}$$

To calculate the Roe's flux, unknown average variables $\bar{\alpha}_i$, $\bar{\lambda}_i$ and $\bar{K}^{(i)}$ has to be calculated. Roe average variables are calculated as;

$$\bar{u} = \frac{\sqrt{\rho_L}u_L + \sqrt{\rho_R}u_R}{\rho_L + \rho_R} \tag{2.111}$$

$$\bar{H} = \frac{\sqrt{\rho_L}H_L + \sqrt{\rho_R}H_R}{\rho_L + \rho_R} \tag{2.112}$$

$$\bar{a} = \sqrt{(\gamma - 1)(\bar{H} - 0.5\bar{u}^2)} \tag{2.113}$$

If eigenvalues and eigenvectors are written in the Roe's average form. The corresponding eigenvalues are written as;

$$\bar{\lambda}_1 = \bar{u} - \bar{a} \tag{2.114}$$

$$\bar{\lambda}_2 = \bar{u} \tag{2.115}$$

$$\bar{\lambda}_3 = \bar{u} + \bar{a} \tag{2.116}$$

The corresponding eigenvectors are written as;

$$\bar{K}^{(1)} = [1, \bar{u} - \bar{a}, \bar{H} - \bar{u}\bar{a}]^T \tag{2.117}$$

$$\bar{K}^{(2)} = [1, \bar{u}, 0.5\bar{u}^2]^T \tag{2.118}$$

$$\bar{K}^{(3)} = [1, \bar{u} + \bar{a}, \bar{H} + \bar{u}\bar{a}]^T \tag{2.119}$$

The waves strengths are calculated from equation 2.101. If equation 2.101 is expanded;

$$\bar{\alpha}_1 + \bar{\alpha}_2 + \bar{\alpha}_3 = \Delta u_1 \tag{2.120}$$

$$\bar{\alpha}_1(\bar{u} - \bar{a}) + \bar{\alpha}_2\bar{u} + \bar{\alpha}_3(\bar{u} + \bar{a}) = \Delta u_2 \tag{2.121}$$

$$\bar{\alpha}_1(\bar{H} - \bar{u}\bar{a}) + \bar{\alpha}_2(0.5\bar{u}^2) + \bar{\alpha}_3(\bar{H} + \bar{u}\bar{a}) = \Delta u_3 \tag{2.122}$$

If the above equation solved for $\bar{\alpha}_i$, the wave strengths given as;

$$\bar{\alpha}_2 = \frac{(\gamma - 1)}{\bar{a}^2} \left[\Delta u_1(\bar{H} - \bar{u}^2) + \bar{u}\Delta u_2 - \Delta u_3 \right] \tag{2.123}$$

$$\bar{\alpha}_1 = \frac{1}{2\bar{a}} \left[\Delta u_1(\bar{u} + \bar{a}) - \Delta u_2 - \bar{a}\bar{\alpha}_2 \right] \tag{2.124}$$

$$\bar{\alpha}_3 = \Delta u_1 - (\bar{\alpha}_1 + \bar{\alpha}_2) \tag{2.125}$$

Now, all the unknowns are calculated, using equation 2.110 inter-cell flux can be calculated. Numerical solution is obtained by the explicit conservative formula.

$$U_i^{n+1} = U_i^n + [F_{i-\frac{1}{2}} - F_{i+\frac{1}{2}}] \tag{2.126}$$

2.7.1   NUMERICAL SOLUTIONS WITH ROE'S METHOD

For testing the Roe's method efficiency, first it is tested with the test case 1 in the section 2.6.2.

Figure 2.18: Comparison of the Roe's method (red symbols) and Godunov's method (black symbols) with exact solution (line) for the test case 1.

At the figure 2.18, Roe's method gives a similar solution with the Godunov's method. Roe's method solves shock in three computing cells as Godunov's method. But Roe's method affects from the entropy glitch more than the Godunov's method. Since Roe's method is approximation of the Riemann problem, it shows same characteristics with the Godunov's method, however some modifications can be done on the Roe's method to fix the entropy glitch. This is the one of the advantages of the approximate Riemann solvers.

2.7.2   ENTROPY FIX

When a sonic rarefaction occurs in a solution, eigenvalue changes sign across the rarefaction wave. When eigenvalue changing its sign there exist a point where $u = a$, which is called a sonic point. This sonic point shows the characteristic of a contact discontinuity. Therefore it is an unphysical discontinuity and it violates the entropy condition. This entropy violation is

called entropy glitch. Entropy glitch is seen at the previous sections, when using Godunov's method. For that reason, Roe's method can be modified for avoiding entropy violating condition.

Harten and Hyman[24] suggest an entropy fix for Roe's method. For left transonic rarefaction;

$$\lambda_1^L = u_L - a_L \qquad \lambda_1^R = u_* - a_{*L} \tag{2.127}$$

If $\lambda_1^L < 0 < \lambda_1^R$ then entropy fix is required. From integral form of the conservation laws,

$$\lambda_1^R(U_{SL} - U_{*L}) + \lambda_1^L(U_L - U_{SL}) = \bar{\lambda}_1(U_L - U_{*L}) \tag{2.128}$$

The above equation can be manipulated as;

$$U_{SL} - U_L = \frac{\lambda_1^R - \bar{\lambda}_1}{\lambda_1^R - \lambda_1^L}(U_{*L} - U_L) \tag{2.129}$$

where the speed $\bar{\lambda}_1$ divided into two smaller jumps. Roe approximation says that

$$(U_{*L} - U_L) = \bar{\alpha}_1 \bar{K}^{(1)} \tag{2.130}$$

The flux jump across the wave is computed using equation 2.129;

$$\Delta F_1^L = \lambda_1^L \frac{\lambda_1^R - \bar{\lambda}_1}{\lambda_1^R - \lambda_1^L} \bar{\alpha}_1 \bar{K}^{(1)} \tag{2.131}$$

so the new wave speed is defined as;

$$\bar{\lambda}_1 = \lambda_1^L \frac{\lambda_1^R - \bar{\lambda}_1}{\lambda_1^R - \lambda_1^L} \tag{2.132}$$

Then inter-cell flux becomes;

$$F_{i+\frac{1}{2}} = F_L + \bar{\alpha}_1 \bar{\lambda}_1 \bar{K}^{(1)} \tag{2.133}$$

Using the same methodology for the right transonic rarefaction wave, inter-cell flux becomes;

$$F_{i+\frac{1}{2}} = F_R - \bar{\alpha}_3 \bar{\lambda}_3 \bar{K}^{(3)} \tag{2.134}$$

The above formulation defines a new wave speed. Using this new wave speed, when calculating the inter-cell flux, removes the entropy glitch because this new wave speed replaces the sonic rarefaction wave speed, so there will no entropy violating condition, therefore entropy glitch has been removed.

At the figure 2.19, entropy distribution of the test case 1 for the Roe's method and Roe's method with entropy fix is given. At the glitch position the entropy is calculated negative

for Roe's method, which is a violation of entropy condition, but Roe's method with entropy fix has a continuous entropy distribution and a positive entropy value at the glitch position. Therefore, from the comparison of the entropy distribution, it has seen that entropy violation is corrected.
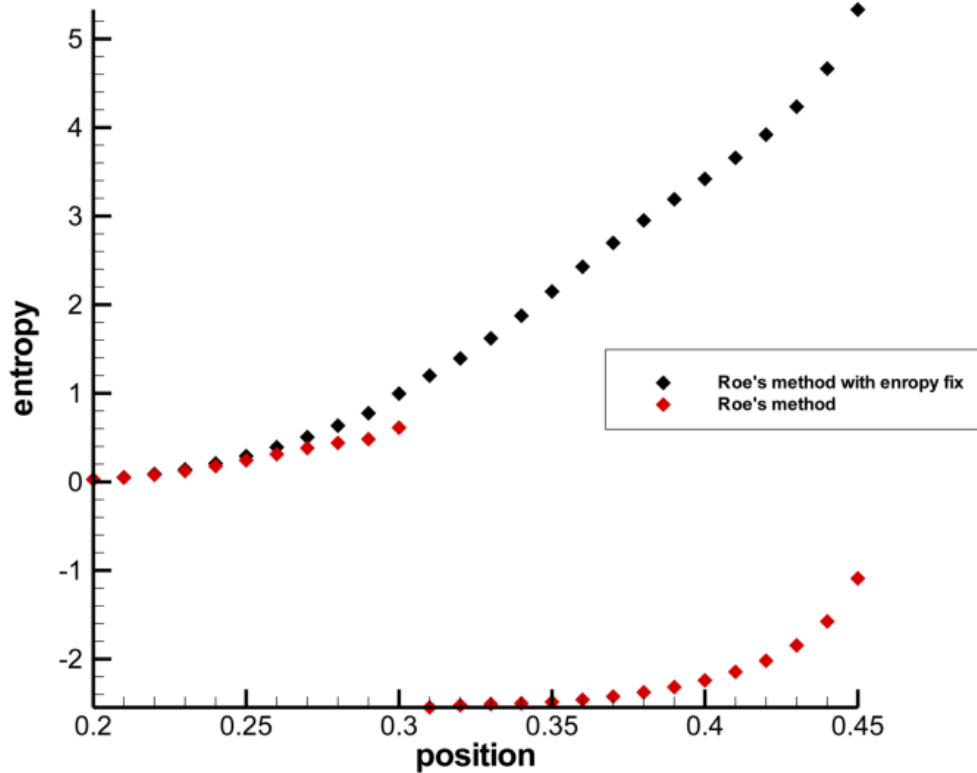
Figure 2.19: Comparison of the Roe's method (black symbols) with Roe's method with entropy fix (red symbols) for the test case 1.

2.7.3 NUMERICAL SOLUTIONS WITH ROE'S METHOD USING ENTROPY FIX

The test case dates are given at table 2.1. For comparison of the numerical schemes, same boundary conditions and same step size evaluation used for Roe's method, Godunov's method and Lax-Friedrichs schemes.

2.7.3.1   Test Case 1

For this test output time is taken as 0.2 units and initial discontinuity position taken as $x_0 = 0.3$.
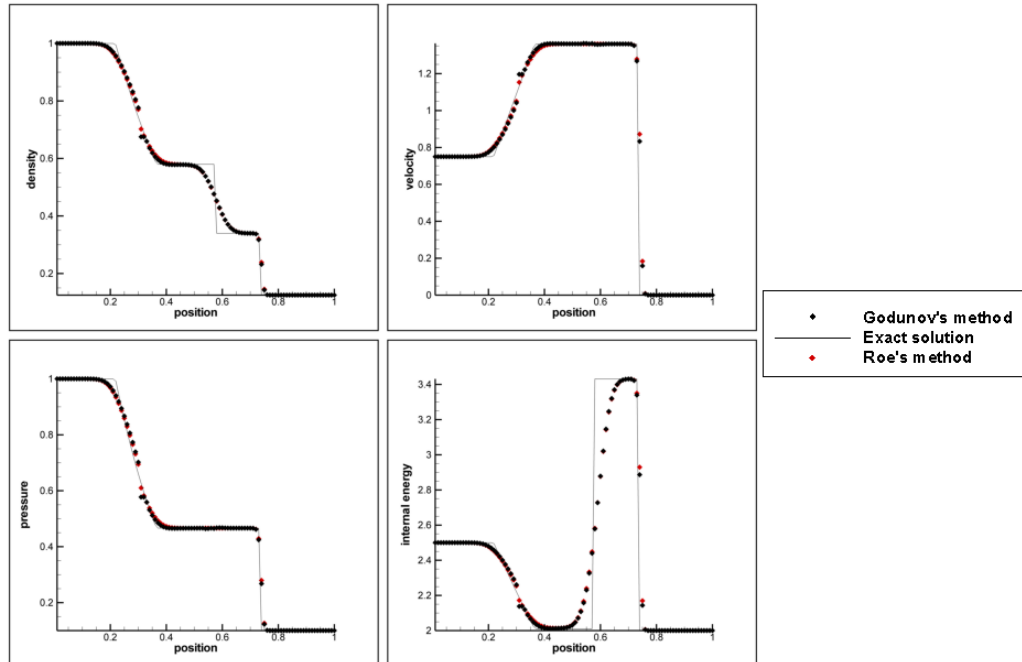
Figure 2.20: Comparison of the Roe's method with entropy fix (red symbols) and Godunov's method (black symbols) with exact solution (line) for the test case 1.

Test case 2 cannot be solved for Roe's method because it is a low density problem. For solving low density problems, Roe's method has to be modified. Because of the oscillations, negative density computed.

2.7.3.2   Test Case 3

For this test output time is taken as 0.012 units and initial discontinuity position taken as $x_0 = 0.5$.
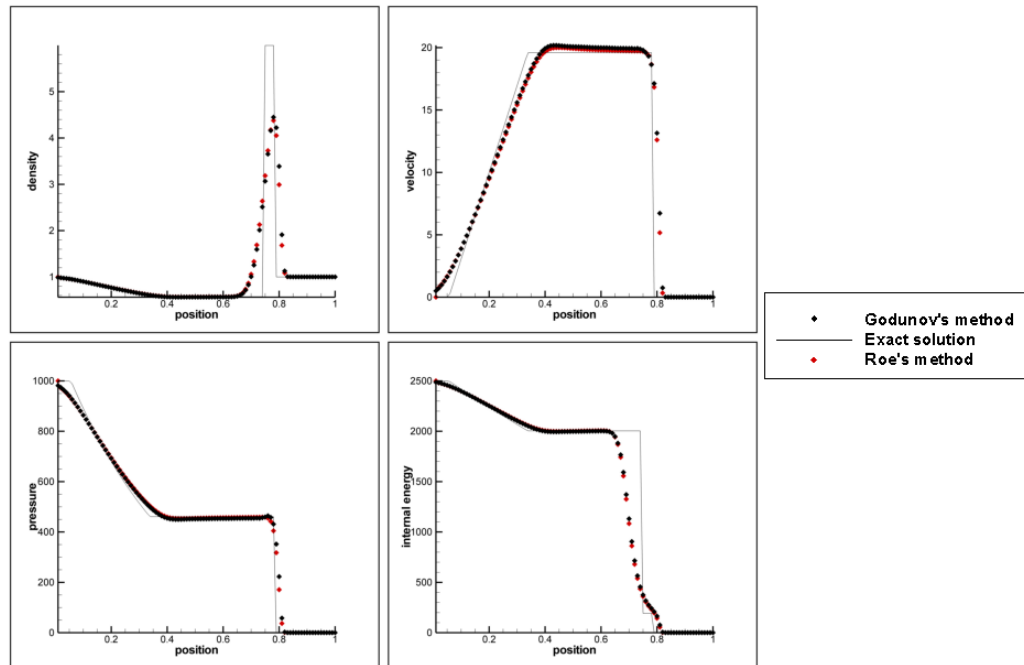
Figure 2.21: Comparison of the Roe's method with entropy fix (red symbols) and Godunov's method (black symbols) with exact solution (line) for the test case 3.

2.7.3.3   Test Case 4

For this test output time is taken as 0.035 units and initial discontinuity position taken as $x_0 = 0.4$.
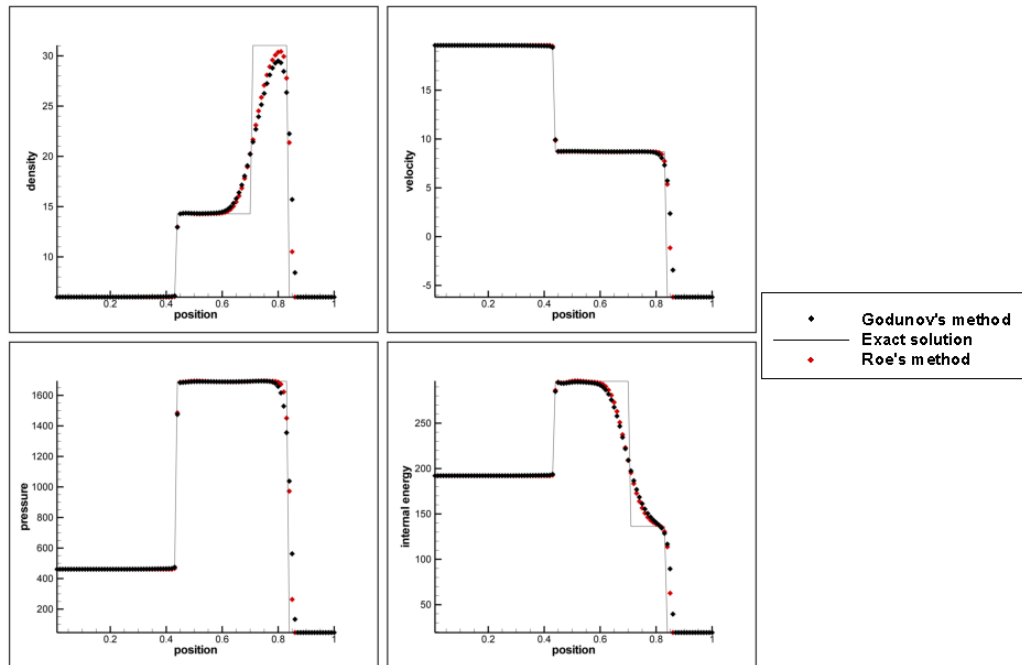
Figure 2.22: Comparison of the Roe's method with entropy fix (red symbols) and Godunov's method (black symbols) with exact solution (line) for the test case 4.

2.7.3.4   Test Case 5

For this test output time is taken as 0.012 units and initial discontinuity position taken as $x_0 = 0.8$.
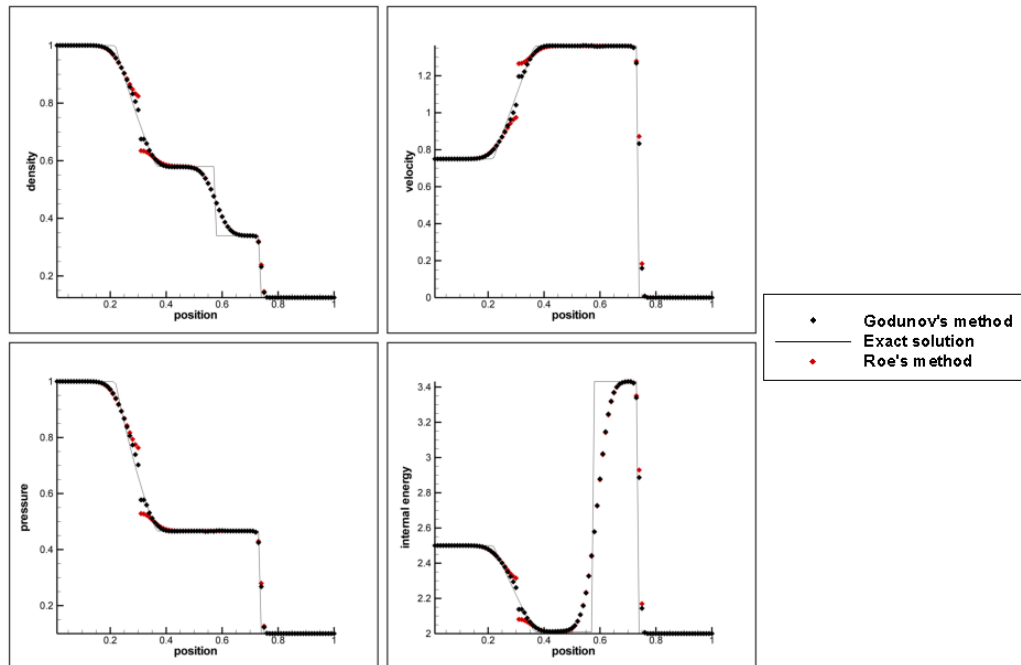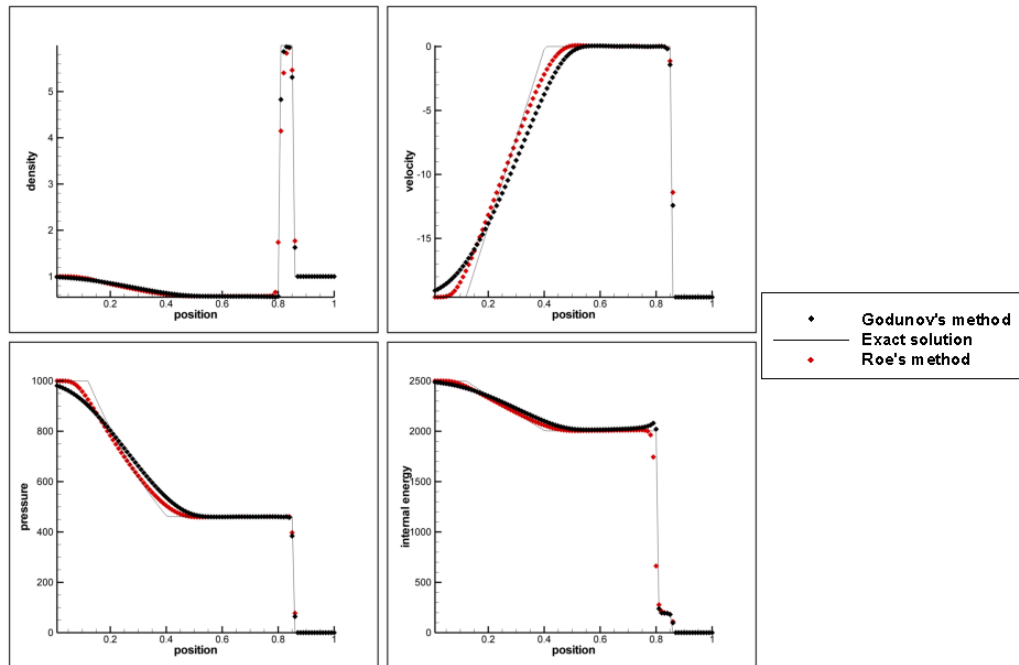

Figure 2.23: Comparison of the Roe's method with entropy fix (red symbols) and Godunov's method (black symbols) with exact solution (line) for the test case 5.

2.7.3.5   Comments on the Numerical Solutions

Roe's method solves the Riemann problem approximately and it is seen from the numerical tests, Roe's method is successful in solving the Riemann problem. However, entropy glitch occurs at the transonic rarefactions and this can be seen at the figure 2.18. An entropy fix is enough to solve that entropy glitch. At the figure 2.20, there is no entropy glitch due to the entropy fix modification done on the Roe's method. In general Roe's method shows same characteristics with the Godunov's method and same comments, that have been done for the Godunov's method at the previous section, can be done for Roe's method. Godunov's method and Roe's method show same accuracy when solving shock waves but Roe's method slightly better when solving smooth regions. At the figure 2.23, Roe's accuracy in the smooth regions is seen clearly. So Godunov's method is diffusive than Roe's method. That makes Roe's method more accurate than the Godunov's method.

CHAPTER 3

HIGH RESOLUTION METHODS

First order methods, Godunov's method, Roe's method, Lax-Friedrichs methods, give poor results in smooth regions and at the discontinuities. Second order methods give, Richtmyer method, good results in smooth regions, but at the discontinuities oscillations may occur and non realistic solutions can be achieved.

To have a better solution, high resolution methods are going to study in this chapter. High resolution methods are the methods that are at least second order accurate on smooth regions and still giving non oscillatory solutions at the discontinuities. As a characteristics of the monotone methods, they do not create unphysical oscillations but they are at most first order[17].

In high resolution methods, the piecewise constant representation of the solution U^n is replaced by a continuous representation of the solution U^n. Using a different representation changes the accuracy of the numerical method. In this thesis, the piecewise linear representation of the solution U^n is used, which makes the numerical method a second order accurate method. Then a slope limiter function is used to increase the accuracy of the second order method at the discontinuous regions.

In this chapter high resolution method is used for solving non-reactive Euler equations. For the high resolution method, second order Roe's method have been used. The importance of monotone and total variation diminishing (TVD) methods with flux limiter and slope limiter has been studied in this chapter.

3.1 MONOTONE AND TVD METHODS FOR CONSERVATION LAWS

The numerical method is a total variation diminishing method if

$$TV(U_{\Delta t}(\cdot, t^{n+1})) \leq TV(U_{\Delta t}(\cdot, t^n)) \tag{3.1}$$

for all grid function, where;

$$TV(U_{\Delta t}(\cdot, t^n)) = \sum_{i=-\infty}^{+\infty} |U_{i+1}^n - U_i^n| \tag{3.2}$$

The numerical method is monotone if

$$V_{\Delta t}(x, t^n) \geq U_{\Delta t}(x, t^n) \tag{3.3}$$

$$V_{\Delta t}(x, t^{n+1}) \geq U_{\Delta t}(x, t^{n+1}) \tag{3.4}$$

for every x in the grid, where $U_{\Delta t}(\cdot, t)$ and $V_{\Delta t}(\cdot, t)$ are the solutions of the conservative formulation.

TVD methods are always monotonicity preserving.

If U^0 the initial data is monotone, then $U_{\Delta t}(\cdot, t)$ is also monotone for all $t > 0$, this property is called monotonicity preserving.

If the numerical method is monotone then the method is always TVD and if a numerical method is TVD, then it is always monotonicity preserving[25].

3.2 FLUX LIMITER METHODS

In flux limiter method, two flux functions is combined to construct a single flux. These two flux functions are chosen from a high order flux, which is accurate in smooth regions, and a low order flux, which is accurate near discontinuities[26].

For studying the flux limiter methods, linear advection equation is solved.

$$\frac{d}{dt}u(x, t) + a\frac{d}{dx}u(x, t) = 0. \tag{3.5}$$

where the $f(u) = au$. $F_{i+\frac{1}{2}}^{(LW)}$ is the Lax-Wendroff numerical flux which is a high order flux and $F_{i+\frac{1}{2}}^{(BU)}$ is the basic upwind numerical flux, which is a low order flux, so these two fluxes are

chosen for studying of flux limiter method. For $a > 0$, when numerical fluxes applied to the equation 3.5;

$$F^{(LW)}_{i+\frac{1}{2}} = F^{(BU)}_{i+\frac{1}{2}} + \frac{1}{2}(1 - a\frac{\Delta t}{\Delta x})(f(u^n_{i+1}) - F^{(BU)}_{i+\frac{1}{2}}) \tag{3.6}$$

Lax-Wendroff function is constructed from a first order basic upwind flux and an anti-diffusive flux. Lax-Wendroff flux is not TVD because it is a second order accurate method, so it is not a monotone function. Monotone functions are at most first order accurate[27].

Function φ, which is a limiter, is added to the flux. Then flux is written as;

$$F^n_{i+\frac{1}{2}} = F^{(BU)}_{i+\frac{1}{2}} + \varphi(\theta^+_{i+\frac{1}{2}})\frac{1}{2}(1 - a\frac{\Delta t}{\Delta x})(f(u^n_{i+1}) - F^{(BU)}_{i+\frac{1}{2}}) \tag{3.7}$$

The limiter φ is written as a function of the ratio of slopes in the upwind direction to detect where the effect of anti diffusive flux is large.. Limiter function φ is chosen as the limited anti-diffusive flux and it is maximized. The scheme still remains as a TVD.

$\theta^+_{i+\frac{1}{2}}$ is written as;

$$\theta^+_{i+\frac{1}{2}} = \frac{u^n_i - u^n_{i-1}}{u^n_{i+1} - u^n_i} \tag{3.8}$$

If the methods unify for $a < 0$ and $a > 0$ numerical flux becomes;

$$F^n_{i+\frac{1}{2}} = F^{(BU)}_{i+\frac{1}{2}} + \varphi(\theta^+_{i+\frac{1}{2}})\frac{1}{2}(1 - a\frac{\Delta t}{\Delta x})(f(u^n_{i+1}) - F^{(BU)}_{i+\frac{1}{2}}) - \varphi(\theta^-_{i+\frac{1}{2}})\frac{1}{2}(1 + a\frac{\Delta t}{\Delta x})(F^{(BU)}_{i+\frac{1}{2}} - f(u^n_i)) \tag{3.9}$$

$$\text{where } \theta^-_{i+\frac{1}{2}} = \frac{u^n_{i+2} - u^n_{i+1}}{u^n_{i+1} - u^n_i} \tag{3.10}$$

The numerical flux defined by the equation 3.9 is a flux limiter method. The flux limiter method is second order and TVD.

Two limiter functions $\varphi(\theta)$ are commonly used. These are Van Leer limiter[28] and Superbee limiter[17]. Van Leer limiter function is;

$$\varphi(\theta) = \frac{|\theta| + \theta}{1 + |\theta|} \tag{3.11}$$

Superbee limiter function is;

$$\varphi(\theta) = max(0, min(1, 2\theta), min(\theta, 2)) \tag{3.12}$$

These limiter functions are non negative functions so sign of the anti diffusivity keeps same. Comparison of these limiter functions can be seen at figure 3.1.
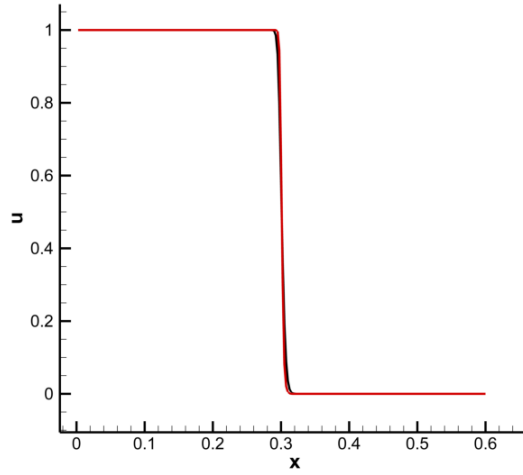
Figure 3.1: Comparison of the Van Leer limiter (black line) with the Superbee limiter (red line).

The limiter functions tested with linear advection equation at $t = 0.3$, where $a = 1$ and $\Delta t = 0.002$ and $\Delta x = 0.0025$ with the initial conditions $u(x,0) = 1$ if $x < 0$ and $u(x,0) = 0$ if $x > 0$.

As it can be seen from figure 3.1, Superbee limiter gives slightly better result than Van Leer limiter, so Superbee limiter is chosen for solving reactive Euler equations.

3.3 SLOPE LIMITER METHODS

In a slope limiter method, piecewise linear representation[29] of the solution U^n is limited by a slope limiter function. By using a slope limiter function, oscillations at the discontinuities tried to be decreased.

Slope limiter method can be represented in the form of the flux limiter method.

$$\delta_i^n = \frac{U_{i+1}^n - U_i^n}{\Delta x} \varphi(\theta_{i+\frac{1}{2}}^+) \tag{3.13}$$

In this thesis Roe's numerical flux is used in high resolution method and then flux becomes;

$$F_{i+\frac{1}{2}}^n = F_{i+\frac{1}{2}}^{(R)} + \frac{1}{2} \sum_{k=1}^{3} \bar{\lambda}_{k,i+\frac{1}{2}} (sgn(\bar{\lambda}_{k,i+\frac{1}{2}}) - \bar{\sigma}_{k,i+\frac{1}{2}}) \Delta x \bar{\delta}_{k,j(k)}^n \bar{\mathbf{r}}_{i+\frac{1}{2}}^{(k)} \tag{3.14}$$

56

$F^{(R)}_{i+\frac{1}{2}}$ is the numerical flux in the equation 2.110, $\bar{\sigma}_{k,i+\frac{1}{2}} = \bar{\lambda}_{k,i+\frac{1}{2}}\frac{\Delta t}{\Delta x}$ and $\bar{\mathbf{r}}^{(k)}_{i+\frac{1}{2}}$ is the right eigenvector.

For slope limiter function $\bar{\delta}^n_{k,i}$ decomposed as;

$$
\bar{\delta}^n_{k,i} = \begin{cases} \dfrac{\bar{\alpha}^n_{k,i-\frac{1}{2}}}{\Delta x}\varphi\left(\dfrac{\bar{\alpha}^n_{k,i+\frac{1}{2}}}{\bar{\alpha}^n_{k,i-\frac{1}{2}}}\right) & \text{if} \quad \bar{\lambda}_{k,i+\frac{1}{2}} < 0, \\[3mm] \dfrac{\bar{\alpha}^n_{k,i+\frac{1}{2}}}{\Delta x}\varphi\left(\dfrac{\bar{\alpha}^n_{k,i-\frac{1}{2}}}{\bar{\alpha}^n_{k,i+\frac{1}{2}}}\right) & \text{if} \quad \bar{\lambda}_{k,i+\frac{1}{2}} > 0, \end{cases}
\tag{3.15}
$$

3.4 NUMERICAL RESULTS

The test case data is given at table 2.1. For comparison of the numerical schemes, same boundary conditions and same step size evaluation used for second order Roe's method, first order Roe's method, Godunov's method and Lax-Friedrichs method.

The description of the test cases are given in chapter 2.

Test case 2 cannot be solved for high resolution method with Roe's flux because it is a low density problem. Roe's method can not solve low density problems. Because of the oscillations in the calculation of the low density or pressure, a negative value is calculated, which is a unphysical property.

Test case 5 is computed without using entropy fix, because there are oscillations due to diffusivity. When entropy fix is used, there are increase in pressure oscillations and negative pressure value calculated. Negative pressure value is very small, it can be neglected but the neglected solution is inaccurate than the solution with no entropy fix.

The solution of the test cases are given with the comparison of the Roe's approximate Riemann solver. Since the most accurate and correct solution is obtained so is from Roe's approximate Riemann solver.

3.4.0.6 Test Case 1

For this test output time is taken as 0.2 units and initial discontinuity position taken as $x_0 = 0.3$.

Figure 3.2: Comparison of the second order Roe's method (black symbols), first order Roe's method (red symbols) with exact solution (line) for the test case 1.

The superiority of the second order Roe's method is seen from the figure 3.2. Solution of the second order Roe's method at the left rarefaction wave is accurate than the first order Roe's method. Second order Roe's method has solved the contact discontinuity in 3 cells, while first order Roe's method has failed when solving the contact discontinuity. The right shock wave has been solved in just 1 cell with second order Roe's method, while first order Roe's method solved it in 3 cells. The solution of the shock wave is important in this thesis, accuracy of the numerical scheme in the shock region is important for that reason. The internal energy is solved with better accuracy with second order Roe's method because the contact discontinuity is solved accurately and that reflected on the internal energy solution.

In this test case, accuracy of the second order method with slope limiter is seen. The accuracy of the second order Roe's method comes from the use of the slope limiter. At the figure 3.3 comparison of the two second order methods can be seen.

Figure 3.3: Comparison of the second order Roe's method (black symbols), Richtmyer method (red symbols) with exact solution (line) for the test case 1.

Accuracy at the smooth regions are nearly same, because of the second order accuracy. But at the discontinuities oscillations is seen. Oscillations created at the contact discontinuity and at the shock wave and unphysical solution have emerged. Using slope limiter, limits these oscillations and gives accurate results and discontinuous regions.

3.4.0.7 Test Case 3

For this test output time is taken as 0.012 units and initial discontinuity position taken as $x_0 = 0.5$.

Figure 3.4: Comparison of the second order Roe's method (black symbols), first order Roe's method (red symbols) with exact solution (line) for the test case 3.

This test case is consists a left rarefaction, a strong contact discontinuity and a strong shock wave. The numerical accuracy when solving the strong shock wave and the strong contact discontinuity is seen from the figure 3.4. The contact discontinuity is solved in the 4 cells, while shock wave is solved in 2 cells. A small inaccurate region is seen at the end of the contact wave and at the start of the shock wave, between $x = 0.75$ and $x = 0.8$, but still solution is better than first order Roe's method, which can not show the peak in density.

Use of a second order method increases the oscillations as seen before, therefore there is a inaccurate region at the end of the right rarefaction wave. This oscillation is seen better at the velocity profile. When looked at the density and the internal energy profiles, this oscillations do not affect the whole solution to much. Still second order Roe's method solves with better accuracy than Roe's method.
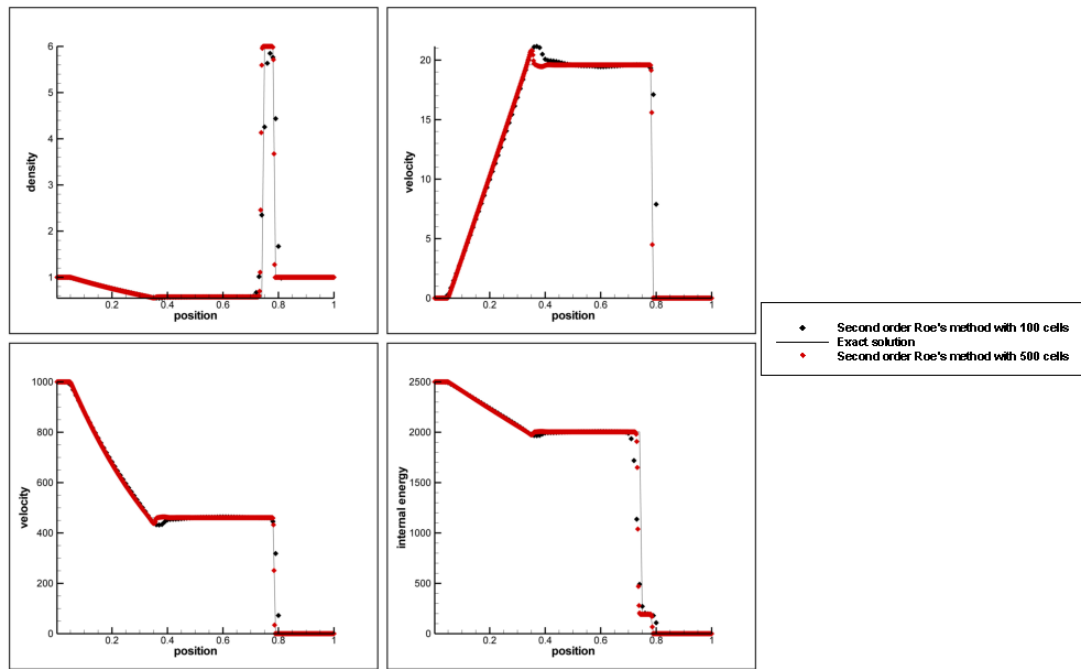
Figure 3.5: Comparison of the second order Roe's method with 100 cells (black symbols), second order Roe's method with 500 cells(red symbols) with exact solution (line) for the test case 3.

At the figure 3.5, the number of the computing cells have been increased from 100 cells to 500 cells. Accuracy of the solution have been increased with increasing cell number. Oscillations at the end of the rarefaction wave have been decreased and the area between the contact wave and the shock wave solved better with higher number of computing cells. The shock wave is resolved in 3 computing cells and the contact wave is resolved in 4 computing cells in both solutions, therefore 100 computing cells have been used for the comparison of the solutions rest of the test cases.

3.4.0.8 Test Case 4

For this test output time is taken as 0.035 units and initial discontinuity position taken as $x_0 = 0.4$.
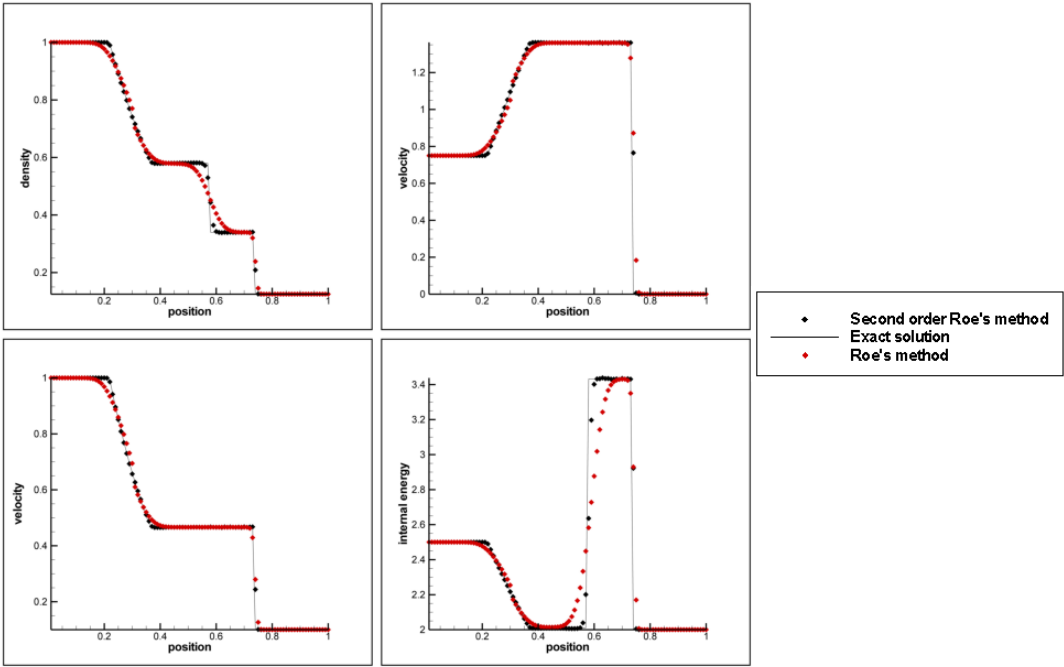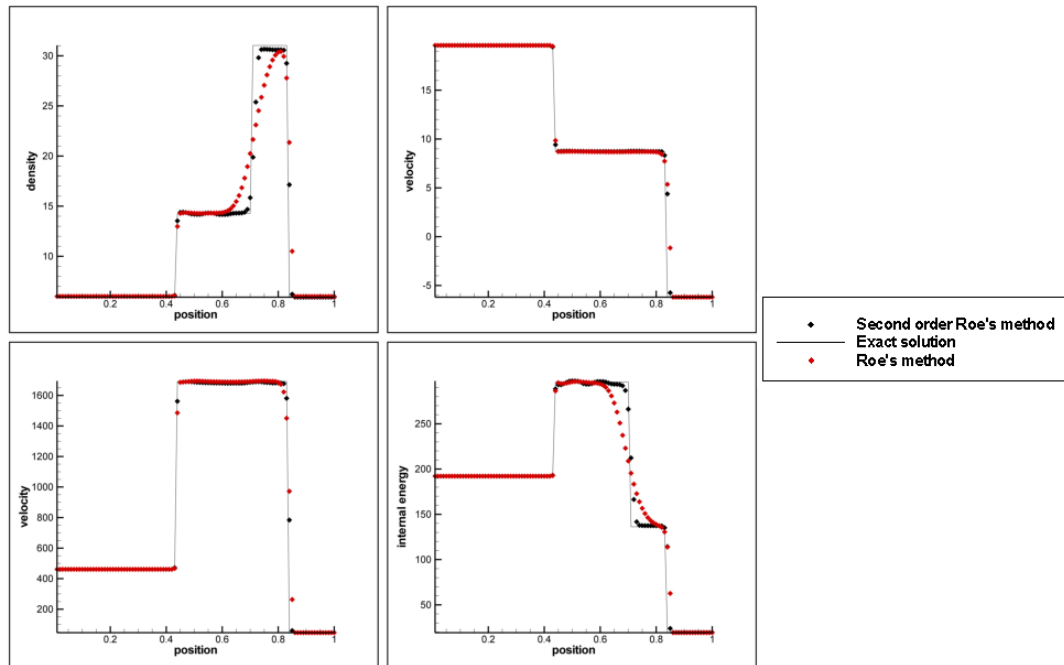

Figure 3.6: Comparison of the second order Roe's method (black symbols), first order Roe's method (red symbols) with exact solution (line) for the test case 4.

The accuracy of the second order method at the shock wave is seen with this case clearly. First shock wave resolved in 1 cell, second shock wave resolved in 2 cells and the contact discontinuity resolved in 4 cells. There are some oscillation before the contact discontinuity but these are not high oscillations. The robustness and the accuracy at the shock waves of the high resolution method is seen more clear in this case, which is better than Roe's method. This is a important property for this thesis.

3.4.0.9 Test Case 5

For this test output time is taken as 0.012 units and initial discontinuity position taken as $x_0 = 0.8$.
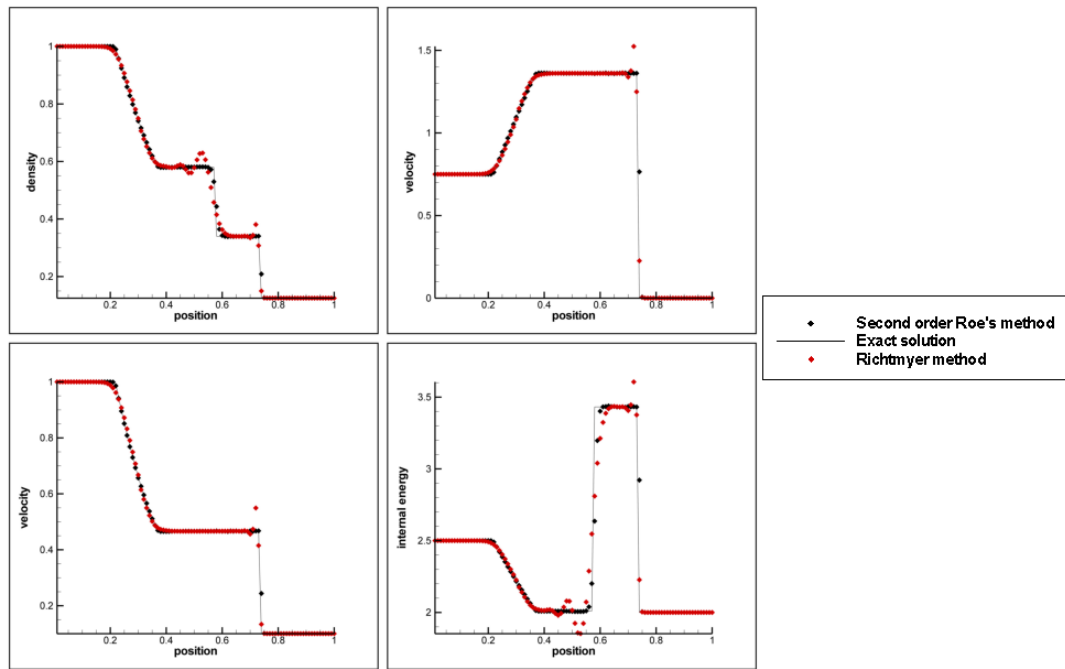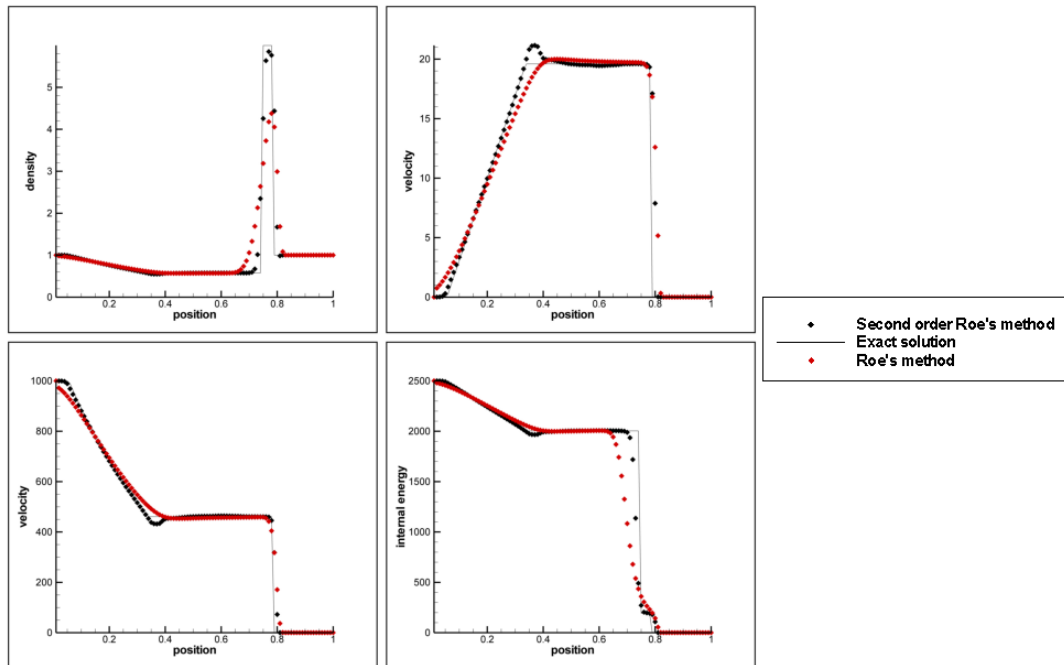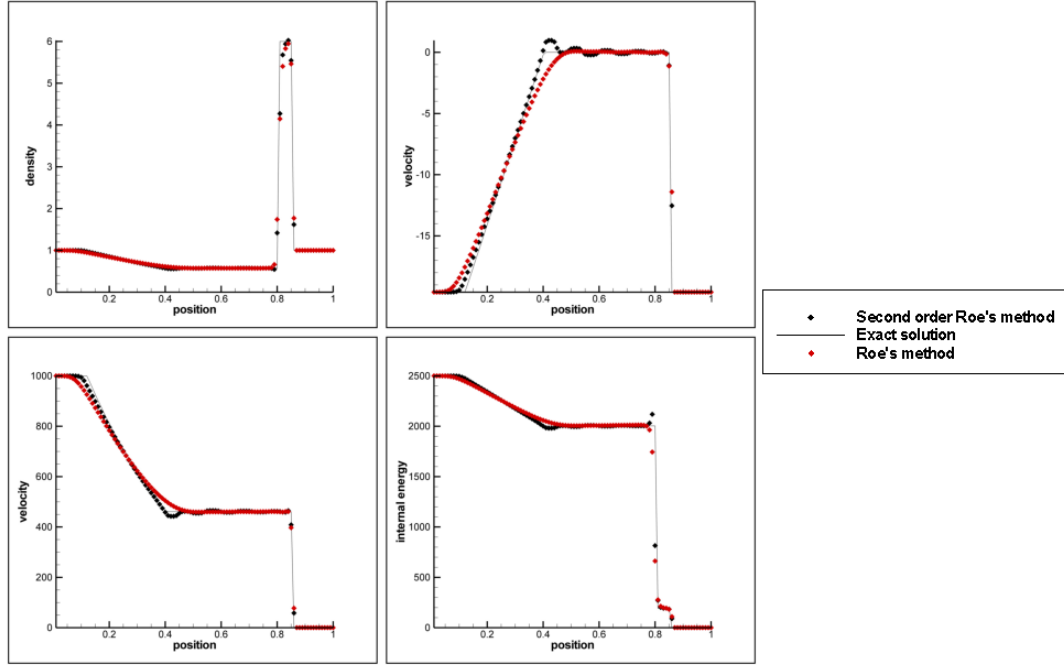

Figure 3.7: Comparison of the second order Roe's method (black symbols), first Roe's method (red symbols) with exact solution (line) for the test case 5.

This case is very similar to the case 3, in this case contact discontinuity is stationary, therefore small oscillations at the velocity affects the solution, which can be seen at the internal energy profile. This is a very challenging problem for the numerical methods.

As a result numerical solution of second order Roe's method compared with the solutions of first order Roe's method, Godunov method and Lax-Friedrichs. Second order Roe's method gives the most accurate results in discontinues regions. As expected there are some oscillations in the smooth regions but they are not affecting the general solution. The robustness and the accuracy of the second order Roe's method is better than other numerical methods that have been studied in this thesis so far. Therefore for solving reactive Euler equations, second order Roe's method is used.

After comparing all the solutions from the studied numerical methods, High Resolution method chosen for solving reactive Euler equations.

CHAPTER 4

ONE-DIMENSIONAL REACTIVE EULER EQUATIONS

In this chapter, reaction is added to the Euler equations and reactive Euler equations have been derived with the following assumptions[5].

The external forces are negligible. Gravity is the only important external force but it is negligible for our problem because detonation happens fast. The mass diffusion caused by pressure and thermal gradients is negligible also for same reason.

All binary diffusion coefficients are equal D. So Fick's law of mass diffusion becomes

$Y_i U_i = -D \frac{\partial}{\partial x} Y_i.$

Bulk viscosity can be neglected because fluid behaves like a Newtonian fluid.

The viscous term in energy equation is negligible. The viscous term is not an important parameter for energy transport in our case.

Heat transfer caused by radiation and gradients are negligible. They are neglected because of the same reason with first assumption.

The gas mixture behaves like an ideal gas.

$$p = \rho R T / W \tag{4.1}$$

where R is the universal gas constant, W is the average molecular mass of the gas mixture. The thermodynamic identity for ideal gas is written as;

$$h = e + \frac{p}{\rho} \tag{4.2}$$

where h and e are the specific enthalpy of the mixture and the specific internal energy.

$$E = e + \frac{1}{2}u^2 \tag{4.3}$$

$$H = h + \frac{1}{2}u^2 = E + \frac{p}{\rho} \tag{4.4}$$

where H and E are the total enthalpy of the mixture and total energy.

Only one chemical reaction takes place and this reaction is exothermic. Heat release is mostly depends on the initial and final composition of the gas mixture and with assuming the reaction is exothermic, one step reaction can be used. Therefore mass fraction of species Y is equal to 1 or 0. Using these assumptions, enthalpy is written as;

$$h = QY + c_p T \tag{4.5}$$

where Q is the heat release and c_p assumed constant.

The reaction rate w is formulated as;

$$w = \begin{cases} 0, & T < T_{ign} \\ -k\rho Y, & T \geq T_{ign} \end{cases} \tag{4.6}$$

where $k = A(T)e^{-\frac{E_a}{RT}}$ and $A(T) = BT^\alpha$. A is the frequency factor and E_a is the activation energy. k assumed to satisfies the Arrhenius's law.

The molecular diffusion, the thermal conduction, the viscous effects and the temperature dependence of the frequency factor in the reaction rate are negligible. From this assumption when calculation reaction rate $\alpha = 0$ and $A(T) = A$ are used.

ZND model will be introduced and in this thesis it is used for solving reactive Euler equations. ZND model describes the wave solution of the reactive Euler Equations.

65

4.1 DIMENSIONLESS FORM OF REACTIVE EULER EQUATIONS

The reactive Euler equations are written in dimensionless form in order to work faster with the numerical results. The dimensionless form is written according to below variables.

$$\rho^* = \frac{\rho}{\rho_{ref}}, \qquad u^* = \frac{u}{u_{ref}}, \qquad x^* = \frac{x}{x_{ref}}, \qquad t^* = t\frac{u_ref}{x_{ref}}$$

$$E^* = \frac{E}{u_{ref}^2}, \qquad p^* = \frac{p}{\rho_{ref}u_{ref}^2}, \qquad w^* = w\frac{t_{ref}}{\rho_{ref}}, \qquad E_a^* = E_a\frac{\rho_{ref}}{Wp_{ref}}$$

$$Q^* = Q\frac{\rho_{ref}}{p_{ref}}, \qquad T^* = T\frac{R\rho_{ref}}{Wp_{ref}}, \qquad k^* = \frac{k}{k_{ref}}, \qquad h^* = h\frac{\rho_{ref}}{p_{ref}},$$

$$a^* = a\sqrt{\frac{\rho_{ref}}{p_{ref}}}$$

(4.7)

To not create a distraction in the equations, $*$ sign is not used in the rest of the formulations. Other useful relations using dimensionless variables are given. The equation of state, thermodynamic identity are written as;

$$p = \rho T \tag{4.8}$$

$$p = (\gamma - 1)\rho(E - 0.5u^2 - QY) \tag{4.9}$$

$$\tag{4.10}$$

Dimensionless form of reactive Euler equations are written as;

$$\frac{\partial(\rho)}{\partial t} + \frac{\partial(\rho u)}{\partial x} = 0 \tag{4.11}$$

$$\frac{\partial(\rho u)}{\partial t} + \frac{\partial(\rho u^2 + p)}{\partial x} = 0 \tag{4.12}$$

$$\frac{\partial(\rho E)}{\partial t} + \frac{\partial(\rho u E + pu)}{\partial x} = 0 \tag{4.13}$$

$$\frac{\partial(\rho Y)}{\partial t} + \frac{\partial(\rho u Y)}{\partial x} = w \tag{4.14}$$

The reaction rate w is calculated from;

$$w = \begin{cases} 0, & T < T_{ign} \\ -Dak\rho Y, & T \geq T_{ign} \end{cases} \tag{4.15}$$

where Y is the mass fraction of species, Da is the Damköhler number[4], k is the rate constant and it is equal to $k = e^{\left(E_a\left(\frac{1}{T_*} - \frac{1}{T}\right)\right)}$. T_{ign} is the ignition temperature. T_* is reference temperature and it is chosen as von Neumann temperature. E_a is the activation energy, T is the temperature.

4.2 THE REACTIVE RANKINE-HUGONIOT EQUATIONS

The reactive Rankine-Hugoniot equations are required in ZND model and it allows constructing a relation between burnt and unburnt state. An assumption is made, which is the flow is steady with the combustion wave . Inspecting the reactive Rankine-Hugoniot conditions on a moving coordinate system, a new variable ξ introduced;

$$\xi(x, t) = x - st \tag{4.16}$$

If the equations 4.11-4.14 is written in the ordinary differential form;

$$-s\frac{\partial(\rho)}{\partial \xi} + \frac{\partial(\rho u)}{\partial \xi} = 0 \tag{4.17}$$

$$-s\frac{\partial(\rho u)}{\partial \xi} + \frac{\partial(\rho u^2 + p)}{\partial \xi} = 0 \tag{4.18}$$

$$-s\frac{\partial(\rho E)}{\partial \xi} + \frac{\partial(\rho u E + pu)}{\partial \xi} = 0 \tag{4.19}$$

$$-s\frac{\partial(\rho Y)}{\partial \xi} + \frac{\partial(\rho u Y)}{\partial \xi} = w \tag{4.20}$$

$$\tag{4.21}$$

Then integrating above equations from $\xi = -\infty$ to $\xi = \infty$, the reactive Rankine-Hugoniot equations become;

$$\rho_u(u_u - s) = \rho_b(u_b - s) = -m \tag{4.22}$$

$$\rho_u(u_u - s)^2 + p_u = \rho_b(u_b - s)^2 + p_b \tag{4.23}$$

$$h_u + \frac{1}{2}(u_u - s)^2 = h_b + \frac{1}{2}(u_b - s)^2 \tag{4.24}$$

where m is the mass flux. s is the wave speed, u subscript represents unburnt species and b subscript represents burnt species.

Rayleigh line is referred to the states at the equations 4.22 and 4.23, which is define as;

$$\frac{p_u - p_b}{\frac{1}{\rho_u} - \frac{1}{\rho_b}} = -m^2 \tag{4.25}$$

The equation of state is written as;

$$\frac{p_u}{\rho_u T_u} = \frac{p_b}{\rho_b T_b} \tag{4.26}$$

and the thermodynamic relation is written as;

$$h_u - Q - \frac{\gamma}{\gamma - 1}T_u = h_b - \frac{\gamma}{\gamma - 1}T_b = 0 \tag{4.27}$$

If all unburnt quantities are given, burnt variables $u_b, \rho_b, p_b, T_b, h_b$ can be calculated using the reactive Rankine-Hugoniot equations (equation from 4.22 to 4.24) and equations 4.26 and 4.27.

4.3 TYPES OF PROCESSES

For describing the possible value along the reaction process, subscript b is not used. Hugoniot function $\mathcal{H}$ is introduced as;

$$\mathcal{H}(v, p) = h(v, p) - h_u - \frac{1}{2}(v + v_u)(p - p_u) \tag{4.28}$$

where $v = 1/\rho$ is the specific volume. The Hugoniot curve has been identified as $\mathcal{H} = 0$. Hugoniot function derived from equation 4.24 by using equation 4.22. Using equation 4.5, Hugoniot curve is written as;

$$p(v) = \frac{2Q - p_u v + \frac{\gamma+1}{\gamma-1} p_u v_u}{\frac{\gamma+1}{\gamma-1} v - v_u} \tag{4.29}$$

The Rayleigh line can be written as;

$$p(v) = -m^2(v - v_u) + p_u \tag{4.30}$$

The intersection of the Rayleigh line and the Hugoniot curve will give the final thermodynamic states.

Since p and v has to be positive, the limits of p and v are given as;

$$0 < p < \infty \tag{4.31}$$

$$\frac{\gamma - 1}{\gamma + 1} v_u < v < 2\frac{Q}{p_u} + \frac{\gamma + 1}{\gamma - 1} v_u \tag{4.32}$$

According to the Hugoniot curve, detonation waves increase the pressure and the density when it is passing through, but deflagration waves decrease pressure and density because the gas is slowed down and expanded.

Hugoniot Curve is divided into two distinct branches

The upper branch is the detonation branch and it is the region with in the limits of;

$$\frac{(\gamma - 1)Q}{v_u} + p_u \le p < \infty \tag{4.33}$$

$$\frac{\gamma - 1}{\gamma + 1} v_u < v \le v_u \tag{4.34}$$

The lower branch is the deflagration branch and it is the region with in the limits of;

$$0 < p \le p_u \tag{4.35}$$

$$v_u + Q\frac{\gamma - 1}{\gamma p_u} \le v < 2\frac{Q}{p_u} + \frac{\gamma 41}{\gamma - 1} v_u \tag{4.36}$$

These limits are written from the definition of the Hugoniot curve and its limits.

There is unique slope of the Rayleigh line for the Rayleigh line passes tangent to the detonation and deflagration branches. The Rayleigh line separates these branches into three different processes. The tangent point of the detonation branch is called point A and the tangent point of the deflagration branch is called B. This can be seen at the figure 4.1
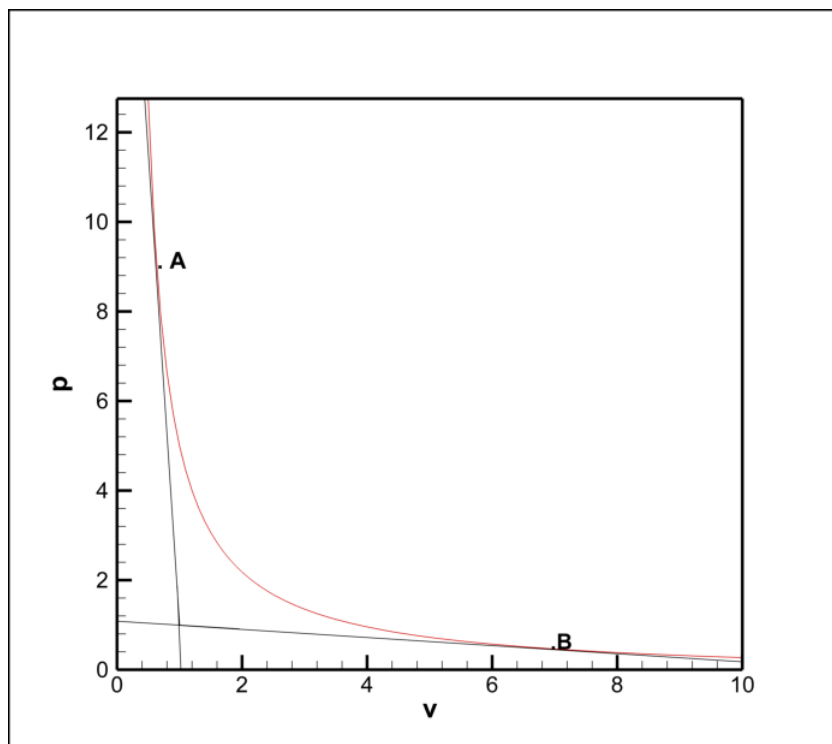
Figure 4.1: A typical Hugoniot Curve with the initial values of $p_u = 1$ and $v_u = 1$, the Rayleigh lines tangent to the Hugoniot curve at the point A and B.

Depending on the final conditions three types of detonations can occur[2, 4, 30].

- Strong detonations.

- Chapman-Jouguet detonations (CJ detonations).

- Weak detonations.

69

Strong detonations occur when the detonation waves with the final conditions on the detonation branch, upper region of the point A until the limited values of p and v. CJ detonations occurs at the point A. Weak detonations occur when the detonation waves with the final conditions on the detonation branch, lower region of the point A until the limited values of p and v.

Depending on the final conditions three types of deflagrations can occur.

- Strong deflagrations.

- Chapman-Jouguet deflagrations (CJ deflagrations).

- Weak deflagrations.

Strong deflagrations occur when the detonation waves with the final conditions on the deflagration branch, lower region of the point B until the limited values of p and v. CJ deflagrations occurs at the point B. Weak deflagrations occur when the detonation waves with the final conditions on the deflagration branch, upper region of the point B until the limited values of p and v.

In this thesis only detonation waves will be considered. From the intersection of Rayleigh line and Hugoniot curve;

$$m_{CJ}^2 = \gamma \frac{p_u}{v_u} + (\gamma^2 - 1)\frac{Q}{v_u^2}\left(1 + \sqrt{1 + \frac{2\gamma p_u v_u}{(\gamma^2 - 1)Q}}\right) \tag{4.37}$$

where subscripts CJ represents CJ detonations, st represents strong detonations and we represents weak detonations.

If $m < m_{CJ}$, there will be no detonations. For $m = m_{CJ}$ there will be a CJ detonation with the thermodynamic quantities;

$$p_{CJ} = \frac{m^2 v_u + p_u}{\gamma + 1} \tag{4.38}$$

$$v_{CJ} = \frac{\gamma(m^2 v_u + p_u)}{m^2(\gamma + 1)} \tag{4.39}$$

$$u_{CJ} = s_{CJ} - v_{CJ}m \tag{4.40}$$

For $m > m_{CJ}$ there will be a strong detonation with the thermodynamic quantities for the

strong detonations;

$$p_{st} = \frac{m^2 v_u + p_u}{\gamma + 1} + \frac{1}{\gamma + 1} \sqrt{(m^2 v_u - \gamma p_u)^2 - 2(\gamma^2 - 1)m^2 Q} \qquad (4.41)$$

$$v_{st} = \frac{\gamma(m^2 v_u + p_u)}{m^2(\gamma + 1)} - \frac{1}{m^2(\gamma + 1)} \sqrt{(m^2 v_u - \gamma p_u)^2 - 2(\gamma^2 - 1)m^2 Q} \qquad (4.42)$$

$$u_{st} = s_{st} - v_{st} m \qquad (4.43)$$

For the weak detonations;

$$p_{we} = \frac{m^2 v_u + p_u}{\gamma + 1} - \frac{1}{\gamma + 1} \sqrt{(m^2 v_u - \gamma p_u)^2 - 2(\gamma^2 - 1)m^2 Q} \qquad (4.44)$$

$$v_{we} = \frac{\gamma(m^2 v_u + p_u)}{m^2(\gamma + 1)} + \frac{1}{m^2(\gamma + 1)} \sqrt{(m^2 v_u - \gamma p_u)^2 - 2(\gamma^2 - 1)m^2 Q} \qquad (4.45)$$

$$u_{we} = s_{we} - v_{we} m \qquad (4.46)$$

Some characteristic properties help to define the various detonation waves. This is called Jouget's rule[30]. From Jouget's rule;

- The gas flow relative to the reaction front is supersonic ahead of a detonation front $(s - u_u > a_u)$.

- The gas flow relative to the reaction front is subsonic behind a strong detonation front $(0 < s - u_b < a_b)$.

- The gas flow relative to the reaction front is sonic behind a CJ detonation front $(s - u_b = a_b)$.

- The gas flow relative to the reaction front is supersonic behind a weak detonation front $(s - u_b > a_b)$.

4.4 THE ZND MODEL FOR DETONATIONS WAVES

The ZND model explains the internal structure of detonation waves, which is developed by Zel'dovich, von Neumann and Döring[2, 4, 30]. The ZND model is used because the reactive Rankine-Hugoniot equations give no explanation to the internal structure of the detonation waves.

71

The ZND model assumes a detonation wave travels with a constant speed of s. Fluid is in the thermo-chemical equilibrium after the fluid dynamical shock wave and it is described by a thermodynamic equation of state. So the reactive Rankine Hugoniot equations can be applied.

Furthermore, the ZND model takes the reaction rate equal to the zero ahead of the shock and finite behind the shock. A non-reacting shock increases the temperature of the unburnt gas and starts a reaction because the temperature is increased to a larger value than ignition temperature.

The shock wave is assumed to be thinner than the reaction zone and the shock wave is considered as a discontinuous jump.

In the ZND model, the Hugoniot curve depends on the mass fraction of the species. If the equation 4.29 written in a general form, it becomes;

$$p(v, Y) = \frac{2Q(1 - Y) - p_u v + \frac{\gamma+1}{\gamma-1} p_u v_u}{\frac{\gamma+1}{\gamma-1} v - v_u} \tag{4.47}$$

When $Y = 0$, then the reaction is completed and all heat is released.

Non-reacting shock wave increases the pressure, density and temperature to a higher value on the Hugoniot curve at $p(\cdot, 1)$, which is called von Neumann spike[2, 4]. The von Neumann spike is the final state behind the non-reacting shock wave if there is no reaction. It is obvious that von Neumann temperature (T_{vN}) is above the ignition temperature. The state point moves down the Rayleigh line until the reaction is completed and the final state on the Hugoniot curve $p(\cdot, 1)$ is reached. For every Y value between zero and one, the reactive Rankine-Hugoniot equations can be used to find the thermodynamic quantities for CJ or strong detonation;

$$p(Y) = \frac{m^2 v_u + p_u}{\gamma + 1} + \frac{1}{\gamma + 1}\beta(Y) \tag{4.48}$$

$$v(Y) = \frac{\gamma(m^2 v_u + p_u)}{m^2(\gamma + 1)} - \frac{1}{m^2(\gamma + 1)}\beta(Y) \tag{4.49}$$

$$u(Y) = s - v(Y)m \tag{4.50}$$

$$\beta(Y) = \sqrt{(m^2 v_u - \gamma p_u)^2 - 2(\gamma^2 - 1)m^2 Q(1 - Y)} \tag{4.51}$$

Y has to depend on a variable in order to calculate the thermodynamic quantities. ξ is intro-

duced, which is the distance between the point x and the shock and formulated as $\xi = x - st$. If the conservation equations for the one-dimensional reactive Euler equations written in the form of a system of ordinary differential equations for $g(x - st) = g(\xi)$. Then equation 4.14 becomes;

$$\frac{\partial Y(\xi)}{\partial \xi} = -\frac{w(Y(\xi))}{m} \qquad (4.52)$$

where ξ less than zero, $\xi = 0$ is the position of the shock. Therefore $w(Y(\xi))$ is continuous for $\xi < 0$.

Weak detonations cannot be solved with the ZND model because weak detonation state can not be reached from von Neumann state and without a shock, the reaction does not start. In this thesis only strong or CJ detonations solved.

Degree of overdrive[31], f is the square of the ratio of the detonation wave speed with the minimum detonation speed, which is the CJ detonation speed. It can be formulated as $f = \left(\frac{s}{s_{cj}}\right)^2$. In order to study strong and CJ detonations in detail, f will be a given parameter.

The half-reaction length $L_{1/2}$ is the distance for half completion of the reaction starting from the front of the detonation wave[2]. $L_{1/2}$ will be given in order to compute Da.

4.5 NUMERICAL TESTS

The ZND model has been solved for a CJ detonation and a strong detonation. The solutions from these test cases will be used for comparison of the numerical solution of the one dimensional reactive Euler equations with the exact ZND solution.

4.5.1 Test Case 1

In this example, $p_u = 1$, $\rho_u = 1$, $u_u = 0$, which are the state before the shock. $E_a = 14$, $Q = 14$, $f = 1$, $T_{vN} = 5.0509$, $\gamma = 1.4$, $L_{1/2} = 1$ and $Da = 0.6488$ are the other given parameters. Da has been chosen small because if Da is large the reaction will be very fast.
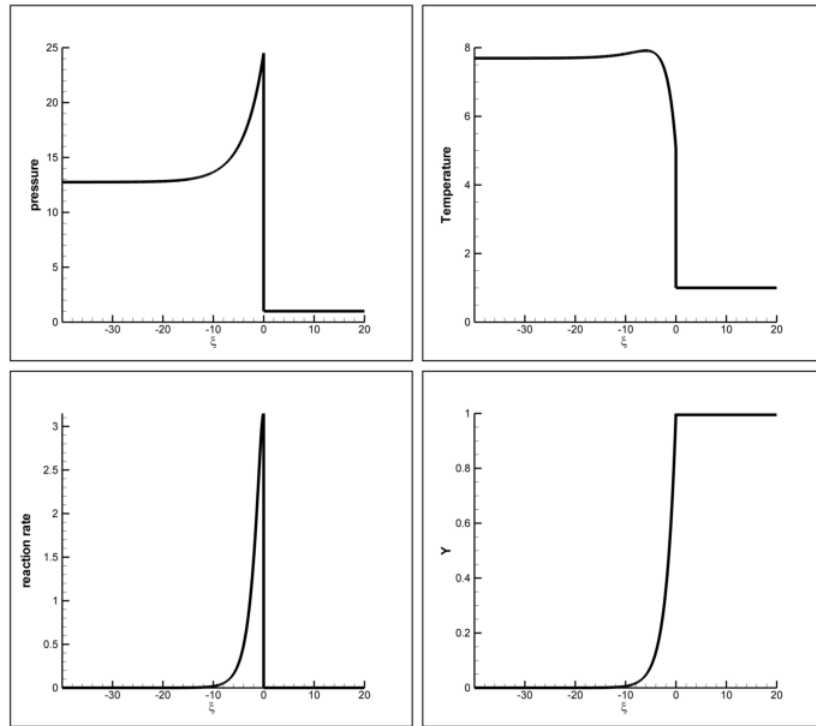
Figure 4.2: Exact solution of the ZND method for pressure, temperature, reaction rate and mass fraction of species for test case 1

In test case 1, $s = 5.44186$, $p_b = 12.7558$, $\rho_b = 1.65829$, $u_b = 2.1602$. If Jouget's rule is checked, $s - u_b = 3.28161$ where $c_b = 3.28161$, which is correct for CJ detonations.

From the figure 4.2, reaction is occurred behind the shock, pressure peek can be seen, which is caused by the reaction. There is no reaction ahead of the shock as expected and therefore the fraction of mass species, Y, is equal to one. The pressure and reaction rate are increasing with the increasing Y value until the reaction is done.

4.5.2 Test Case 2

In this example, $p_u = 1$, $\rho_u = 1$, $u_u = 0$, which are the state before the shock. $E_a = 150$, $Q = 50$, $f = 1.8$, $T_{vN} = 7.8801$, $\gamma = 1.2$ and $Da = 0.63293$ are the other given parameters.
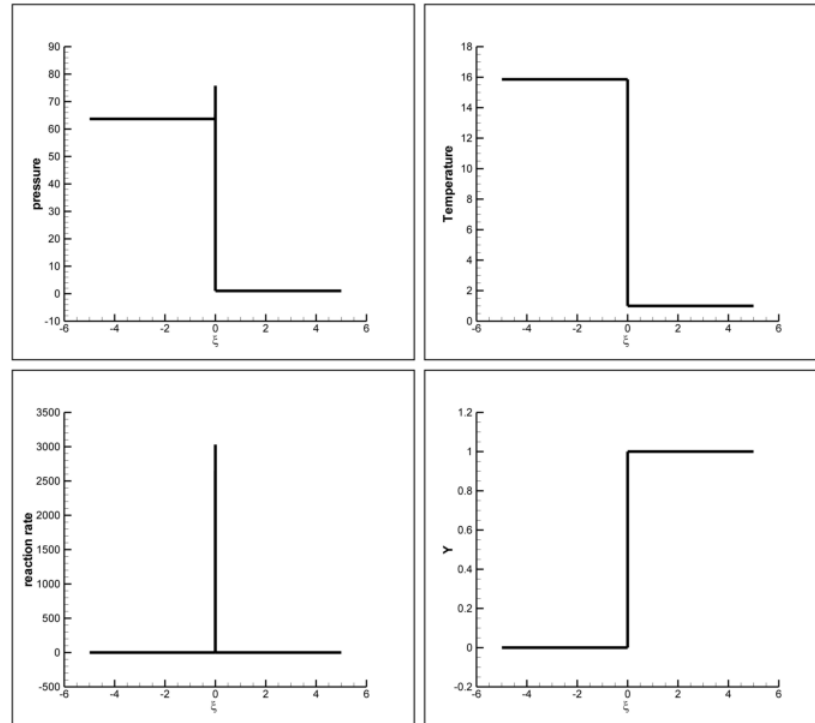
Figure 4.3: Exact solution of the ZND method for pressure, temperature, reaction rate and mass fraction of species for test case 2

In test case 2, $s = 9.13687$, $p_b = 63.6802$, $\rho_b = 4.01581$, $u_b = 6.86089$. If Jouget's rule is checked, $s - u_b = 2.27489$ where $c_b = 4.36221$, therefore we can say that $s - u_b < c_b$, which is correct for strong detonations.

Because of the higher activation energy, reaction rate is higher for this case. Normally Da constant defines the reactions speed but even using similar Da at test cases 1 and 2. Every fast detonation occurred due to high activation energy.

CHAPTER 5

SIMPLIFIED DETONATION MODEL

In this chapter, a simplified detonation model will be solved[32]. Simplified detonation model consists of Burgers' equation and a chemical reaction. In this model,the reaction starts when $u \geq u_{ign}$, otherwise there is no reaction.

In order to solve the simplified detonation model, first, an analogue will be created with reactive Rankine-Hugoniot equations and ZND model[2, 4, 30]. With the help of this analogue, exact ZND solution of the model is solved for different cases. After obtaining the exact solution, simplified detonation model is solved with first order splitting method. Finally simplified detonation model is solved with second order Roe's method using second order splitting method.

System of equations for simplified detonation model is written as;

$$\frac{\partial u}{\partial t} + \frac{\partial \frac{u^2}{2}}{\partial x} = -Qw(u, Y) \tag{5.1}$$

$$\frac{\partial Y}{\partial t} = w(u, Y) \tag{5.2}$$

The reaction rate w is idealized for this model, using Arrhenius' behavior;

$$w(u, Y) = \begin{cases} 0, & u < u_{ign} \\ -DaY, & u \geq u_{ign} \end{cases} \tag{5.3}$$

where u_{ign} is the needed ignition velocity to start the reaction.

5.1 REACTIVE RANKINE-HUGONIOT EQUATIONS

For simplified detonation model, s is assumed constant and $s > 0$ along the positive x-direction. From the equations 5.1 and 5.2, the reactive Rankine-Hugoniot equation becomes;

$$s(u_b - u_u - Q) = \frac{1}{2}u_b^2 - \frac{1}{2}u_u^2 \tag{5.4}$$

For our system Hugoniot curve and Rayleigh line written as;

$$\mathcal{H}(u) = \frac{1}{2}u^2 \tag{5.5}$$

$$\mathcal{R}(u) = s(u - u_u - Q) + \frac{1}{2}u_u^2 \tag{5.6}$$

$$\tag{5.7}$$

The intersection point of $\mathcal{H}$ and $\triangle$ determines the final state of u. From the equations 5.5 and 5.6, s_{cj} calculated as;

$$s_{cj} = u_u + Q + \sqrt{Q^2 + 2u_u Q} \tag{5.8}$$

If $s < s_{cj}$, there will be no detonation, if $s = s_{cj}$, there will be a CJ (Chapman-Joguet) detonation and if $s > s_{cj}$, there will be a strong detonation. u is calculated as;

$$u_{st} = s + \sqrt{(s - u_u)^2 - 2sQ} \tag{5.9}$$

$$u_{cj} = s_{cj} \tag{5.10}$$

$$\tag{5.11}$$

Jouguet's rule can be written for this system as;

- For detonation waves $s > u_u$

- For strong detonations $s < u_{st} = u_b$

- For CJ detonations $s = u_{cj} = u_b$

5.2 THE ZND (ZELDOVICH, VON NEUMANN AND DÖRING) MODEL

The ZND model for simplified detonation model is done from making a generalization from the ZND model for Euler Equations. The Hugoniot curve depends on the Y ,the mass fraction of species, and it is written as;

$$\mathcal{H}(u, Y) = \frac{1}{2}u^2 - sQY \tag{5.12}$$

Using the ZND theory, u is written depending on Y as for strong or CJ detonation;

$$u(Y) = s + \sqrt{(s - u_u)^2 - 2sQ(1 - Y)} \tag{5.13}$$

Y is written depending on ξ, where $\xi = x - st$. $u(\xi) = u_u)$ for $\xi > 0$ because it represents the unburnt state. Y written in the ordinary differential form as;

$$\frac{d}{d\xi}Y(\xi) = -\frac{DaY(\xi)}{s} \quad \text{for } \xi < 0 \tag{5.14}$$

$\xi = 0$ is the position of the shock so; $Y(0) = 1$. The exact ZND solution is obtained for equation 5.1 and 5.2 as;

$$Y(x, t) = Y(\xi) = \begin{cases} 1 & \xi > 0 \\ e^{Da\xi/s} & \xi \leq 0 \end{cases} \tag{5.15}$$

$$u(x, t) = u(\xi) = \begin{cases} u_u & \xi > 0 \\ s + \sqrt{(s - u_u)^2 - 2sQ(1 - Y(\xi))} & \xi \leq 0 \end{cases} \tag{5.16}$$

For this model $L_{1/2}$ is given by;

$$L_{1/2} = \frac{s}{Da}\ln(2) \tag{5.17}$$

$L_{1/2}$ can be used for calculation of Da, it is obvious from above equation.

5.2.1 Test Case 1

In this example, $u_u = 0$, which are the state before the shock. $Q = 0.5$, $f = 1$, $L_{1/2} = 1$ and $Da = 0.6931$ are the other given parameters. This is a CJ detonation case, where $s = s_{cj}$.

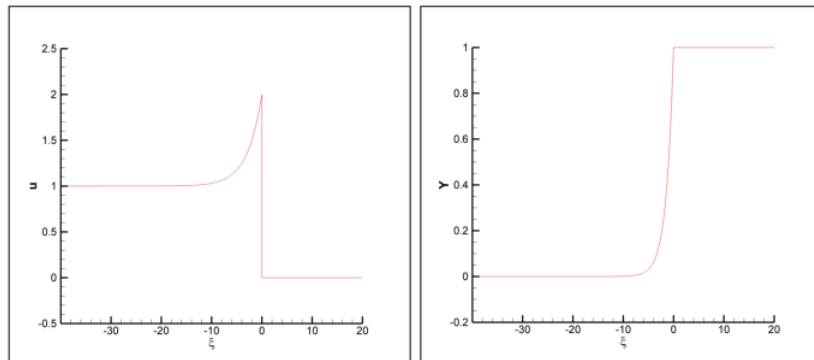Figure 5.1: Exact solution of the ZND method for u and Y for test case 1

In test case 1, $s = 1$, $u_b = 1$. From figure 5.1, u variable is climb to the von Neumann state, where $u = 2$ as expected right before the shock.

5.2.2 Test Case 2

In this example, $u_u = 0$, which are the state before the shock. $Q = 2$, $f = 1.265625$, $L_{1/2} = 0.1$ and $Da = 3.1192$ are the other given parameters. This is a strong detonation case.
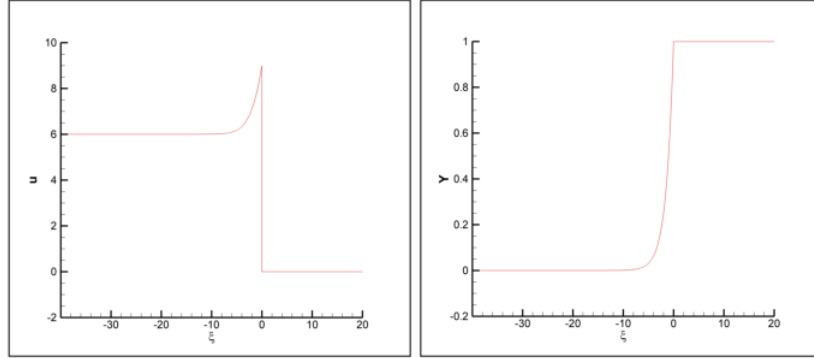
Figure 5.2: Exact solution of the ZND method for u and Y for test case 2

In test case 2, $s = 4.5$, $u_b = 6$. From figure 5.2, u variable is climb to the con Neumann state, where $u = 9$ as expected right before the shock.

5.3   NUMERICAL COMPUTATION OF THE SIMPLIFIED DETONATION

The simplified detonation model solved numerically in this section. First, the simplified detonation model is solved using first order splitting method. This method consists of two steps. In the first step equations solved without the source term. In the second step, no convection assumed.

For the first step, Roe's flux is used for computation of the Burgers' equation. The second step is solved by the backward Euler method. For the initial conditions, the exact ZND solution of the problem is used.

For the numerical solution of the simplified detonation model, two solutions are obtained. First solution is the CJ detonation, second solution is the strong detonation. Solutions are compared with the exact solution. This preliminary calculations are done in order to check the results accuracy of the written FORTRAN code in a simple case.

5.3.1 CJ Detonation

The initial conditions are given as; $u_u = 0$, $\Delta t = 0.01$, $\Delta x = 0.1$, $Q = 2$, $f = 1$, output time is 1, $Da = 31.192$ and $u_{ign} = 0.1$

Figure 5.3: Comparison of the numerical solution of the Burgers' equation (black symbols) with the exact ZND solution (black line)

From looking at the figure above, the inaccuracy of the solution is seen from the variable u profile. The numerical solution can not show the same peak for this problem. When a high resolution method is used to solve this problem, better peak value will be obtained.

5.3.2 Strong Detonation

The initial conditions are given as; $u_u = 0$, $\Delta t = 0.01$, $\Delta x = 0.1$, $Q = 2$, $f = 1.265625$, output time is 4, $Da = 31.192$ and $u_{ign} = 0.1$

Figure 5.4: Comparison of the numerical solution of the Burgers' equation (black symbols) with the exact ZND solution (black line)

The peak value can not be achieved in the strong detonation as in the CJ detonation. More accurate numerical methold will be used in order to get an more accurate solution.

5.3.3 High Resolution Method

For the solution of the high resolution method, Roe's flux with Superbee limiter is used. This time a different splitting method has been used, which is called second order splitting method of Strang[5, 33]. First equation set solved without convective term at time $t + \Delta t/2$, then equation set solved without source term at time $t + \Delta t/2$ and finally the equation set solved again without convective term at time $t + \Delta t$.

5.3.3.1 CJ Detonation

The initial conditions are given as; $u_u = 0$, $\varDelta t = 0.01$, $\varDelta x = 0.1$, $Q = 2$, $f = 1$, output time is 1, $Da = 31.192$ and $u_{ign} = 0.1$
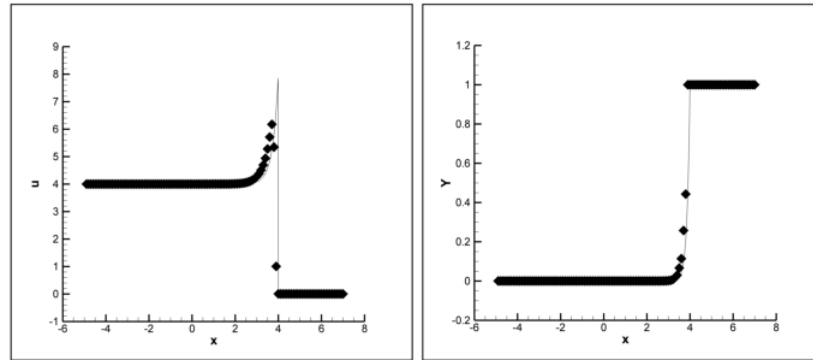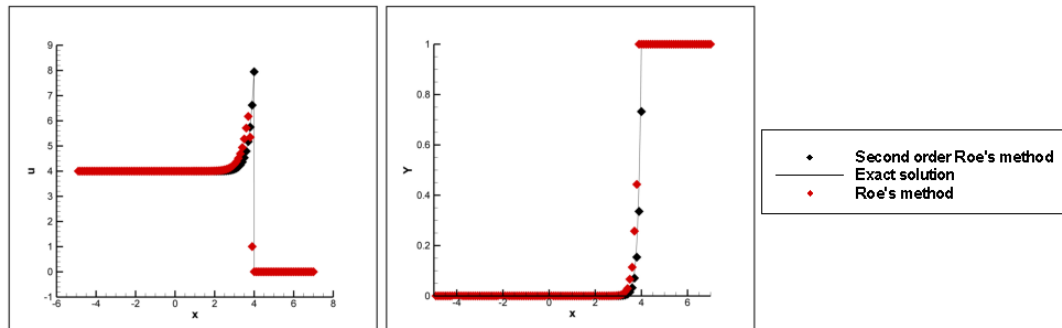

Figure 5.5: Comparison of the numerical solution of the Burgers' equation with second order Roe's method (black symbols) and Roe's method (red symbols) with the exact ZND solution (black line)

The comparison at the figure 5.5 shows the accuracy of the second order Roe's method in a simple case. The peak location and value at the variable u computed accurately.

5.3.3.2 Strong Detonation

The initial conditions are given as; $u_u = 0$, $\Delta t = 0.01$, $\Delta x = 0.1$, $Q = 2$, $f = 1$, output time is 1, $Da = 31.192$ and $u_{ign} = 0.1$

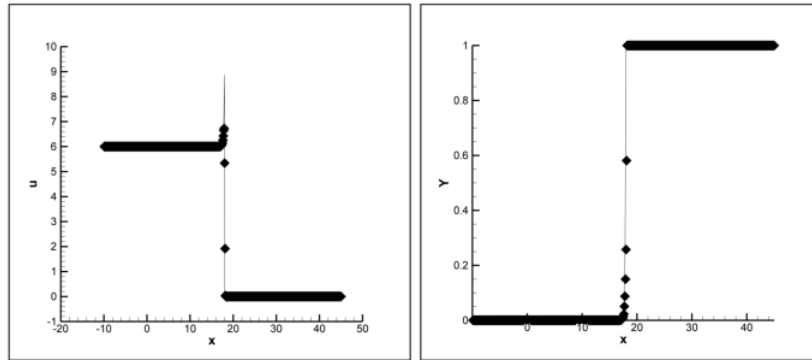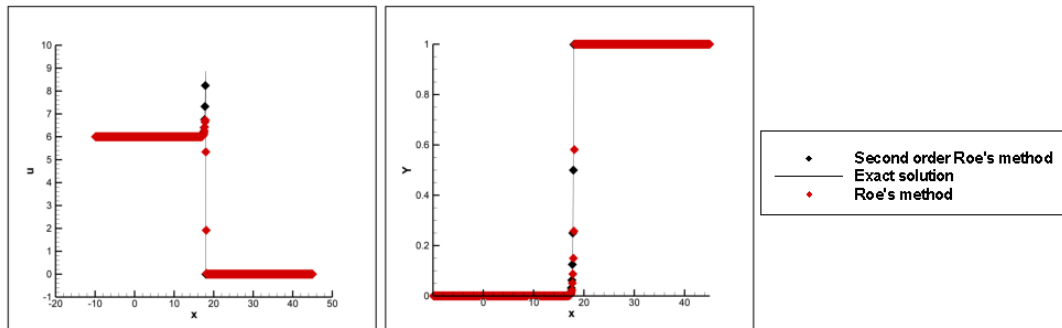Figure 5.6: Comparison of the numerical solution of the Burgers' equation with second order Roe's method (black symbols) and Roe's method (red symbols) with the exact ZND solution (black line)

At the above figure, second order Roe's method's accuracy is compared with a first order method. The peak location and value of u variable is not calculated correctly in the first order method. High resolution method solves the strong detonation with better accuracy than the first order method, but it is not successful as the numerical solution of the CJ detonation with high resolution method. Strong shocks is harder to solve as seen at the chapter 3.

More detailed results will be compared for the reactive Euler equation, using high resolution method with Superbee limiter using Roe's flux and the Strang time splitting method used. The detailed information on Strang time splitting method[33] is given at the chapter 6.

CHAPTER 6

NUMERICAL SOLUTION OF THE REACTIVE EULER EQUATIONS

In this chapter, the reactive Euler equations are solved numerically. The numerical solutions are obtained by using high resolution method. For high resolution method, Roe's flux is used with the slope limiter, Superbee limiter. For detailed information on the numerical method, one can refer to the chapter 3.

Solutions are obtained for two different detonations, CJ detonations and strong detonation. In these detonations, effects of the ignition temperature, activation energy, heat release and number of computing cells have been compared for different cases.

A FORTRAN code have been used in solving the reactive Euler equations. Flowchart of the FORTRAN code is given in the following sections.

The Strang splitting method used for the time splitting method. The Strang splitting method is given as;

$$U_{\Delta t}(.,t^{n+1}) = \mathcal{L}^c_{\Delta t/2}\mathcal{L}^f_{\Delta t}\mathcal{L}^c_{\Delta t/2}U_{\Delta t}(.,t^n) \tag{6.1}$$

where $\mathcal{L}^c_{\Delta t/2}$ is the solution operator for the solution of the chemical part of the problem, which is the case with the non-convective flux in this thesis and $\mathcal{L}^f_{\Delta t}$ is the solution operator for the solution of the fluid dynamical part, which the case with the no source term.

6.1 SOLUTION PROCEDURE

The system of the reactive Euler equations are given as;

$$\frac{\partial(\rho)}{\partial t} + \frac{\partial(\rho u)}{\partial x} = 0 \tag{6.2}$$

$$\frac{\partial(\rho u)}{\partial t} + \frac{\partial(\rho u^2 + p)}{\partial x} = 0 \tag{6.3}$$

$$\frac{\partial(\rho E)}{\partial t} + \frac{\partial(\rho u E + pu)}{\partial x} = 0 \tag{6.4}$$

$$\frac{\partial(\rho Y)}{\partial t} + \frac{\partial(\rho u Y)}{\partial x} = w \tag{6.5}$$

$$\tag{6.6}$$

where the reaction rate w calculated from;

$$w = \begin{cases} 0, & T < T_{ign} \\ -Dak\rho Y, & T \geq T_{ign} \end{cases} \tag{6.7}$$

where $k = e^{[Ea(1/T_{VN}-1/T)]}$.

When solving this problem numerically, the problem is separated into two parts, the chemical part and the fluid dynamic part. The chemical part is the part where the reaction of the equation is solved. So the convective flux term $\frac{\partial(.)}{\partial x}$ terms assumed to be zero, when solving chemical part. The fluid dynamic part is solved with assuming no source term, this way effects of the convective fluxes have been seen.

The FORTRAN code consist of 5 subroutines. These are READER, DOMAIN, BOUNDARY, SOLVER and OUTPUT. The READER subroutine is used for entering/reading the initial data for the problem. DOMAIN subroutine used to generate the domain and separate the left and right states for the problem. BOUNDARY subroutine applies the wanted boundary conditions on the problem. SOLVER subroutine is used for the numerical solution of the problem. The time splitting method, fluxes and advancing in time is done at this subroutine. Finally OUTPUT subroutine is used for the taking out of the output file. The flow chart of the FORTRAN code is given at the figure 6.1.
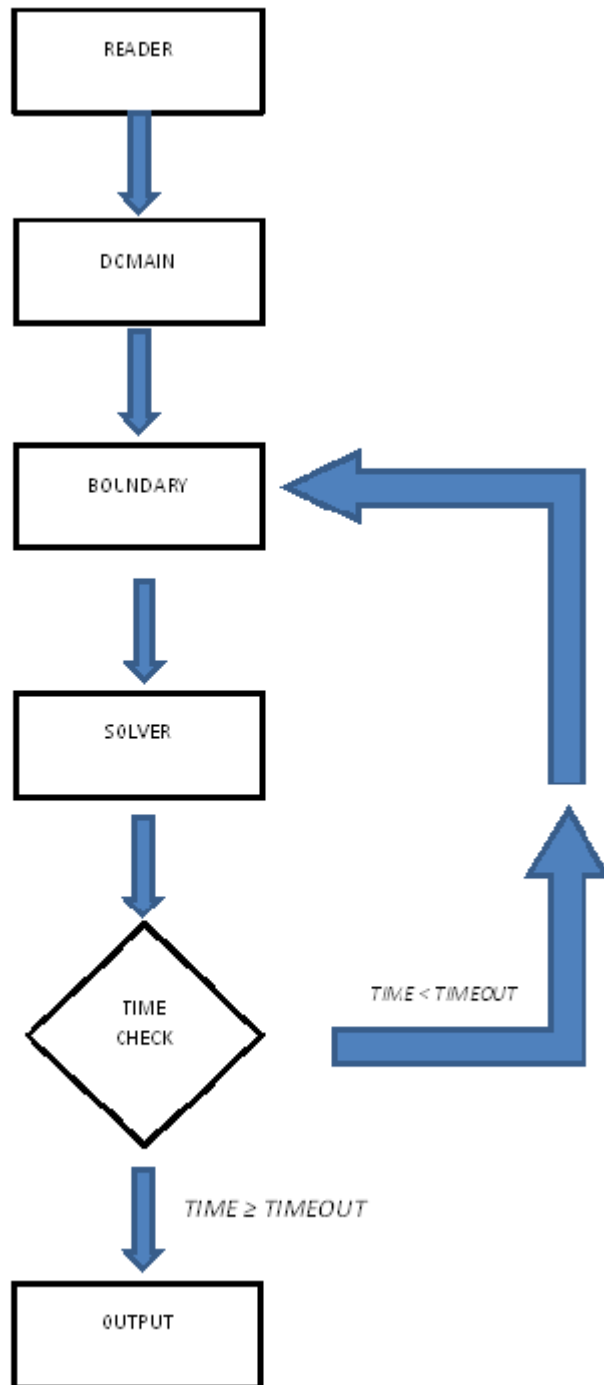
Figure 6.1: Flowchart of the FORTRAN code used to solve the reactive Euler equations

When solving the reactive Euler equations numerically, transmissive boundary conditions are used. which are;

$$U_0 = U_1 \qquad U_M = U_{M+1} \tag{6.8}$$

M is the number of the cells.

6.1.1 Computation of the Roe's flux

Roe's flux is computed from the equation 2.110. For the computation of the flux, $\bar{\alpha}_i$, $\bar{\lambda}_i$ and $\bar{K}^{(i)}$, needed to calculated.

In order to calculate eigenvalues, $\bar{\lambda}_i$ averaged Jacobian matrix has to be calculated first. The calculation steps of the averaged Jacobian matrix is given at the appendix A.

$$
\begin{bmatrix}
0 & 1 & 0 & 0 \\
-\frac{1}{2}(3-\gamma)\bar{u}^2 & (3-\gamma)\bar{u} & \gamma-1 & -(\gamma-1)Q \\
\bar{u}\left(\frac{1}{2}(\gamma-1)\bar{u}^2 - \bar{H}\right) & \bar{H}-(\gamma-1)\bar{u}^2 & \gamma\bar{u} & -(\gamma-1)Q\bar{u} \\
-\bar{Y}\bar{u} & \bar{Y} & 0 & \bar{u}
\end{bmatrix}
\tag{6.9}
$$

The averaged variables are calculated as;

$$
\bar{u} = \frac{\sqrt{\rho_L}u_L + \sqrt{\rho_R}u_R}{\rho_L + \rho_R}
\tag{6.10}
$$

$$
\bar{H} = \frac{\sqrt{\rho_L}H_L + \sqrt{\rho_R}H_R}{\rho_L + \rho_R}
\tag{6.11}
$$

$$
\bar{Y} = \frac{\sqrt{\rho_L}Y_L + \sqrt{\rho_R}Y_R}{\rho_L + \rho_R}
\tag{6.12}
$$

$$
\bar{a} = \sqrt{(\gamma-1)(\bar{H}-0.5\bar{u}^2}
\tag{6.13}
$$

$$
\tag{6.14}
$$

According to the averaged Jacobian matrix eigenvalues $\bar{\lambda}_i$ are calculated as;

$$
\bar{\lambda}_1 = \bar{u} - \bar{a}
\tag{6.15}
$$

$$
\bar{\lambda}_2 = \bar{u}
\tag{6.16}
$$

$$
\bar{\lambda}_3 = \bar{u}
\tag{6.17}
$$

$$
\bar{\lambda}_4 = \bar{u} - \bar{a}
\tag{6.18}
$$

$$
\tag{6.19}
$$

From the founded eigenvalues, right eigenvectors, $\bar{K}^{(i)}$, calculated as;

$$\bar{K}^{(1)} = [1, \bar{u} - \bar{a}, \bar{H} - \bar{u}\bar{a}, \bar{Y}]^T \tag{6.20}$$

$$\bar{K}^{(2)} = [1, \bar{u}, 0.5\bar{u}^2, 0]^T \tag{6.21}$$

$$\bar{K}^{(3)} = [0, 0, Q, 1]^T \tag{6.22}$$

$$\bar{K}^{(4)} = [1, \bar{u} + \bar{a}, \bar{H} + \bar{u}\bar{a}, \bar{Y}]^T \tag{6.23}$$

$$\tag{6.24}$$

The computation of the eigenvalues and eigenvector are given in the appendix B. The methodology for the computation of the Jacobian matrix, eigenvalues and eigenvector is given at the chapter 1.

From the equation 2.101 wave strengths, $\bar{\alpha}_i$ computed as;

$$\bar{\alpha}_2 = \Delta u_1(Q\bar{Y} + \bar{u}^2 - \bar{H}) - \Delta u_2\bar{u} + \Delta u_3 - Q\Delta u_4 \tag{6.25}$$

$$\bar{\alpha}_3 = \bar{\alpha}_2\bar{Y} + \Delta u_4 - \bar{Y}\Delta u_1 \tag{6.26}$$

$$\bar{\alpha}_4 = \frac{\Delta u_2 + (\bar{a} - \bar{u})\Delta u_1 - \bar{\alpha}_2\bar{a}}{2\bar{a}} \tag{6.27}$$

$$\bar{\alpha}_1 = \Delta u_1 - \bar{\alpha}_4 - \bar{\alpha}_2 \tag{6.28}$$

$$\tag{6.29}$$

with the given matrix;

$$\Delta U = \begin{bmatrix} \rho_R - \rho_L \\ (\rho u)_R - (\rho u)_L \\ (\rho E)_R - (\rho E)_L \\ (\rho Y)_R - (\rho Y)_L \end{bmatrix} = \begin{bmatrix} \Delta u_1 \\ \Delta u_2 \\ \Delta u_3 \\ \Delta u_4 \end{bmatrix} \tag{6.30}$$

The computation of the wave strengths is given at the appendix C.

6.1.2 Computation of the Fluid Dynamic Part

Assuming no source term, reactive Euler equations become;

$$\frac{\partial(\rho)}{\partial t} + \frac{\partial(\rho u)}{\partial x} = 0 \tag{6.31}$$

$$\frac{\partial(\rho u)}{\partial t} + \frac{\partial(\rho u^2 + p)}{\partial x} = 0 \tag{6.32}$$

$$\frac{\partial(\rho E)}{\partial t} + \frac{\partial(\rho u E + pu)}{\partial x} = 0 \tag{6.33}$$

$$\frac{\partial(\rho Y)}{\partial t} + \frac{\partial(\rho u Y)}{\partial x} = 0 \tag{6.34}$$

$$\tag{6.35}$$

The above equation set can be calculated using second order Roe's method. Detailed information is given at the chapter 3.

6.1.3 Computation of the Chemical Part

Assuming the convective flux term to be zero, reactive Euler equations become;

$$\frac{\partial(\rho Y)}{\partial t} + \frac{\partial(\rho u Y)}{\partial x} = 0 \tag{6.36}$$

The solution of the above ordinary differential equation is solved by implicit Euler method. Implicit Euler method is formulated as;

$$Y_i^{n+1} = Y_i^n + \Delta t f(Y_i^{n+1}) \tag{6.37}$$

where f function is the derivate of the Y.

6.2 RESULTS

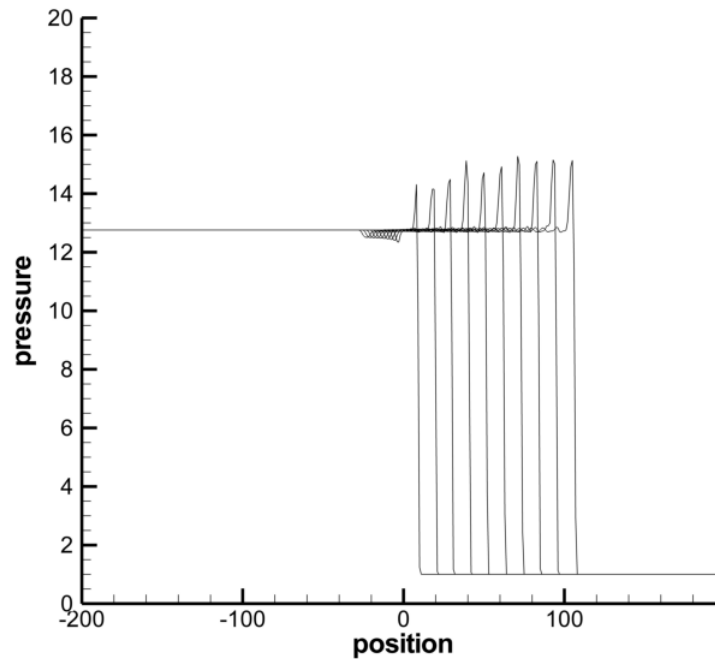First movement of the detonation wave is analyzed.

Figure 6.2: Movement of the detonation wave with output time at 2, 4, 6, 8, 10, 12, 14, 16, 18 and 20 units.

From the figure 6.2, the movement of the detonation wave is seen with an increase in time. At the first time steps, the peak value has not been reached for the pressure. With an increase in time, pressure peak value has been increased and come to a stable peak value. Therefore for examining the numerical solution of the reactive Euler equations, 30 unit output time will be used.

As the detonation wave moves, there exist oscillations at the start of the shock wave. These oscillations follow the movement of the detonation wave. These oscillations occur because of the Strang time splitting method. The Strang time splitting method creates errors at discontinuous regions but these errors are not affecting the whole solution[5].

90

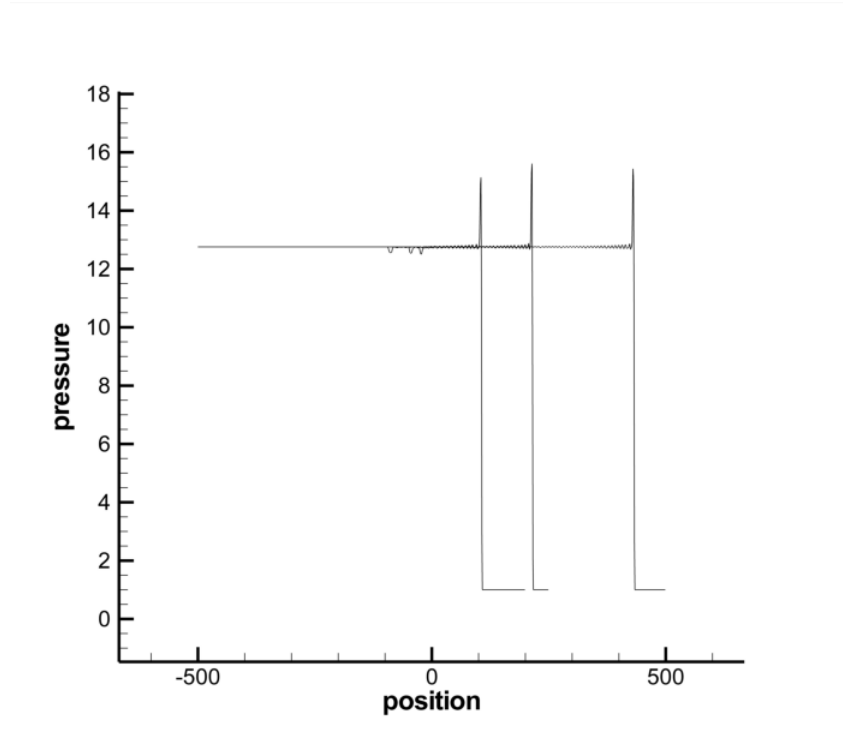Figure 6.3: Movement of the detonation wave with output time at 20, 40 and 80 units.

To understand the movement of the oscillations, more detailed view is given at the figure 6.3. From the detailed view, it is seen that, oscillations continue in the solution domain as the detonation wave moves and oscillations follow the detonation wave.
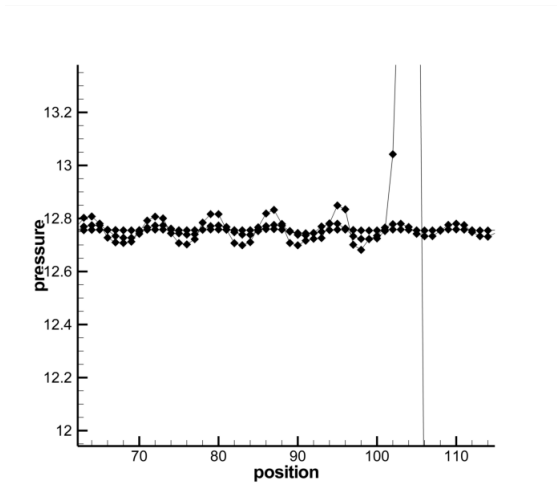
Figure 6.4: Detailed view of the oscillation at output time 20.
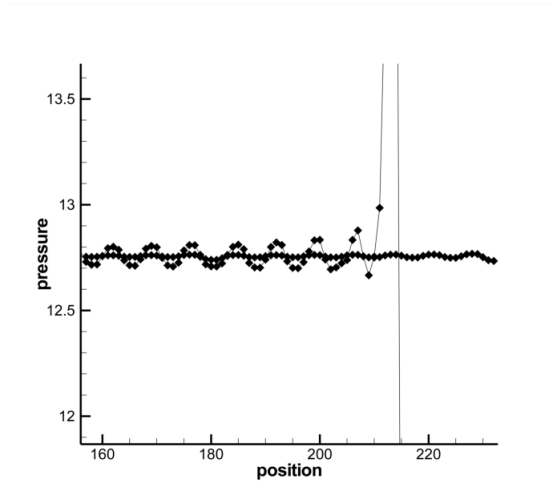
Figure 6.5: Detailed view of the oscillation at output time 40.
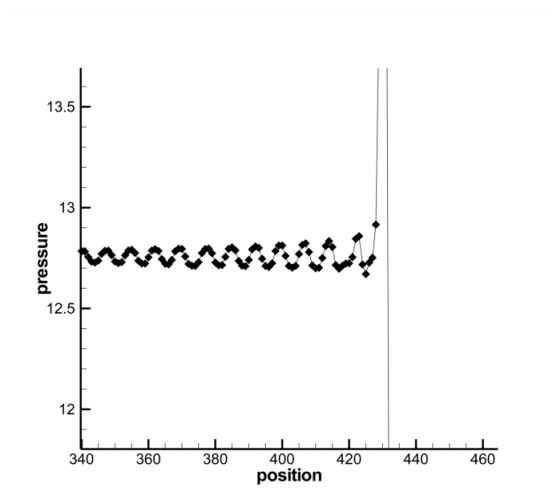
Figure 6.6: Detailed view of the oscillation at output time 80

From looking at the figures 6.4, 6.5 and 6.6 the amplitude of the oscillation is seen. The amplitude of the oscillation is slightly increased with movement of the detonation wave. But this increase is small enough to neglect. Because it does not affect the solution.

After investigation of movement of the detonation problem, the detonation problem will be studied in two section, the CJ detonation and the strong detonation. Comparison of the results and comments on the results are given below. To check the numerical accuracy, pressure and mass fraction values are compared with the exact solution.

6.2.1 CJ Detonation

For CJ detonation, degree of overdrive, $f = 1.0$.

6.2.1.1 Test case 1

For the test case 1, $\rho_u = 1$, $u_u = 0$, $p_u = 1$, discontinuity position is at, $x_0 = 0$, domain length is between $[-250, 250]$, cell number is $M = 500$, $\gamma = 1.4$, $Da = 64.88$, $E_a = 14$, $Q = 14$, output time is at 30 with $\Delta t = 0.1$, the reference temperature, $T_{VN} = 5.0509$, $T_{ign} = 4.0$. The speed of the detonation wave is calculated as 5.44186.

At the figures 6.7 and 6.8, the numerical solution of the test case 1 compared with the exact ZND solution for that case. For this case, a fast detonation takes place. There is a sudden peak value at the solution. Because Da is large, the detonation has to be fast. When looked at the comparison of the pressure peak, the numerical solution can not reach the pressure peak calculated in the exact solution case but an increase is seen at the pressure value. Nevertheless, pressure peaks are resolved in 5 cells.

Figure 6.7: Numerical solution of the reactive Euler equations (red symbols) for CJ detonation, comparing with the exact ZND solution (black line) for the test case 1.

Figure 6.8: Numerical solution of the reactive Euler equations (red symbols) for CJ detonation, comparing with the exact ZND solution (black line) for the test case 1.

6.2.1.2 Test case 2

For the test case 2, Da number have been decreased. $\rho_u = 1$, $u_u = 0$, $p_u = 1$, discontinuity position is at, $x_0 = 0$, domain length is between $[-250, 250]$, cell number is $M = 500$, $\gamma = 1.4$, $Da = 0.6488$, $E_a = 14$, $Q = 14$, output time is at 30 with $\Delta t = 0.1$, the reference temperature, $T_{VN} = 5.0509$, $T_{ign} = 4.0$. The speed of the detonation wave is calculated as 5.44186.

The figures 6.9 and 6.10 show a slower chemical reaction due to Da number. At the previous chapters it has been told, numerical solution of the discontinuities is hard to compute with a good accuracy, when a slow chemical reaction takes place. From these figures it is seen that, for low Da number, numerical solution is not computed accurately. There exist a small discontinuity at the start of the detonation, when looked at the pressure peak. It is a weak detonation and at the weak detonation, all heat is released and the CJ detonation can not be occur. In the ZND theory, weak detonations are not expected, so this case is a numerically wrong solution.
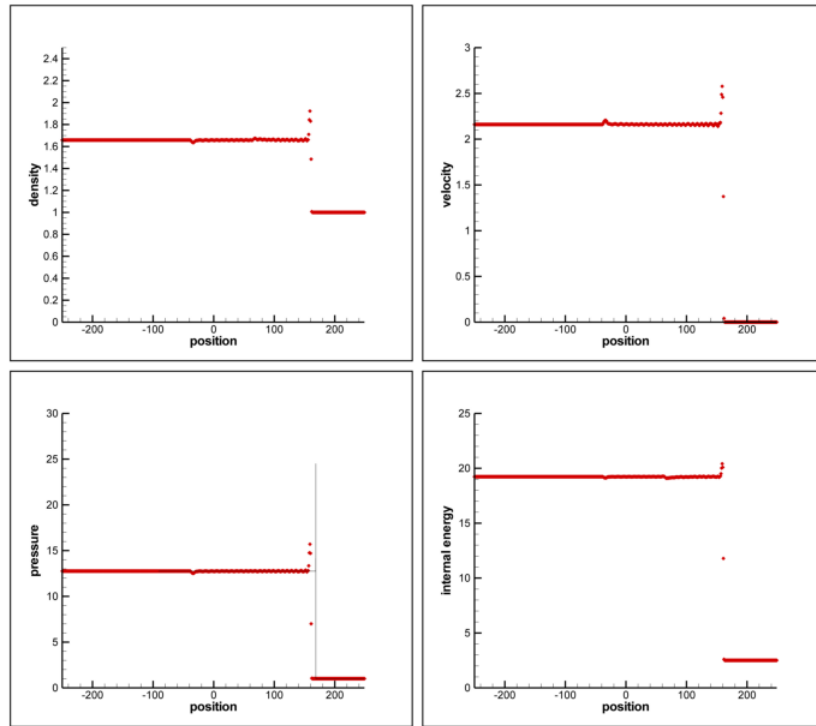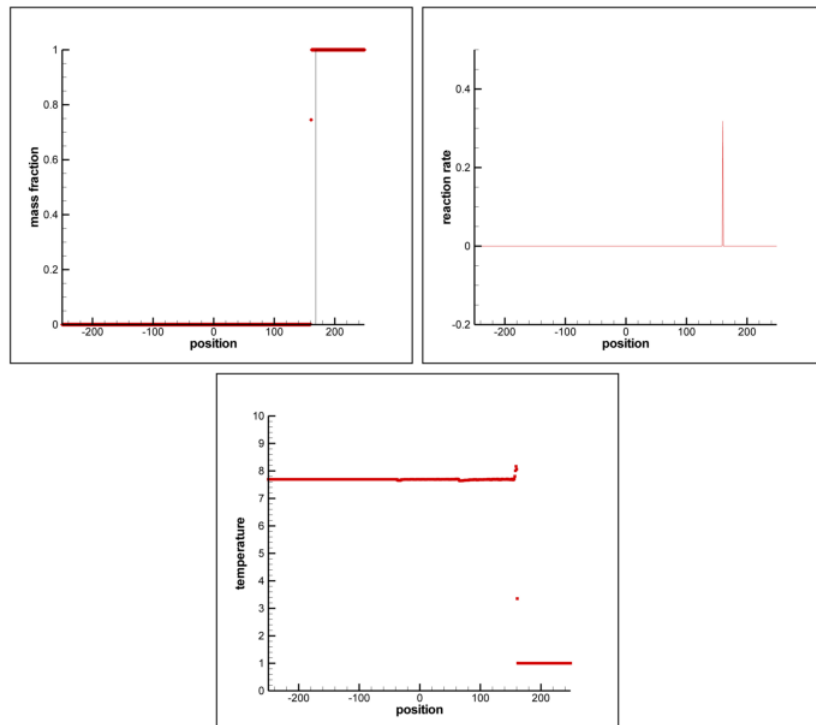
Figure 6.9: Numerical solution of the reactive Euler equations (red symbols) for CJ detonation, comparing with the exact ZND solution (black line) for the test case 2.

Figure 6.10: Numerical solution of the reactive Euler equations (red symbols) for CJ detonation, comparing with the exact ZND solution (black line) for the test case 2.

6.2.1.3 Test case 3

For the test case 3, Da number have been increased. $\rho_u = 1$, $u_u = 0$, $p_u = 1$, discontinuity position is at, $x_0 = 0$, domain length is between $[-250, 250]$, cell number is $M = 500$, $\gamma = 1.4$, $Da = 6488$, $E_a = 14$, $Q = 14$, output time is at 30 with $\Delta t = 0.1$, the reference temperature, $T_{VN} = 5.0509$, $T_{ign} = 4.0$. The speed of the detonation wave is calculated as 5.44186.

The figures 6.11 and 6.12 show a faster chemical reaction due to Da number. As it seen from the figure, the numerical solution is have the same accuracy as in the solution of the test case 1. The pressure peak values calculated nearly the same as test case 1 and the mass fractions are in the same behavior. But in this case the chemical reaction happens fast, so the reaction rate can not calculated accurately. For calculating the reaction rate accurately, cells number has to be increased. For faster chemical reactions finer mesh is required in order to collect a true solution.
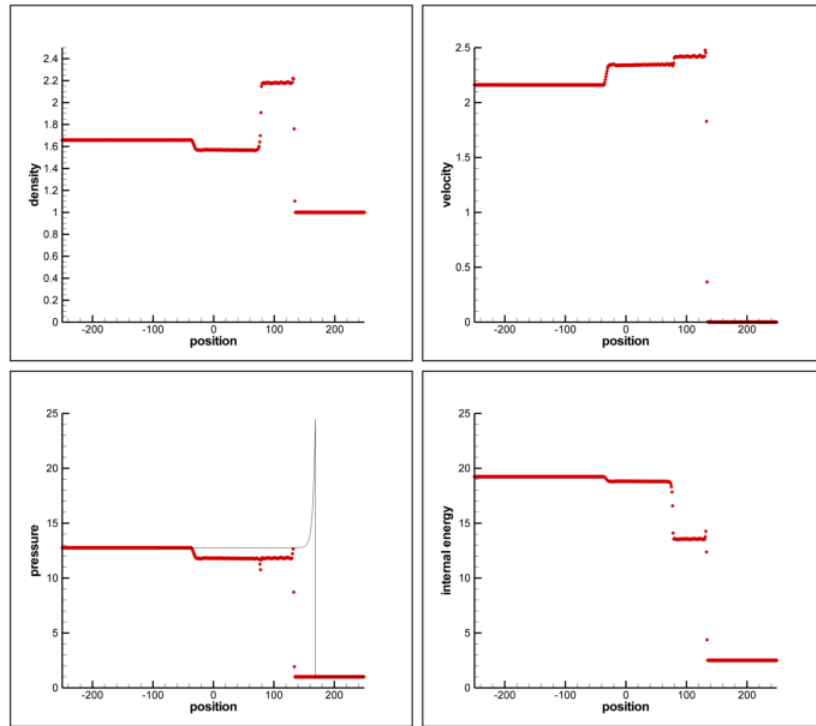
Figure 6.11: Numerical solution of the reactive Euler equations (red symbols) for CJ detonation, comparing with the exact ZND solution (black line) for the test case 3.

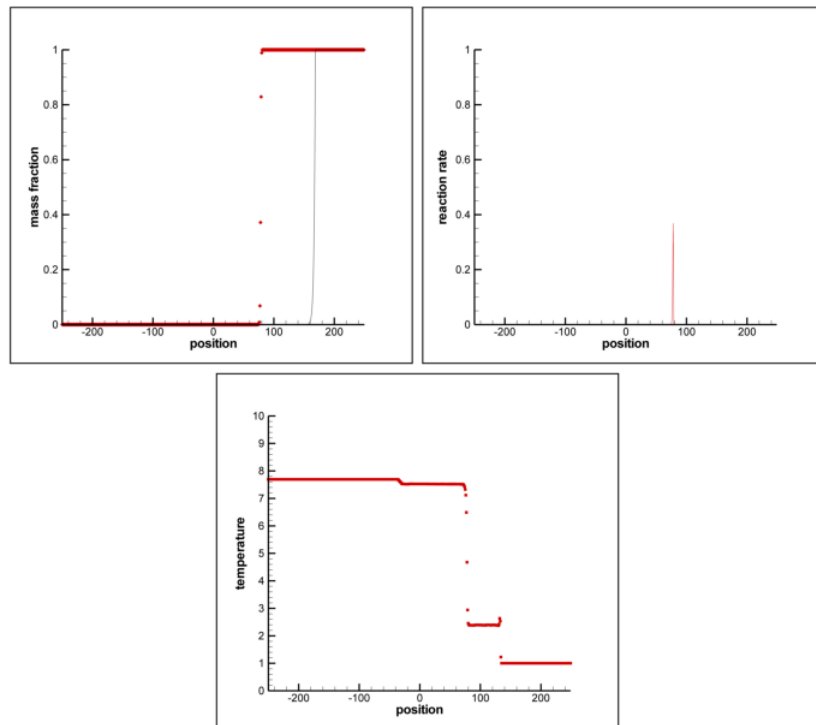
Figure 6.12: Numerical solution of the reactive Euler equations (red symbols) for CJ detonation, comparing with the exact ZND solution (black line) for the test case 3.

6.2.1.4 Test case 4

For the test case 4, cell number have been increased and time step is decreased to $\Delta t = 0.0125$. $\rho_u = 1$, $u_u = 0$, $p_u = 1$, discontinuity position is at, $x_0 = 0$, domain length is between $[-250, 250]$, cell number is $M = 4000$, $\gamma = 1.4$, $Da = 6488$, $E_a = 14$, $Q = 14$, output time is at 30 with $\Delta t = 0.0125$, the reference temperature, $T_{VN} = 5.0509$, $T_{ign} = 4.0$. The speed of the detonation wave is calculated as 5.44186.

At the previous test case, the reaction rate is not computed accurately, therefore the cell number has been increased. With increasing the cell number of the solution domain, time step has to be chosen smaller because of the stability reasons. Otherwise solution can not be obtained. From looking at figures 6.13 and 6.14, finer mesh results in a more accurate solution. The error due to oscillations have been decreased with a finer mesh but still reaction rate can not be calculated correctly. Therefore more finer mesh required. As mentioned before, the increase in the cell number requires decrease in the time step, which results in a more expensive solution.
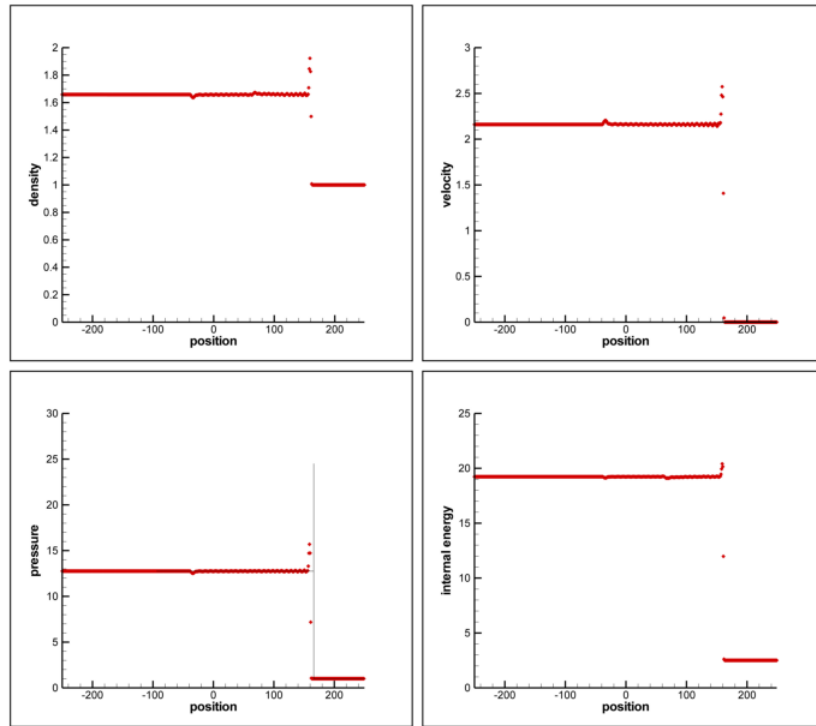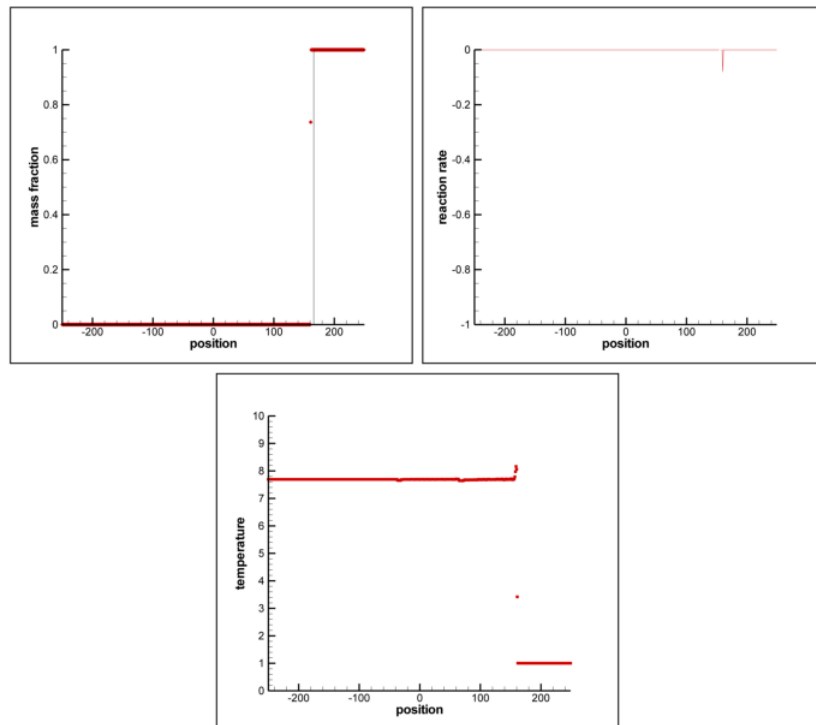
Figure 6.13: Numerical solution of the reactive Euler equations (red symbols) for CJ detonation, comparing with the exact ZND solution (black line) for the test case 4.

Figure 6.14: Numerical solution of the reactive Euler equations (red symbols) for CJ detonation, comparing with the exact ZND solution (black line) for the test case 4.

6.2.1.5   Test case 5

For the test case 5, cell number have been increased and time step is decreased to $\Delta t = 0.005$. $\rho_u = 1$, $u_u = 0$, $p_u = 1$, discontinuity position is at, $x_0 = 0$, domain length is between $[-250, 250]$, cell number is $M = 10000$, $\gamma = 1.4$, $Da = 6488$, $E_a = 14$, $Q = 14$, output time is at 30 with $\Delta t = 0.005$, the reference temperature, $T_{VN} = 5.0509$, $T_{ign} = 4.0$. The speed of the detonation wave is calculated as 5.44186.

This time computing cell number is increased to 40000, which is higher than test case 4. At test case 5, reaction rate can be calculated in exchange of longer numerical solution time. The finer mesh is seen at figures 6.15 and 6.16. There is a small increase at pressure peak value with finer mesh. Because of the detonation phenomena happens fast, capturing peak value with more computing cells is very expensive.

Figure 6.15: Numerical solution of the reactive Euler equations (red symbols) for CJ detonation, comparing with the exact ZND solution (black line) for the test case 5.

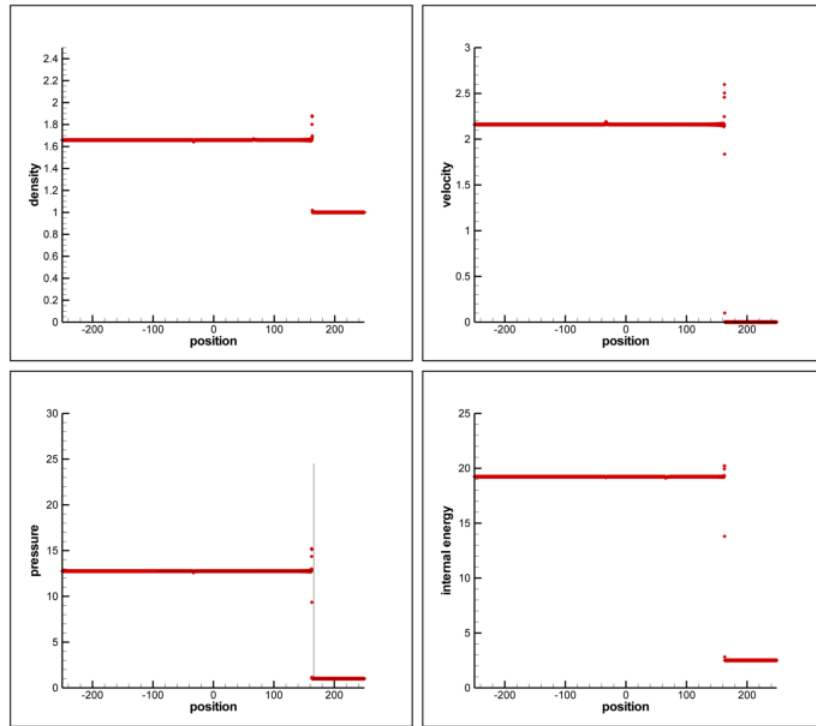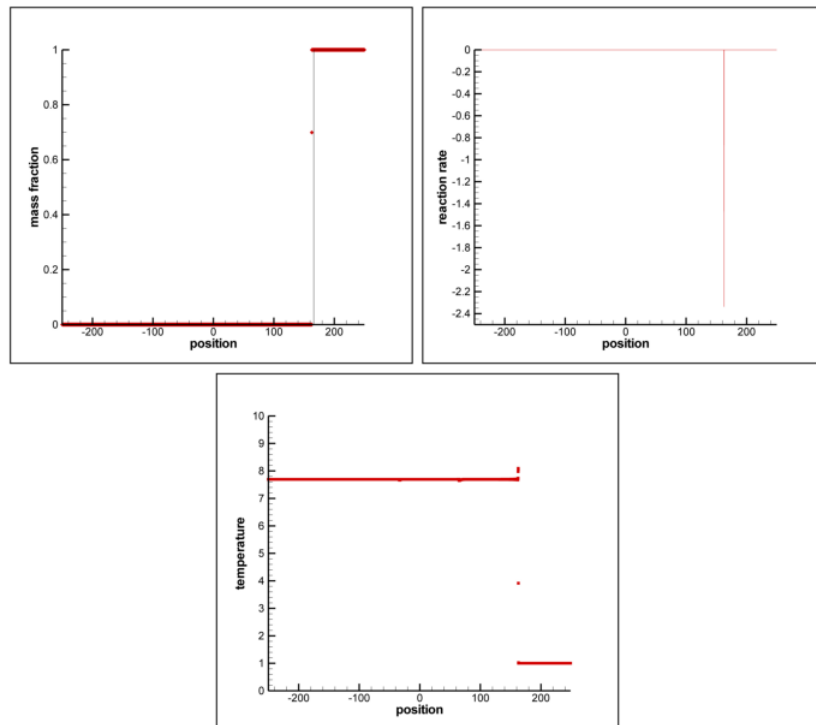
Figure 6.16: Numerical solution of the reactive Euler equations (red symbols) for CJ detonation, comparing with the exact ZND solution (black line) for the test case 5.

6.2.1.6 Test case 6

For the test case 6, cell number have been decreased and time step is stayed constant. $\rho_u = 1$, $u_u = 0$, $p_u = 1$, discontinuity position is at, $x_0 = 0$, domain length is between $[-250, 250]$, cell number is $M = 4000$, $\gamma = 1.4$, $Da = 6488$, $E_a = 14$, $Q = 14$, output time is at 30 with $\Delta t = 0.00125$, the reference temperature, $T_{VN} = 5.0509$, $T_{ign} = 4.0$. The speed of the detonation wave is calculated as 5.44186.

The only difference between test case 5 and test case 6 is the number of computing cells. But there are huge differences at the solution of test case 5 and test case 6. The solution of the test case 6 is given at figures 6.17 and 6.18. From comparison of the test case 5 and test case 6 shows that appropriate number of computing cells has to be chosen with the time step. Otherwise, unrealistic solutions or inaccurate solutions can be calculated.

Figure 6.17: Numerical solution of the reactive Euler equations (red symbols) for CJ detonation, comparing with the exact ZND solution (black line) for the test case 6.
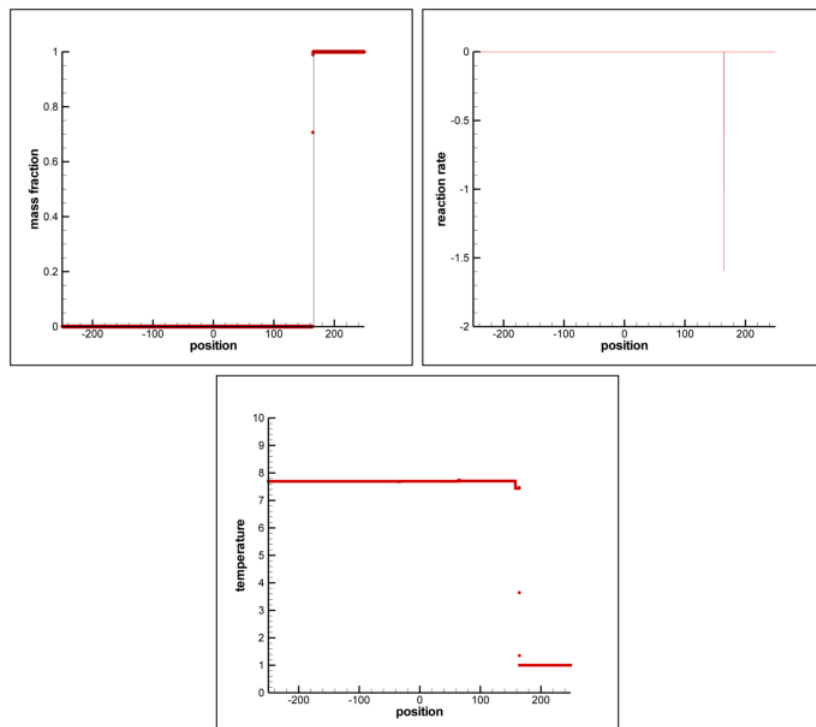
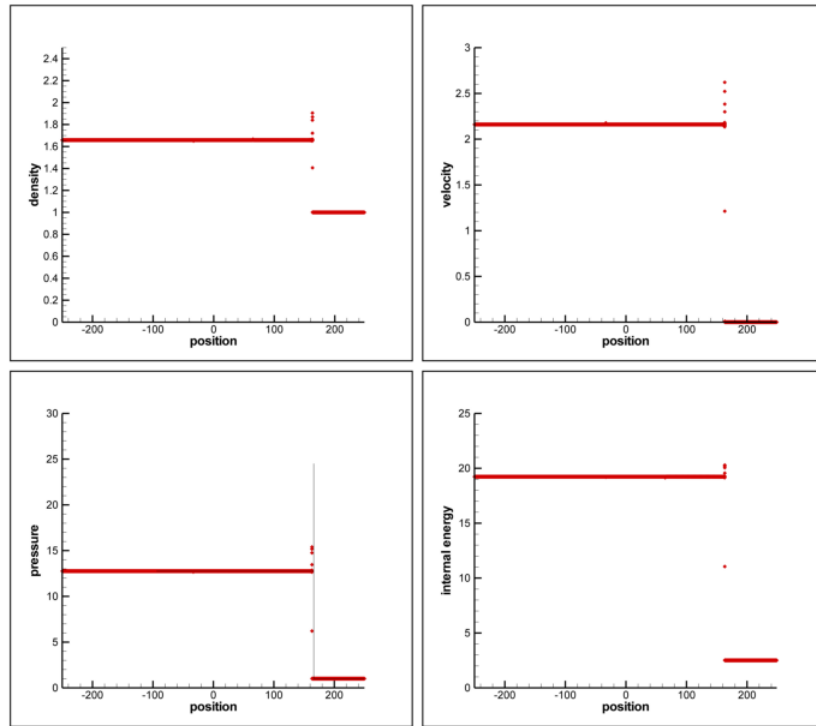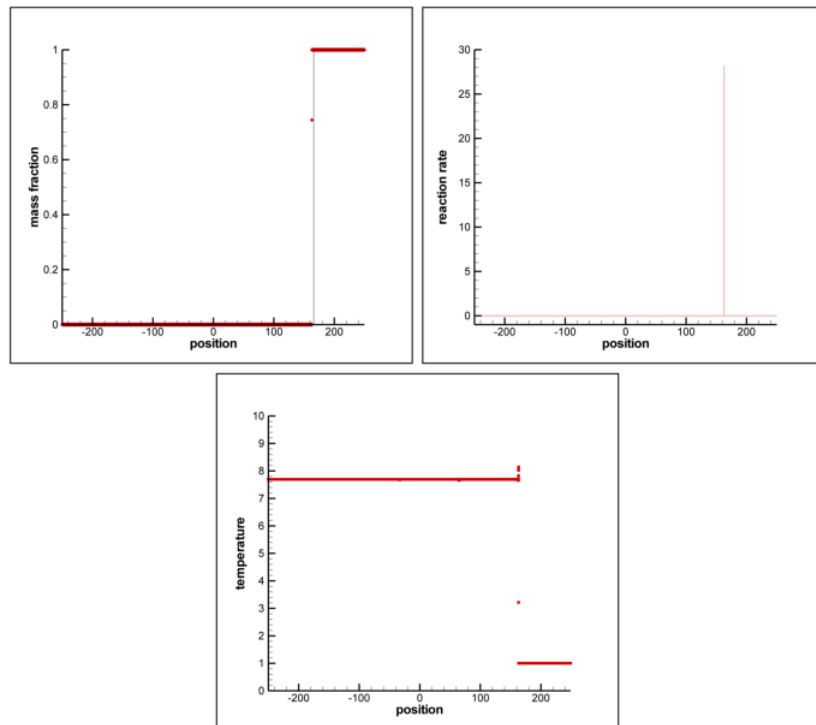
Figure 6.18: Numerical solution of the reactive Euler equations (red symbols) for CJ detonation, comparing with the exact ZND solution (black line) for the test case 6.

6.2.1.7 Test case 7

For the test case 7, activation energy have been increased to 50 and heat release increased to 25. $\rho_u = 1$, $u_u = 0$, $p_u = 1$, discontinuity position is at, $x_0 = 0$, domain length is between $[-250, 250]$, cell number is $M = 500$, $\gamma = 1.4$, $Da = 0.6488$, $E_a = 14$, $Q = 14$, output time is at 30 with $\Delta t = 0.1$, the reference temperature, $T_{VN} = 5.0509$, $T_{ign} = 4.0$. The speed of the detonation wave is calculated as 7.12470.

As seen from the figures 6.19 and 6.20, with the increasing the activation energy and heat release, a slow chemical reaction due to small Da number is solved by numerically. The increase in the activation energy have increased the burned pressured value, so a stronger shock is observed. Because of the strong shock, oscillations behind the shock increases and the misalignment between the start of the detonation at the numerical solution and at the exact solution increase.

Figure 6.19: Numerical solution of the reactive Euler equations (red symbols) for CJ detonation, comparing with the exact ZND solution (black line) for the test case 7.

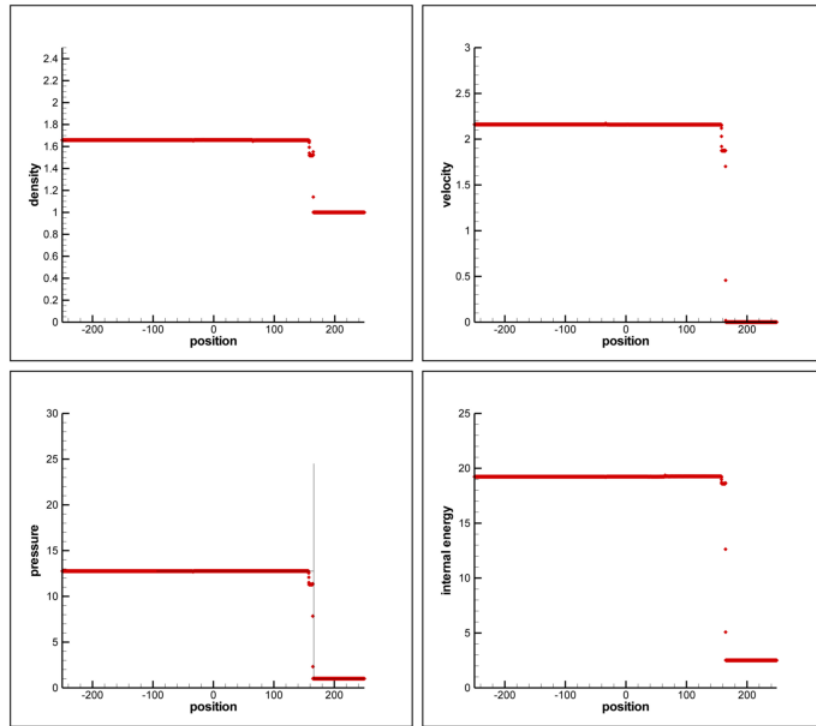
Figure 6.20: Numerical solution of the reactive Euler equations (red symbols) for CJ detonation, comparing with the exact ZND solution (black line) for the test case 7.

6.2.2   Strong Detonation

For strong detonation, degree of overdrive has to be, $f > 1$.

6.2.2.1   Test case 1

For the test case 1, degree of overdrive, $f = 1.1$, $\rho_u = 1$, $u_u = 0$, $p_u = 1$, discontinuity position is at, $x_0 = 0$, domain length is between $[-250, 250]$, cell number is $M = 5000$, $\gamma = 1.4$, $Da = 66.201$, $E_a = 10$, $Q = 10$, output time is at 30 with $\Delta t = 0.01$, the reference temperature, $T_{VN} = 5.2838$, $T_{ign} = 4.0$. The speed of the detonation wave is calculated as 4.90934.

The numerical solution of the strong detonation is seen from the figures 6.21 and 6.22. The reaction rate is sampled for strong detonation case successfully. The reaction rate for strong detonation is higher than CJ detonation case even for a low degree of overdrive, so it is easier to compute numerically. There are still some oscillations behind the shock. The peak value could not achieved numerically as seen from the pressure comparison.

Figure 6.21: Numerical solution of the reactive Euler equations (red symbols) for strong detonation, comparing with the exact ZND solution (black line) for the test case 1.
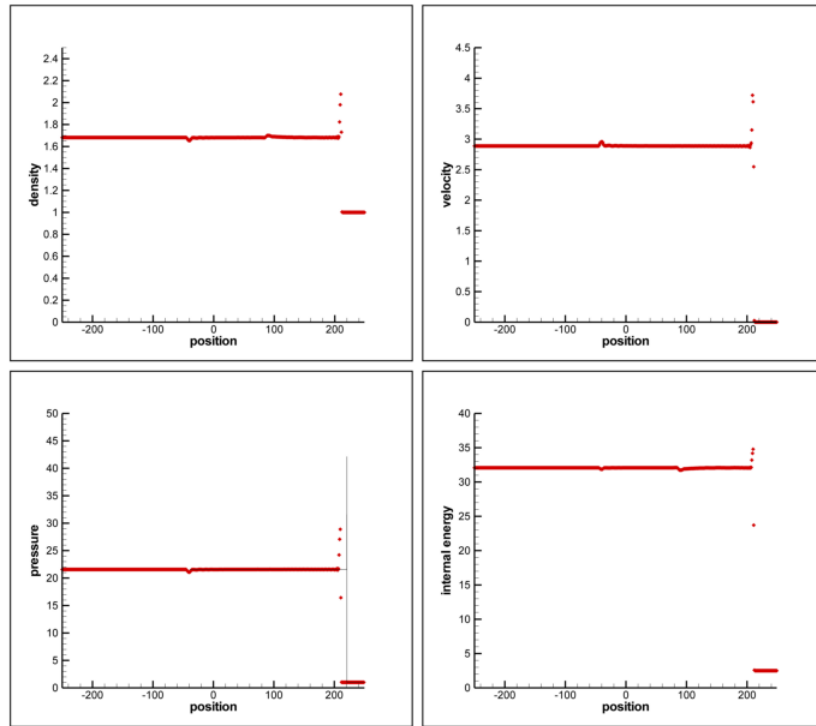

Figure 6.22: Numerical solution of the reactive Euler equations (red symbols) for strong detonation, comparing with the exact ZND solution (black line) for the test case 1.
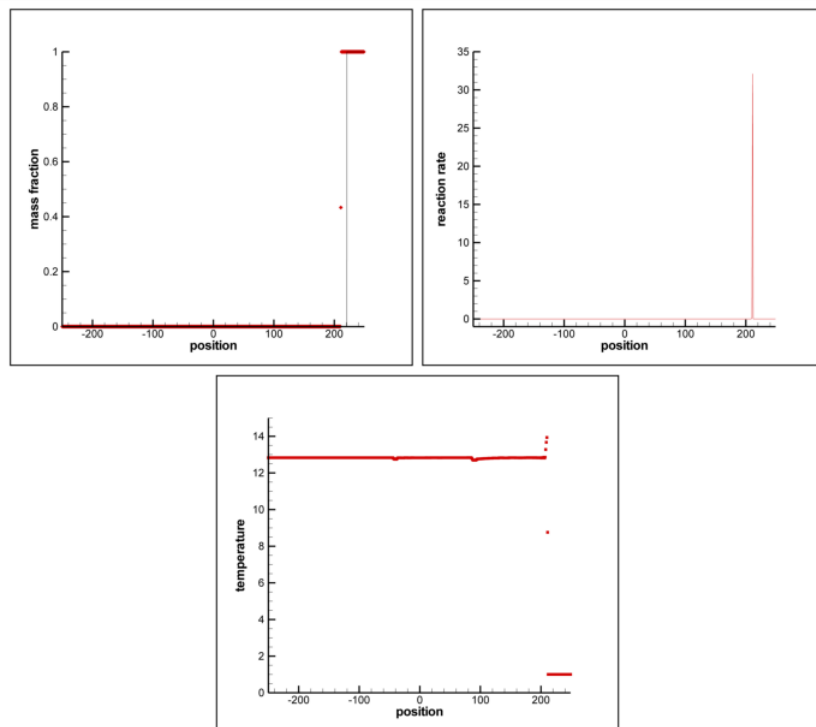
6.2.2.2 Test case 2

For the test case 2, degree of overdrive has been increased, $f = 1.7$, $\rho_u = 1$, $u_u = 0$, $p_u = 1$, discontinuity position is at, $x_0 = 0$, domain length is between $[-250, 250]$, cell number is $M = 5000$, $\gamma = 1.4$, $Da = 66.201$, $E_a = 10$, $Q = 10$, output time is at 30 with $\Delta t = 0.01$, the reference temperature, $T_{VN} = 5.2838$, $T_{ign} = 4.0$. The speed of the detonation wave is calculated as 6.10311.

In test case 2 at figures 6.23 and 6.24, detonation speed has been increased with increasing the degree of overdrive. Increase in the detonation speed decreases oscillations that are come from the time splitting method. The reason of this, is peak value can not be calculated so effect of the chemical part of the solution have been decreased. Therefore with increasing the detonation speed, numerical solution requires finer mesh.

Figure 6.23: Numerical solution of the reactive Euler equations (red symbols) for strong detonation, comparing with the exact ZND solution (black line) for the test case 2.
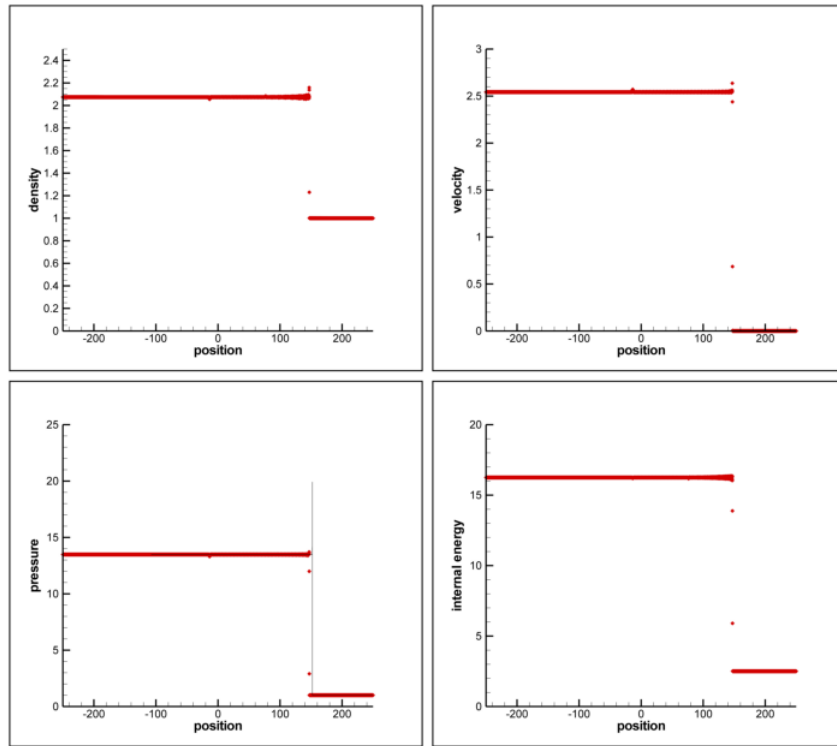

Figure 6.24: Numerical solution of the reactive Euler equations (red symbols) for strong detonation, comparing with the exact ZND solution (black line) for the test case 2.

6.2.2.3 Test case 3

For the test case 3, degree of overdrive has been increased, $f = 2.5$, $\rho_u = 1$, $u_u = 0$, $p_u = 1$, discontinuity position is at, $x_0 = 0$, domain length is between $[-250, 250]$, cell number is $M = 5000$, $\gamma = 1.4$, $Da = 66.201$, $E_a = 10$, $Q = 10$, output time is at 30 with $\Delta t = 0.01$, the reference temperature, $T_{VN} = 5.2838$, $T_{ign} = 4.0$. The speed of the detonation wave is calculated as 7.40111.

In this case, degree of overdrive is increased furthermore. Now, detonation speed is higher than test case 2. From the figures 6.25 and 6.26, there is not any peak in the solution, therefore oscillations are lost. The effect of the chemical part is decreased and when looked at the exact solution of the pressure peak value, effect of the chemical reaction in the exact solution is also decreased.
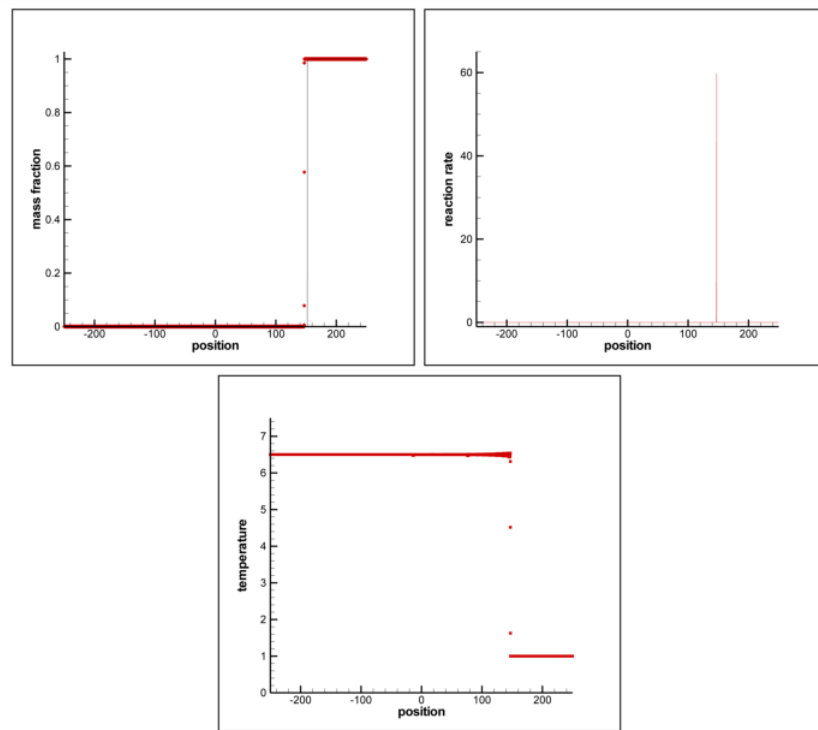
Figure 6.25: Numerical solution of the reactive Euler equations (red symbols) for strong detonation, comparing with the exact ZND solution (black line) for the test case 3.

Figure 6.26: Numerical solution of the reactive Euler equations (red symbols) for strong detonation, comparing with the exact ZND solution (black line) for the test case 3.

6.2.2.4 Test case 4

For the test case 4, ignition temperature has been decreased, $f = 1.1, \rho_u = 1$, $u_u = 0$, $p_u = 1$, discontinuity position is at, $x_0 = 0$, domain length is between $[-250, 250]$, cell number is $M = 5000$, $\gamma = 1.4$, $Da = 66.201$, $E_a = 10$, $Q = 10$, output time is at 30 with $\Delta t = 0.01$, the reference temperature, $T_{VN} = 5.2838$, $T_{ign} = 1.01$. The speed of the detonation wave is calculated as 4.90934.

When looked figures 6.27 and 6.28, numerical solution of the conservative variables seems to be same with the test case 1, which has higher ignition temperature. But at test case 4, at the calculation of the reaction rate, there seems to be a difference with test case 1. Because of the higher ignition temperature, reaction happens faster than test case 4, because when temperature drops below the ignition temperature, chemical reaction stops. Therefore with higher ignition temperature, reaction rate has to be larger.
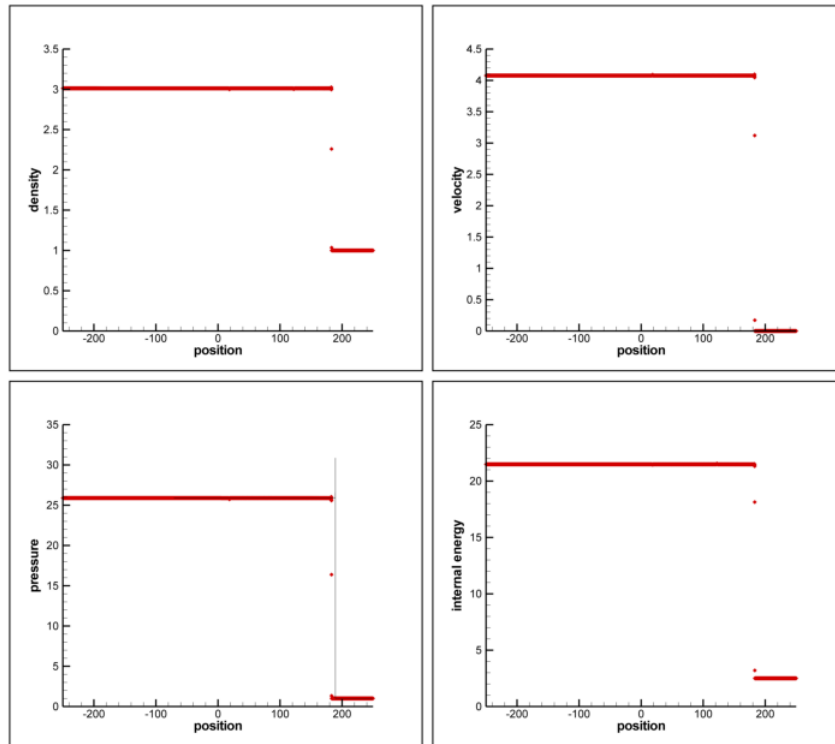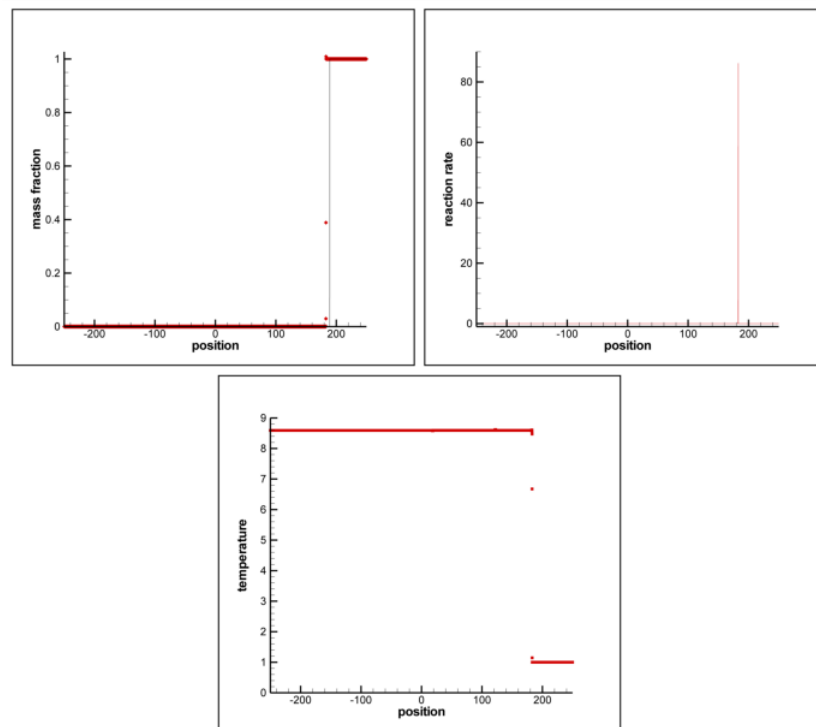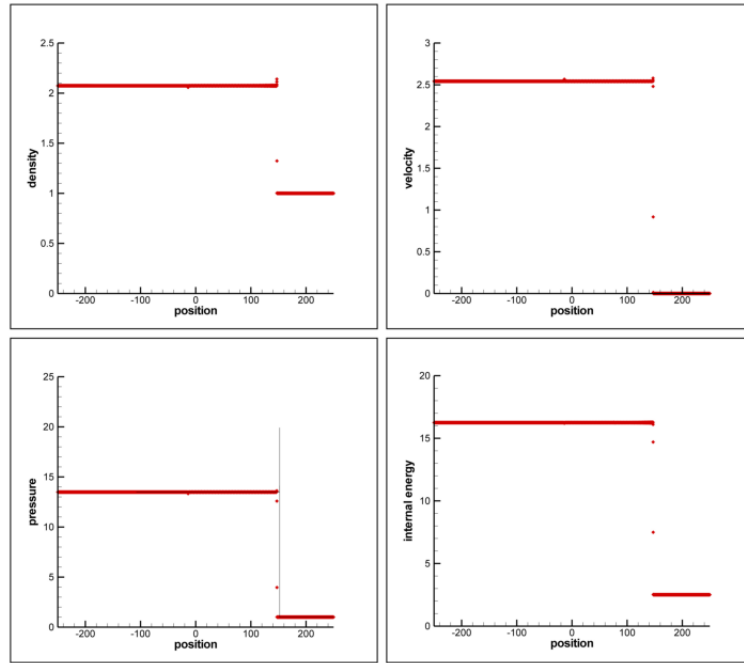
Figure 6.27: Numerical solution of the reactive Euler equations (red symbols) for strong detonation, comparing with the exact ZND solution (black line) for the test case 4.
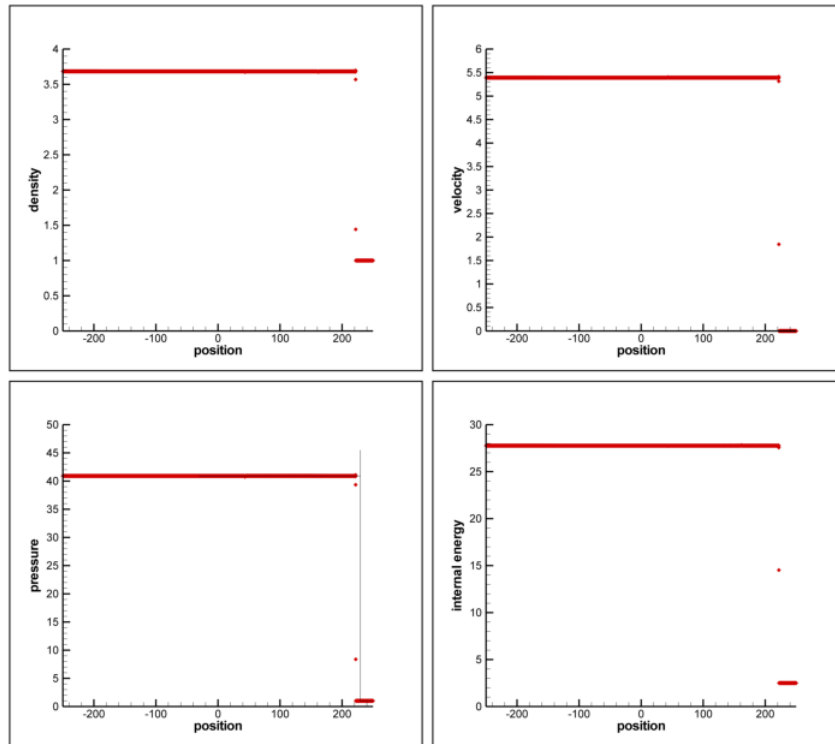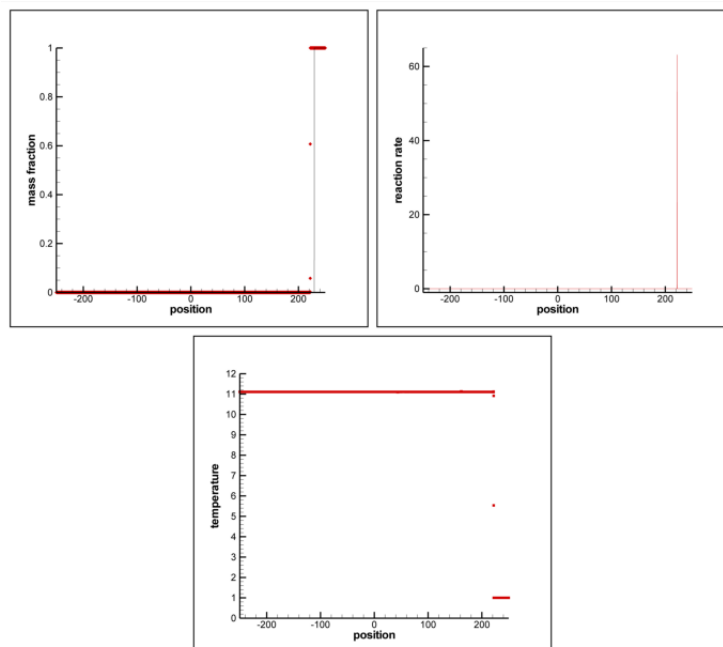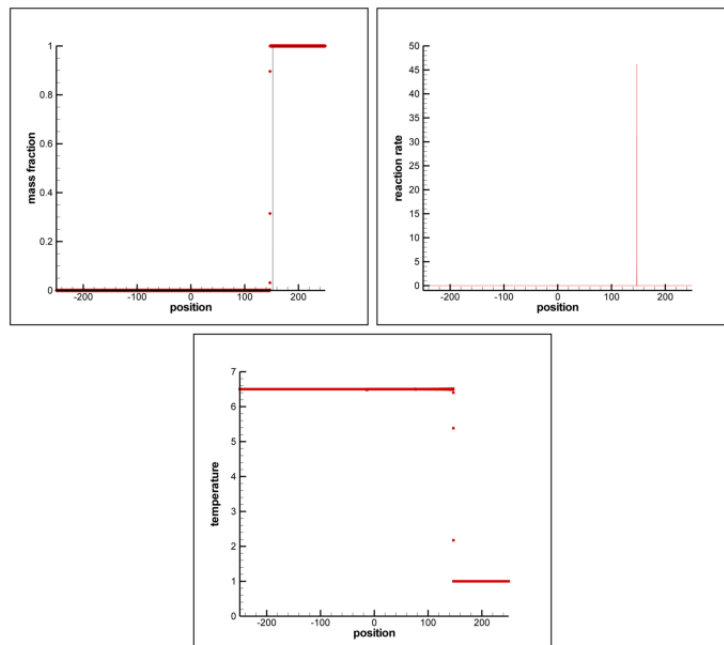

Figure 6.28: Numerical solution of the reactive Euler equations (red symbols) for strong detonation, comparing with the exact ZND solution (black line) for the test case 4.

6.3 CONCLUSION

As a conclusion, detonation tube problem is solved numerically applying high resolution methods on the reactive Euler equations. Solutions are obtained from a written FORTRAN code. For the detonation tube problem, several cases have been tested according to the input variables. With these numerical tests, accuracy of the numerical method for solving detonation tube problem has been seen. Numerical solutions compared with the exact ZND solution of the problem, with this comparison accuracy of the numerical methods have been seen. In general, high resolution method gives fine solution, it shows the pressure peaks at the detonation, but for slow moving waves, numerical method is inaccurate. The construction of the mesh is important for capturing the strong or CJ detonations, otherwise weak detonations can be seen, which is an unphysical solution for the ZND theory. ApAdjust the ratio of the $\Delta t/\Delta x$ is important when constructing a fine mesh. An accurate solution can be collected when ratio of $\Delta t/\Delta x$ is equal to 0.1. Otherwise numerical method can give inaccurate or an error due negative pressure or density.

For the future works, one can study to capture the pressure peaks with more accuracy then high resolution methods. A modification needed to done in order to solve the slow moving waves accurately. The oscillations created by the Strang time splitting method can be decreased by changing the splitting method. For use in engineering purposes, a two dimensional analyses of the detonation tube problem can be done in future. B

REFERENCES

[1] Glassman, I. *Combustion*, Academic Press, 2nd Edition, 1987.

[2] Fickett, W., Davis, W. C., *Detonation*, University of California Press, 1979.

[3] Li, J., Qiu, H., Yan, C. and Wang, Y., *Preliminary study of a pulse normal detonation wave engine*, Aerospace Science and Technology, Volume 14, Issue 3 ,pp. 161-167, May 2010.

[4] Strehlow, R. A., *Combustion Fundamentals* McGraw-Hill, New York, 1984.

[5] Berkenbosch, A. C., *Capturing Detonation Waves for the Reactive Euler Equations*, 1995.

[6] Toro, E. F., *Riemann Solvers and Numerical Methods for Fluid Dynamic*, Springer, 3rd Edition, 2009.

[7] Godunov, S. K., *A Finite Difference Method for the Computation of Discontinuous Solutions of the Equations of Fluid Dynamics*, Mat. Sb., 47:357-393, 1959.

[8] Lax, P. D., *Hyperbolic Systems of Conservation Laws and the Mathematical Theory of Shock Waves*, Society for Industrial and Applied Mathematics, Philadelphia, 1990.

[9] Sod, G. A., *A Survey of Several Finite Difference Methods for Systems of Nonlinear Hyperbolic Conservation Laws*, J. Comput. Phys., 27:1-31, 1978.

[10] Einfeldt, B., Munz, C. D., Roe, P. L. and Sjögreen, B., *On Godunov-Type Methods near Low Densities*, J. Comput. Phys., 92:273-295, 1991.

[11] Woodward, P. and Colella, P. *The Numerical Simulation of Two-Dimensional Fluid Flow with Strong Shocks*, J. Comput. Phys., 54:115-173, 1984.

[12] Toro, E. F., *NUMERICA: A Library of Source Codes for Teaching, Research and Applications*, Numeritek Ltd., www.numeritek.com, 1999.

[13] Anderson, D. A., Tannehill, J. C. and Pletcher, R. H. *Computational Fluid Mechanics and Heat Transfer*, Hemisphere Publishing Corporation, 1984.

[14] Hirsch, C. *Numerical Computation of Internal and External Flows, Vol. I: Fundamentals of Numerical Discretization*, Wiley, 1988.

[15] Hirsch, C. *Numerical Computation of Internal and External Flows, Vol. II: Computational Methods for Inviscid and Viscous Flows.*, Wiley, 1990.

[16] Hoffmann, K. A., *Computational Fluid Dynamics for Engineers*, Engineering Education Systems, Austin, Texas, USA, 1989.

[17] LeVeque, R. J. *Numerical Methods for Conservation Laws*, Birkhäuser Verlag, 1992.

[18] LeVeque, R. J. *Finite Volume Methods for Hyperbolic Problems*, Cambridge University Press, 2002.

[19] Hou, T. Y. and Le Floch, P. G., *Why Nonconservative schemes converge to wrong solutions: Error Analysis*, Mathematics of Computation, Volume 62, Number 206, pp. 497-530, April 1994.

[20] Lax, P. D., *Weak Solutions of Nonlinear Hyperbolic Equations and Their Numerical Computation*, Comm. Pure. Appl. Math., VII:159-193, 1954.

[21] Lax, P. D. and Wendroff, B. *Systems of Conservation Laws* Comm. Pure Appl.Math., 13:217-237, 1960.

[22] Quirk, J. J., *A Contribution to the Great Riemann Solver Debate*, International Journal for Numerical Methods in Fluids, vol 18, pp. 555-574, 1994.

[23] Roe, P. L., *Approximate Riemann Solvers, Parameter Vectors, and Difference Schemes* J. Comput. Phys., 43:357-372, 1981.

[24] Harten, A. and Hyman, J. M., *Self Adjusting Grid Methods for One-Dimensional Hyperbolic Conservation Laws*, J. Comput. Phys., 50:235-269, 1983.

[25] Harten, A., *On a Class of High Resolution Total-Variation-Stable Finite-Difference schemes*, SIAM J. Numer. Anal. 21:1-23, 1984.

[26] Sweby, B. K., *High Resolution Schemes Using Flux Limiters for Hyperbolic Conservation Laws*, SIAM J. Numer. Anal. 21:995-1011, 1984.

[27] Osher, S., *Riemann Solvers, the Entropy Condition and Difference Approximations* SIAM J. Numer. Anal. 21:217-235, 1984.

[28] van Leer, B., *Towards the Ultimate Conservative Difference Scheme II. Monotonicity and Conservation Combined in a Second Order Scheme*, J. Comput. Phys. 14:361-370, 1974.

[29] Goodman, J. B. and LeVeque, R. J., *A geometric Approach to High Resolution TVD Schemes*, SIAM J. Numer. Anal. 25:268-284, 1988.

[30] Courant, R. and Friedrichs K. O., *Supersonic Flow and Shock Waves*, Wiley, New York, 1948.

[31] Bourlioux, A., Majda, A. and Roytburd, V., *Theoretical and Numerical Structure for Unstable One-Dimensional Detonations*, SIAM J Appl. Math. 51:303-343, 1991.

[32] Majda, A., *A Qualitative Model for Dynamic Combustion*, SIAM J. Appl. Math. 41:70-93, 1981.

[33] Stang, G., *On the Construction and Comparison of Difference Schemes*, SIAM J. Numer. Anal. 5:506-517, 1968.

[34] Bourlioux, A. *Numerical Study of Unstable Detonations*, Ph.D. Thesis, Princeton University, Princeton, 1991.

[35] Quirk, J.J. *Godunov-type Schemes Applied to Detonation Flows*, Institute for Computer Applications in Science and Engineer, Hampton, 1993.

[36] Papalexandris, M. V., Leonard, A. and Dimotakis, P. E., *Unsplit Schemes for Hyperbolic Conservation Laws with Source Terms in One Space Dimension*, J. Comput. Phys., 134:31-61, 1997.

[37] Sharpe, G.J. and Falle, A. E. G., *One-dimensional Numerical Simulations of Idealized Detonations*, Math. Phys. and Engineering Sciences, 455:1203-1214, 1999.

[38] Zucrow, M. J. and Hoffman, J. D., *Gas Dynamics Volume I*, John Wiley and Sons, 1976.

APPENDIX A

JACOBIAN MATRIX OF THE REACTIVE EULER EQUATIONS

The general formulation of the Jacobian matrix is;

$$A(U) = \frac{\partial F}{\partial U} = \begin{bmatrix} \frac{\partial f_1}{\partial u_1} & \frac{\partial f_1}{\partial u_2} & \frac{\partial f_1}{\partial u_3} & \frac{\partial f_1}{\partial u_4} \\ \frac{\partial f_2}{\partial u_1} & \frac{\partial f_2}{\partial u_2} & \frac{\partial f_2}{\partial u_3} & \frac{\partial f_2}{\partial u_4} \\ \frac{\partial f_3}{\partial u_1} & \frac{\partial f_3}{\partial u_2} & \frac{\partial f_3}{\partial u_3} & \frac{\partial f_3}{\partial u_4} \\ \frac{\partial f_4}{\partial u_1} & \frac{\partial f_4}{\partial u_2} & \frac{\partial f_4}{\partial u_3} & \frac{\partial f_4}{\partial u_4} \end{bmatrix} \tag{A.1}$$

The variable vector U is written as;

$$U = \begin{bmatrix} \rho \\ \rho u \\ \rho E \\ \rho Y \end{bmatrix} = \begin{bmatrix} u_1 \\ u_2 \\ u_3 \\ u_4 \end{bmatrix} \tag{A.2}$$

The flux vector F is written as;

$$U = \begin{bmatrix} \rho u \\ \rho u^2 + p \\ \rho u E + u p \\ \rho u Y \end{bmatrix} = \begin{bmatrix} f_1 \\ f_2 \\ f_3 \\ f_4 \end{bmatrix} \tag{A.3}$$

In order to take the derivatives of the F, F is written in terms of U as;

$$f_1 = u_2$$

$$f_2 = \gamma E \rho - E \rho + \frac{3 - \gamma}{2} \rho u^2 - (\gamma - 1) Q \rho Y$$

$$f_2 = \gamma u_3 - u_3 + \frac{3 - \gamma}{2} \frac{u_2^2}{u_1} - (\gamma - 1) Q u_4$$

$$f_3 = \gamma \rho u E - \frac{\gamma - 1}{2} \rho u^3 - (\gamma - 1) Q \rho u Y \qquad \text{(A.4)}$$

$$f_3 = \gamma \frac{u_2 u_3}{u_1} - \frac{\gamma - 1}{2} \frac{u_2^3}{u_1^2} - (\gamma - 1) Q \frac{u_2 u_4}{u_1}$$

$$f_4 = \frac{u_2 u_4}{u_1}$$

Then the derivatives can be calculated.

$$\frac{\partial f_1}{\partial u_1} = 0, \qquad \frac{\partial f_1}{\partial u_2} = 1, \qquad \frac{\partial f_1}{\partial u_3} = 0, \qquad \frac{\partial f_1}{\partial u_4} = 0,$$

$$\frac{\partial f_2}{\partial u_1} = -\frac{3 - \gamma}{2} \frac{u_2^2}{u_1}$$

$$\frac{\partial f_2}{\partial u_2} = (3 - \gamma) \frac{u_2}{u_1}$$

$$\frac{\partial f_2}{\partial u_3} = (\gamma - 1)$$

$$\frac{\partial f_2}{\partial u_4} = -(\gamma - 1) Q$$

$$\frac{\partial f_3}{\partial u_1} = (\gamma - 1) \frac{u_2^3}{u_1} - \gamma \frac{u_2 u_3}{u_1^2} + (\gamma - 1) Q \frac{u_2 u_+}{u_1^2} \qquad \text{(A.5)}$$

$$\frac{\partial f_3}{\partial u_2} = \gamma \frac{u_3}{u_1} - \frac{3(\gamma - 1)}{2} \frac{u_2^2}{u_1} - (\gamma - 1) Q \frac{u_4}{u_1}$$

$$\frac{\partial f_3}{\partial u_3} = \gamma \frac{u_2}{u_1}$$

$$\frac{\partial f_3}{\partial u_4} = -(\gamma - 1) Q \frac{u_2}{u_1}$$

$$\frac{\partial f_4}{\partial u_1} = -\frac{u_2 u_4}{u_1}, \qquad \frac{\partial f_4}{\partial u_2} = \frac{u_4}{u_1}, \qquad \frac{\partial f_4}{\partial u_3} = 0, \qquad \frac{\partial f_4}{\partial u_4} = -\frac{u_2}{u_1},$$

Then the Jacobian matrix becomes;

$$A = \begin{bmatrix} 0 & 1 & 0 & 0 \\ -\frac{3 - \gamma}{2} u^2 & (3 - \gamma) u & \gamma - 1 & -(\gamma - 1) Q \\ (\gamma - 1) u^3 - \gamma u E + (\gamma - 1) Q u Y & \gamma E - \frac{3(\gamma - 1)}{2} u^2 - (\gamma - 1) Q Y & \gamma u & -(\gamma - 1) Q u \\ -u Y & Y & 0 & u \end{bmatrix}$$

(A.6)

To simplify the Jacobian matrix, γE will be written as;

$$\gamma E = \frac{p}{\rho} + E + \frac{(\gamma - 1)}{2} u^2 - Q Y (\gamma - 1) \qquad \text{(A.7)}$$

120

If γE put into the Jacobian matrix, and using $H = E + p/\rho$, the final Jacobian matrix becomes;

$$A = \begin{bmatrix} 0 & 1 & 0 & 0 \\ -\frac{3-\gamma}{2}u^2 & (3-\gamma)u & \gamma-1 & -(\gamma-1)Q \\ u\left(\frac{1}{2}(\gamma-1)u^2 - H\right) & H-(\gamma-1)u^2 & \gamma u & -(\gamma-1)Qu \\ -uY & Y & 0 & u \end{bmatrix} \tag{A.8}$$

APPENDIX B

CALCULATION OF THE EIGENVALUES AND EIGENVECTORS OF THE REACTIVE EULER EQUATIONS

In order to calculate the eigenvalues of the reactive Euler equations without the source term, the equation set is written in the primitive variable form. The equation set is given as;

$$U_t + F(U)_x = 0$$

$$U = \begin{bmatrix} \rho \\ \rho u \\ \rho E \\ \rho Y \end{bmatrix} \qquad F = \begin{bmatrix} \rho u \\ \rho u^2 + p \\ u(\rho E + p) \\ \rho u Y \end{bmatrix} \tag{B.1}$$

Then primitive variable formulation will be written in terms of vector $W = [\rho, u, p, Y]^T$. To write the equation set in the primitive variable form, the differential form of the equation will be written in more explicit form. The conservation of mass is written as;

$$\rho_t + \rho u_x + u\rho_x = 0 \tag{B.2}$$

The conservation of momentum is written as;

$$u\rho_t + \rho u_t + u\rho u_x + u^2\rho_x + u\rho u_x + p_x = 0$$
$$u[\rho_t + \rho u_x + u\rho_x] + \rho[u_t + uu_x + \frac{1}{\rho}p_x] = 0 \tag{B.3}$$

Using the conservation of mass, conservation of momentum equation becomes;

$$u_t + uu_x + \frac{1}{\rho}p_x = 0 \tag{B.4}$$

The conservation of species is written as;

$$Y\rho_t + \rho Y_t Y(\rho u)_x + u\rho Y_x = 0$$
$$Y[\rho_t + \rho u_x + u\rho_x] + \rho[Y_t + uY_x] = 0 \tag{B.5}$$

122

Using the conservation of mass, conservation of species equation becomes;

$$Y_t + uY_x = 0 \tag{B.6}$$

The conservation of energy is written as;

$$\left[\rho\left(\frac{p}{\rho(\gamma-1)} + 0.5u^2 + QY\right)\right]_t + \left[\rho u\left(\frac{p}{\rho(\gamma-1)} + 0.5u^2 + QY\right)\right]_x + up_x + pu_x = 0$$

$$\frac{p_t}{\gamma-1} + \rho u u_t + 0.5u^2\rho_t + Q(\rho Y)_t + \frac{u}{\gamma-1}p_x + \frac{p}{\gamma-1}u_x + Q(\rho u Y)_x$$

$$+ 0.5\rho u^2 u_x + u^3\rho_x + \rho u^2 u_x + up_x + pu_x = 0 \tag{B.7}$$

$$0.5u^2[\rho_t + \rho u_x + u\rho_x] + \rho u[u_t + uu_x + \frac{1}{\rho}p_x]$$

$$+ Q[Y\rho_t + \rho Y_t Y(\rho u)_x + u\rho Y_x] + \frac{1}{\gamma-1}[p_t + up_x + (\gamma-1)pu_x + pu_x] = 0$$

Using the conservation of mass, momentum and species, the conservation of energy is written as;

$$p_t + up_x + \gamma p u_x = 0 \tag{B.8}$$

The primitive formulation of the variables can be written as;

$$W_t + AW_x = 0$$

$$W = \begin{bmatrix} \rho \\ u \\ p \\ Y \end{bmatrix} \qquad A = \begin{bmatrix} u & \rho & 0 & 0 \\ 0 & u & \frac{1}{\rho} & 0 \\ 0 & \gamma p & u & 0 \\ 0 & 0 & 0 & u \end{bmatrix} \tag{B.9}$$

A is the characteristic matrix. Using the matrix A the eigenvalues are calculated.

$$det|A - \lambda I| = 0$$

$$det\begin{bmatrix} u-\lambda & \rho & 0 & 0 \\ 0 & u-\lambda & \frac{1}{\rho} & 0 \\ 0 & \gamma p & u-\lambda & 0 \\ 0 & 0 & 0 & u-\lambda \end{bmatrix} = 0 \tag{B.10}$$

$$(u-\lambda)\left[(u-\lambda)\left((u-\lambda)^2 - \frac{\gamma p}{\rho}\right)\right] = 0$$

$$(u-\lambda)^2[(u-\lambda)^2 - a^2] = 0$$

Solving the above equation, the eigenvalues are calculated as;

$$\lambda_1 = u - a, \qquad \lambda_2 = u, \qquad \lambda_3 = u, \qquad \lambda_4 = u + a \tag{B.11}$$

123

Using the calculated eigenvalues and the Jacobian matrix calculated in appendix A. The eigenvector can be calculated.

$$(A - \lambda)K = 0 \tag{B.12}$$

For $\lambda_1 = u - a$;

$$
\begin{bmatrix}
-u + a & 1 & 0 & 0 \\
-\frac{3-\gamma}{2}u^2 & (3-\gamma)u - u + a & \gamma - 1 & -(\gamma-1)Q \\
u\left(\frac{1}{2}(\gamma-1)u^2 - H\right) & H - (\gamma-1)u^2 & \gamma u - u + a & -(\gamma-1)Qu \\
-uY & Y & 0 & a
\end{bmatrix}
\begin{bmatrix}
x_1 \\ x_2 \\ x_3 \\ x_4
\end{bmatrix} = 0
$$

$$(-u + a)x_1 + x_2 = 0 \tag{B.13}$$

$$-\frac{3-\gamma}{2}u^2 x_1 + ((3-\gamma)u - u + a)x_2 + (\gamma-1)x_3 - (\gamma-1)Qx_4 = 0$$

$$u\left(\frac{1}{2}(\gamma-1)u^2 - H\right)x_1 + (H - (\gamma-1)u^2)x_2 + (\gamma u - u + a)x_3 + -(\gamma-1)Qux_4 = 0$$

$$-uYx_1 + Yx_2 + ax_4 = 0$$

Assuming $x_1 = 1$, from the first relation $x_2 = u - a$. From the fourth relation $x_4 = Y$. Using the second relation and putting the founded variables, $x_3 = H - ua$.

For $\lambda_{2,3} = u$;

$$
\begin{bmatrix}
-u & 1 & 0 & 0 \\
-\frac{3-\gamma}{2}u^2 & (3-\gamma)u - u & \gamma - 1 & -(\gamma-1)Q \\
u\left(\frac{1}{2}(\gamma-1)u^2 - H\right) & H - (\gamma-1)u^2 & \gamma u - u & -(\gamma-1)Qu \\
-uY & Y & 0 & 0
\end{bmatrix}
\begin{bmatrix}
x_1 \\ x_2 \\ x_3 \\ x_4
\end{bmatrix} = 0
$$

$$-ux_1 + x_2 = 0 \tag{B.14}$$

$$-\frac{3-\gamma}{2}u^2 x_1 + ((3-\gamma)u - u)x_2 + (\gamma-1)x_3 - (\gamma-1)Qx_4 = 0$$

$$u\left(\frac{1}{2}(\gamma-1)u^2 - H\right)x_1 + (H - (\gamma-1)u^2)x_2 + (\gamma u - u)x_3 + -(\gamma-1)Qux_4 = 0$$

$$-uYx_1 + Yx_2 = 0$$

For λ_2, assuming $x_1 = 1$, from the first relation $x_2 = u$. Using the second and third relations, $x_3 = 0.5u^2$ and $x_4 = 0$.

For λ_3, assuming $x_1 = 0$, from the first relation $x_2 = 0$. Using the second and third relations, $x_3 = Q$ and $x_4 = 1$.

For $\lambda_4 = u + a$;

$$\begin{bmatrix} -u - a & 1 & 0 & 0 \\ -\frac{3-\gamma}{2}u^2 & (3-\gamma)u - u - a & \gamma - 1 & -(\gamma-1)Q \\ u\left(\frac{1}{2}(\gamma-1)u^2 - H\right) & H - (\gamma-1)u^2 & \gamma u - u - a & -(\gamma-1)Qu \\ -uY & Y & 0 & -a \end{bmatrix}\begin{bmatrix} x_1 \\ x_2 \\ x_3 \\ x_4 \end{bmatrix} = 0$$

$$(-u - a)x_1 + x_2 = 0 \tag{B.15}$$

$$-\frac{3-\gamma}{2}u^2 x_1 + ((3-\gamma)u - u - a)x_2 + (\gamma-1)x_3 - (\gamma-1)Qx_4 = 0$$

$$u\left(\frac{1}{2}(\gamma-1)u^2 - H\right)x_1 + (H - (\gamma-1)u^2)x_2 + (\gamma u - u - a)x_3 + -(\gamma-1)Qux_4 = 0$$

$$-uYx_1 + Yx_2 - ax_4 = 0$$

Assuming $x_1 = 1$, from the first relation $x_2 = u + a$. From the fourth relation $x_4 = Y$. Using the second relation and putting the founded variables, $x_3 = H + ua$.

Then the right eigenvector are written as;

$$K^{(1)} = \begin{bmatrix} 1 \\ u - a \\ H - ua \\ Y \end{bmatrix} \quad K^{(2)} = \begin{bmatrix} 1 \\ u \\ 0.5u^2 \\ 0 \end{bmatrix} \quad K^{(3)} = \begin{bmatrix} 0 \\ 0 \\ Q \\ 1 \end{bmatrix} \quad K^{(4)} = \begin{bmatrix} 1 \\ u + a \\ H + ua \\ Y \end{bmatrix} \tag{B.16}$$

APPENDIX C

CALCULATION OF THE WAVE STRENGTHS

From the definition, the wave strength formulated as;

$$\Delta U = \sum_{1}^{4} \alpha_i K^{(i)}$$

$$\begin{bmatrix} \Delta u_1 \\ \Delta u_2 \\ \Delta u_3 \\ \Delta u_4 \end{bmatrix} = \alpha_1 \begin{bmatrix} 1 \\ u-a \\ H-ua \\ Y \end{bmatrix} + \alpha_2 \begin{bmatrix} 1 \\ u \\ 0.5u^2 \\ 0 \end{bmatrix} + \alpha_3 \begin{bmatrix} 0 \\ 0 \\ Q \\ 1 \end{bmatrix} + \alpha_4 \begin{bmatrix} 1 \\ u+a \\ H+ua \\ Y \end{bmatrix}$$

$$\begin{bmatrix} \Delta u_1 \\ \Delta u_2 \\ \Delta u_3 \\ \Delta u_4 \end{bmatrix} = \begin{bmatrix} 1 & 1 & 0 & 1 \\ u-a & u & 0 & u+a \\ H-ua & 0.5u^2 & Q & H+ua \\ Y & 0 & 1 & Y \end{bmatrix} \begin{bmatrix} \alpha_1 \\ \alpha_2 \\ \alpha_3 \\ \alpha_4 \end{bmatrix}$$

(C.1)

Using Gaussian elimination method;

$$
\begin{array}{c|cccc}
\varDelta u_1 & 1 & 1 & 0 & 1 \\
\varDelta u_2 - u\varDelta u_1 & -a & 0 & 0 & a \\
\varDelta u_3 & H - ua & 0.5u^2 & Q & H + ua \\
\varDelta u_4 & Y & 0 & 1 & Y
\end{array}
$$

$$
\begin{array}{c|cccc}
\varDelta u_1 & 1 & 1 & 0 & 1 \\
\varDelta u_2 - u\varDelta u_1 & -a & 0 & 0 & a \\
\varDelta u_3 - u(\varDelta u_2 - u\varDelta u_1) & H & 0.5u^2 & Q & H \\
\varDelta u_4 & Y & 0 & 1 & Y
\end{array}
$$

$$
\begin{array}{c|cccc}
\varDelta u_1 & 1 & 1 & 0 & 1 \\
\varDelta u_2 - u\varDelta u_1 & -a & 0 & 0 & a \\
\varDelta u_3 - u(\varDelta u_2 - u\varDelta u_1) - H\varDelta u_1 & 0 & 0.5u^2 - H & Q & 0 \\
\varDelta u_4 - Y\varDelta u_1 & 0 & -Y & 1 & 0
\end{array}
$$

$$
\begin{array}{c|cccc}
\varDelta u_1 & 1 & 1 & 0 & 1 \\
\varDelta u_2 + (a - u)\varDelta u_1 & 0 & a & 0 & 2a \\
\varDelta u_3 - u(\varDelta u_2 - u\varDelta u_1) - H\varDelta u_1 & 0 & 0.5u^2 - H & Q & 0 \\
\varDelta u_4 - Y\varDelta u_1 & 0 & -Y & 1 & 0
\end{array}
$$

(C.2)

Then equations become;

$$
\begin{aligned}
& \alpha_1 + \alpha_2 + \alpha_4 = \varDelta u_1 \\
& a\alpha_2 + 2a\alpha_4 = \varDelta u_2 + (a - u)\varDelta u_1 \\
& (0.5u^2 - H)\alpha_2 + Q\alpha_3 = \varDelta u_3 - u(\varDelta u_2 - u\varDelta u_1) - H\varDelta u_1 \\
& - Y\alpha_2 + \alpha_3 = \varDelta u_4 - Y\varDelta u_1
\end{aligned}
$$

(C.3)

Then combining the third and fourth equations ;

$$
\alpha_2 = \frac{\varDelta u_1(QY + u^2 - H) - \varDelta u_2 u + \varDelta u_3 - \varDelta u_4 Q}{0.5u^2 + QY - H}
$$

(C.4)

After finding the α_2, α_3 can be calculated from fourth equation easily. After that α_4 calculated as;

$$
\alpha_4 = \frac{\varDelta u_1(a - u) + \varDelta u_2 - \alpha_2 a}{2a}
$$

(C.5)

Finally α_1 is calculated from the first equation as;

$$
\alpha_1 = \varDelta u_1 - \alpha_2 - \alpha_4
$$

(C.6)